Investigation of a Circulating Fluidised Adsorption Refrigeration (CFAR) System for Continuous Operation Mode

By

Modupe Atinuke Oluleye

BEng, MSc

Thesis Submitted to the University of Nottingham

for the Degree of Doctor of Philosophy

November 2023

Abstract

Energy economy, nature conservation and sustainability remain the focal points of the global world. Due to the increase in the global consumption of limited primary energy and the ecological consideration for refrigerants choice, solid desiccant refrigeration systems powered by low grade heat sources have been the subject of extensive research for cooling applications geared to meet the fast growing refrigeration needs of the rural areas of developing countries.

Some merits of adsorption cooling systems include but are not restricted to low energy intensity, use of low grade heat sources and being environmentally benign i.e., both their ozone depletion potential (ODP) and global warming potential (GWP) are zero, thereby meeting the current global regulations. However, this technology has not been able to fully compete with, let alone replacing vapour compression refrigeration system (VCRS) because of some identified bottlenecks.

The overall aim of this research is to develop a novel energy efficient adsorption refrigeration system for application in rural areas of developing countries that addresses the technical limitations (e.g. refrigeration production intermittency, adsorbent deterioration, refrigerant leakage, poor heat transfer, mechanical complexities, and thermal stress induction) of existing adsorption systems without compromising the system simplicity. Hence, a novel circulating fluidised adsorption refrigeration (CFAR) system using G32-H, a coconut-derived activated carbon/methanol as working pair for continuous operation mode is investigated in this work.

The novel CFAR system comprises three interconnected circuits [the circulatory circuit (CC), the separation circuit (SC) and the refrigeration circuit (RC)] that work in tandem. This configuration has been proved effective for the continuous circulation of the fluidized adsorbate-laden-solid desiccant by means of a gas-solid cyclone separator.

Detailed computer modelling of the novel design to investigate its performance parameters was carried out which involved model formulation for the separation circuit (cyclone) and mathematical formulations for the modelling of the heat and mass transfer of the adsorption cooling/heating circuit. The performance of the separation circuit (cyclone) was investigated by writing a computer code using MATLAB software to determine the speed of adsorbent flow. Subsequently, from the discretised governing equations of energy and mass conservation (developed by finite difference scheme (FDS)) combined with the associated boundary conditions and the adsorbent flow speed already determined, a computer code using MATLAB software was developed for easy implementation on a personal computer to determine and optimize the overall system performance parameters.

The simulation result shows that the designed cyclone is an energy efficient, high efficiency one as it has an overall separation of 99%. Moreover, it was shown that with the ambient temperature of 26.9 ℃, maximum adsorption capacity of 0.38 kg/kg, desiccant flow velocity of 0.49 m/s, evaporator and condenser temperatures being controlled at 15℃ and 35 ℃ respectively, a desorption temperature of 87 ℃ was reached and the resulting COP ranged from 0.24 – 0.40 while the SCP ranged from 73.1 W/kg – 152.0 W/kg.

Furthermore, the impact of some operational and design parameters that play a significant role in the CFAR system performance was evaluated in a parametric study using the developed numerical model. The computer model was validated with experimental data from the literature and a good agreement was recorded.

Therefore, the concept of this novel CFAR configuration with its pertinent potentials (including continuous cold production, eradication of the issue of unnecessary load on the evaporator, maximum optimization of both adsorption and desorption processes due to the spatial separation of both desorber and adsorber, absence of thermal stress induction in the bed as heat source and heat sink heat exchangers are localised), has been proved to meet the fast growing refrigeration needs of the rural areas of developing countries thereby maintaining the energy conservation and sustainable development of her environment.

Keywords: Adsorption, Desorption, Refrigeration, Fluidized, Circulating, Continuous mode, Solid desiccant, Cyclone.

To Delight, my beloved late daughter who I lost in the course of this study. You remain in my heart forever.

Publications

- Oluleye M. A. & Rabah Boukhanouf, (2019). *Development Trend of Solar-powered Adsorption Refrigeration Systems: A Review of Technologies, Cycles, Applications, Challenges and Future Research Directions.* Journal of Multidisciplinary Engineering Science and Technology (JMEST), 6(8), 10491- 10504.

Acknowledgement

We are an aggregate of what we have learnt from all who have taught or influenced us by some means both great and small. Foremost, I appreciate God Almighty, the fountain of all inspirations and the source of my strength, for sustaining me this far.

I would like to express my profound gratitude to my supervisor, Associate Prof. Dr. Rabah Boukhanouf for his patience, understanding, motivation, enthusiasm, and immense knowledge. His supportive guidance, valuable inputs and stimulating suggestions had undoubtedly helped me in all the period of my research journey under his painstaking supervision. I could not have imagined having a better supervisor and mentor for my Ph.D study. Thank you for your continuous believe in me over the years. Those thoughtful words and the crucial role you played during the demise of my daughter had immensely made the completion of this work possible.

I am deeply indebted to the Nigeria Tertiary Education Trust Fund (TETFund) for sponsoring my Ph.D study in the United Kingdom.

I wish to also record my special thanks of gratitude to the Faculty of Engineering, University of Nottingham, United Kingdom for awarding me with the financial means (50% yearly tuition reduction) to complete this work.

I owe my endless gratitude to my caring husband who endured this long process with me. Thank you Papa for your patience, unconditional love, unequivocal support and for granting permission for this programme. I revere your courage and heart which is never shaken by whatsoever.

With a heart of gratitude, I would also want to acknowledge the endless supports and encouragement from my children, family, friends and colleagues. You are all accorded a due appreciation.

Table of contents

Abstract.....i

Dedication.....iv
Publications.....v
Acknowledgement.....vi
Table of contents.....vii
Nomenclature.....xi
List of figures.....xiv
List of tables.....xvii
Chapter 1: Introduction.....1
1.1 Background.....1
1.1.1 The increase in global consumption of limited primary energy (energy crisis in developing countries) 2
1.1.2 Ecological consideration for refrigerant choice.....4
1.2 Need for alternative refrigeration system in rural areas of developing countries.....5
1.3 Research aims and objectives.....6
1.3.1 Research aims.....6
1.3.2 Research objectives.....6
1.4 Research methodology.....7
1.4.1 Review of literature.....7
1.4.2 Designs, investigation and evaluation of the various possible alternative configurations of solid desiccant cooling/heating systems to evaluate the credits and limitations of each.....8
1.4.3 Design and definition of the broad characteristics of a novel system.....9
1.4.4 Computer modelling of the novel design to investigate its performance parameters.....9
1.5 Problem statements.....10
1.5.1 Adsorption deterioration.....10
1.6 Thesis layout.....11

Chapter 2: Overview of refrigeration/cooling technologies.....13
2.1 Classification of cooling technologies.....13
2.2 Types of cooling technology.....14
2.2.1 Ejector refrigeration technology……...14
2.2.2 Vapour-compression refrigeration technology…….16
2.2.3 Absorption refrigeration technology……18
2.2.4 Run-around solid desiccant for dehumidification…….20
2.2.5 Organic Rankine cycle refrigeration technology……..21
2.2.6 Adsorption refrigeration technology.....23
2.2.6.1 Principle of adsorption refrigeration.....23

2.2.6.2 Basic adsorption refrigeration cycle.....24
2.2.6.3 Adsorbents general requirements.....26
2.2.6.4 Choice of adsorbate.....26
2.2.6.5 Selection of working pair.....27
2.2.6.6 Important advantages of the adsorption refrigeration technology.....28
2.3 Summary.....29

Chapter 3: Development trend in adsorption cooling technology.....31
3.1 Development history of adsorption cooling technology.....31
3.2 A review of development trends.....32
3.2.1 Basic or intermittent cycles.....33
3.2.2 Advanced continuous cycles.....39
3.2.2.1 Heat recovery adsorption refrigeration cycle....40
` 3.2.2.2 Heat and mass recovery adsorption refrigeration cycle.....41
3.2.2.3 Thermal wave adsorption refrigeration cycle...44
3.2.2.4 Convective thermal wave adsorption refrigeration cycle.....46
3.2.2.5 Cascaded cycle.....47
3.2.2.6 Multi bed and multi stage cycle.....48
3.2.2.7 Fluidised bed technology.....50
3.2.2.8 Constant temperature adsorption refrigeration (CTAR) cycle.....51
3.2.2.9 Hybrid systems.....53
3.3 Analysis of reviewed works on development history of adsorption cooling technology……..56
3.4 Summary.....64

Chapter 4: Alternative adsorption refrigeration system design configurations.....65
4.1 Introduction.....65
4.2 Proposed adsorption design arrangements.....66
4.2.1 Design arrangement 1: Adsorption-partial resorption out-of-phase configuration.....66
4.2.2 Design arrangement 2: The rotary desiccant wheel configuration.....68
4.2.3 Design arrangement 3: Desiccant-circulator-aided fluidised adsorbent bed.....69
4.2.4 Design arrangement 4: Circulating fluidised adsorption refrigeration (CFAR) system.....71
4.2.4.1 CFAR system description.....72
4.2.4.2 Operation principle and components of the system.....73

4.2.4.3 Desiccant circuit.....75
4.2.4.4 Refrigerant/adsorbate circuit.....76
4.2.4.5 Desiccant separation.....77
4.2.4.6 System design considerations.....78
4.2.4.7 Theoretical analysis for the separation circuit.....81
4.3 Summary.....86

Chapter 5: Design and mathematical modelling of the proposed circulating fluidised adsorption refrigeration system configuration.....88
5.1 Introduction……...88
5.2 Model formulation for the separation circuit 88
5.2.1 Cyclone design.....88
5.2.2 Cyclone geometry.....88
5.2.3 Assumptions.....89
5.2.4 Estimation of pressure drop, (ΔP) 91
5.2.5 Estimation of the cut size diameter, x50.....93
5.2.6 Cyclone overall separation/collection efficiency, ηt.....94
5.2.7 Number of effective turns, Ne.....96
5.2.8 Power requirement, P.....96
5.2.9 Solid circulating rate, Msc.....96
5.2.10 Gas residence time, τR.....96
5.2.11 Terminal settling velocity of solid adsorbent, usc.....97
5.2.12 Determination of mass of solid adsorbent collected, mc.....97
5.3 Model formulation for the adsorption refrigeration circuit.....97
5.3.1 Assumptions.....98
5.3.2 The isotherm equation.....99
5.3.3 Adsorber/desorber configuration.....99
5.3.4 Energy balance.....101
5.3.5 The overall mass balance/conservation.....102
5.3.6 Initial and boundary conditions.....103
5.3.7 Method of numerical solution.....103
5.3.8 Discretization of the governing equations.....104
5.3.9 Computer model algorithm/solution procedure.....106
5.3.10 System performance indices.....108
5.4 Summary.....110

Chapter 6: Results analysis and discussion.....112
6.1 Cyclone simulation results.....112

6.1.1 Validation of the numerical model.....113

6.1.2 Effects of the cyclone operational parameters on its performance.....115
6.1.2.1 Effects of particle exit diameter on the cyclone pressure drop.....116
6.1.2.2 Effects of particle exit diameter on the cyclone cut size diameter.....118
6.1.2.3 Effects of particle exit diameter on the cyclone collection efficiency.....119
6.2 Adsorption refrigeration circuit simulation results.....120
6.2.1 Temperature profile along the desorber and adsorber.....123
6.2.1.1 In the first 60 s.....123
6.2.1.2 Within the second 60 s.....124
6.2.1.3 After the first 60 s.....126
6.2.2 Pressure profile along the desorber and adsorber.....127
6.2.2.1 In the first 60 s.....127
6.2.2.2 Within the second 60 s.....129
6.2.2.3 After the first 60 s.....131
6.2.3 Adsorption quantity profile along the desorber and adsorber.....132
6.2.3.1 In the first 60 s.....132
6.2.3.2 Within the second 60 s.....134
6.2.3.3 After the first 60 s.....135
6.3 Parametric analysis.....137
6.3.1 Effect of cycle time.....137
6.3.2 Effect of desiccant flow velocity.....139
6.3.3 Effect of desorber bed temperature.....140
6.3.4 Effects of adsorber bed temperature.....141
6.4 Summary.....143

Chapter 7: Conclusion and future work.....148
7.1 Conclusion.....148
7.1.1 Design novelty.....148
7.1.2 Contribution.....149
7.2 Future work.....151
References.....152
Appendices.....160
Appendix A: Computer code written in MATLAB script file for the separation circuit (cyclone).....160
Appendix B: Computer code written in MATLAB script file for the adsorption refrigeration circuit.....164

Nomenclature

Abbreviations

CFAR	Circulating Fluidised Adsorption Refrigeration
SC	Separation circuit,
RC	Refrigeration circuit
CC	Circulatory circuit

Nomenclature

A	Adsorptive property
A_R	The total surface area of the inside of the cyclone contributing to the frictional drag, (m^2)
B	Adsorptive property
c_o	Incoming solid loading/ loading ratio in cyclone inlet, (kg/kg)
c_{o_2}	Incoming solid loading/ loading ratio in cyclone inlet, (kg/m^3)
$C_{P_{sc}}$	Specific heat of adsorbent, ($J/(kg.K)$)
$C_{P_{ads}}$	Specific heat of adsorbate (adsorbed phase), ($J/(kg.K)$)
$c_{p,v}$	Specific heat of vapour at constant pressure, (kJ/kgK)
$c_{p,z}$	Specific heat of adsorbent at constant pressure, (kJ/kgK)
$c_{p,a}$	Specific heat of adsorbate at constant pressure, (kJ/kgK)
$C_{p,adst}$	Specific heat of adsorbent, (kJ/kgK)
$C_{p,r}$	Specific heat of adsorbate, (kJ/kgK)
$C_{p,bed}$	Specific heat of adsorbent bed, (kJ/kgK)
D	Adsorptive property
D_S	Adsorbent effective diffusion coefficient, (m^2/s)
g	acceleration due to gravity, (m^2/s)
h_{vz}	Heat transfer coefficient between vapour and adsorbent, (W/m^2K)
H_S	Heat of sorption, (J/kg)
ΔH	Heat of adsorption, (J/kg)
k	Characteristic parameter of adsorption pair
k_z, k_{sc}	Adsorbent thermal conductivity, ($W/(m.K)$)
k_v	Vapour thermal conductivity, ($W/(m.K)$)
L_E	Latent heat of vaporization of adsorbate, (J/kg)
M_{ads}	Molar mass of adsorbate, ($kg/mole$)
$\dot{M}_{sc}$	Mass flow rate of adsorbent, (kg/s)
m_{Sf}	Mass of solid fed into the cyclone, (kg)
m_g	Mass of circulating gas entering into the cyclone, (kg)
m_c	Mass of solid adsorbent collected, (kg)
m_{bed}	Mass of adsorbent bed/adsorber, (kg)
m_{ads}	Mass of adsorbent, (kg)
m	Slope of grade efficiency curve

n	Characteristic parameter of adsorption pair, number of size fraction
P_{ads}	Vapour pressure of adsorbate, (Pa)
P_s	Saturation pressure corresponding to saturation temperature T_s, (Pa)
P_{sat}	Saturation pressure corresponding to the adsorbent temperature, (Pa)
P, p	equilibrium pressure, (Pa)
q	Mass adsorption capacity, (kg/kg)
q_o	Maximum adsorption capacity, q_{max} (kg/kg)
q_{min}	Minimum adsorption capacity, (kg/kg)
$\dot{Q}$	Gas (particle laden) volumetric flow rate, (m^3/s)
$\dot{Q}_{ref}$	Amount of refrigeration produced, (Watts)
r	Cyclone radius, (m)
r_v	Radius of vortex finder, (m)
r_{cm}	Mean cyclone radius, (m)
r_{in}	Radial position of the center of cyclone/mean inlet radius, (m)
Re_P	Particle Reynolds number
R	Universal gas constant, ($J/(mole.K)$)
t	Time, (s)
T_C	Condenser temperature, (*K*)
T_z, T	Adsorbent temperature, (*K*)
T_v	Vapour temperature, (*K*)
u_{t50}	Terminal (radial) velocity of x_{50} in the inner vortex, (m/s)
u_x	Tangential velocity of the conveying gas at the inner core (vortex) radius (at r_v), (m/s)
u_c	Tangential velocity in the vicinity of (near) the cyclone wall (at r), (m/s)
$\bar{u}_{sc}$	Speed of adsorbent flow, (m/s)
u	Velocity component in x direction, (m/s)
u_v	Velocity component of vapour adsorbate in x direction,(m/s)
v_{in}	Mean gas inlet velocity, (m/s)
v_m	Mean (wall) axial velocity, (m/s)
v_x	Mean axial velocity in the vortex finder, (m/s)
W_i	ith mass fraction of the total mass of adsorbent feed
x_{50}	Cut point diameter (diameter of particle which has 50% probability of capture from the inner vortex), (m)
x	Axial coordinate, (m)
x	Adsorption capacity/amount of adsorbate, (kg/kg)
x_i	ith particle diameter, (m)
x_o	Maximum adsorption capacity/ maximum amount of adsorbate, (kg/kg)
z	Axial coordinate, (m)

Greek symbols

$\int$	Total friction coefficient including the reaction of the solid phase to the gas flow
$\int_{sw}$	Gas friction factor for smooth cyclone wall
$\int_{rw}$	Gas friction factor for rough cyclone wall
α	Entrance constriction coefficient
ϵ	Absolute roughness of the inside surface of the cyclone wall, (m)
ε	Adsorbent porosity
μ_g	Gas dynamic viscosity, (Pa s)
ρ_g	Gas density, (kg/m^3)
ρ_p, ρ_{sc}	Adsorbent particle density, (kg/m^3)
ρ_v	Vapour adsorbate density, kg/m^3
ρ_z	Adsorbent density, kg/m^3
η_t	Overall separation/Collection efficiency (%)
η_i	Collection efficiency of the average particle size of ith fraction (%)
τ_R	Gas residence time, (s)
ρ_{ads}	Concentration/density of adsorbate vapour, (kg/m^3)

List of Figures

Fig 1-1 United Nations 2022 World population growth projection [6]……..3
Fig 1-2 Research aims and objectives…….7
Fig 1-3 System configuration flowchart……...10
Fig 2-1 Classification of cooling technologies [10]……..14
Fig 2-2 (A) Representation of ejector structure (B) Schematic diagram of a basic ejector refrigeration system [10]……..16
Fig 2-3 Schematic diagram of a vapour compression refrigeration system…..17
Fig 2-4 Schematic diagram of a basic absorption refrigeration cycle [15]…...18
Fig 2-5 Schematic diagram of a single-effect absorption refrigeration system [16]…… ……...20
Fig 2-6 Schematic diagram of a run-around system with moving solid desiccant [18]……21
Fig 2-7 Schematic diagram of an organic Rankine cycle refrigeration system [10]……23
Fig 2-8 Schematic diagram of basic adsorption refrigeration system……...24
Fig 2-9 Thermodynamic cycle of the basic adsorption system…….25
Fig 3-1 Classification of adsorption refrigeration cycle based on development history [23]…….33
Fig 3-2 Schematic diagram of heat recovery two-bed adsorption refrigeration system [56, 57]…….41
Fig 3-3 (a) Principle of mass recovery (b) Diagram of heat and mass recovery cycle [23]……42
Fig 3-4 Schematic diagram of a thermal wave cycle [61]……44
Fig 3-5 Adsorption refrigeration system with convective thermal wave cycle [78]……...47
Fig 3-6 Adsorption–absorption cascading multi-effect refrigeration cycle: (1) adsorption cycle; (2) high pressure absorption cycle and (3) low pressure absorption cycle [61]……..49
Fig 3-7 Schematic diagram of the constant temperature adsorption cooling cycle [89]……...51
Fig 3-8 Clapeyron diagram for the constant temperature adsorption cooling cycle [89]……...52
Fig 3-9 Schematic diagram of the proposed CO-SAR system [90]……..52

Fig 3-10 Schematic representation of continuous hybrid adsorption refrigeration system [95]……...54
Fig 4-1 Schematic of proposed design arrangement 1……..67
Fig 4-2 Schematic of proposed design arrangement 2……..68
Fig 4-3 Schematic of proposed design arrangement 3……..70
Fig 4-4 Schematic representation of the CFAR system……72
Fig 4-5 Clapeyron diagram for the CFAR cycle……...75
Fig 4-6 The schematic of the desiccant circuit……76
Fig 4-7 The schematic of the refrigerant circuit……...77
Fig 4-8 A typical cyclone separator [103]……78
Fig 4-9 Cyclone classification based on gas inlet and dust discharge configuration [103]…….……..85
Fig 4-10 Cyclones installed for industrial applications [116]……..85
Fig 5-1 Schematic diagram of the proposed cyclone separator……90
Fig 5-2 A schematic representation of the Desorber/Adsorber……..101
Fig 5-3 Elemental discretized volume of the model……...104
Fig 5-4 Computer Model Flowchart……...109
Fig 6-1 Comparison between the experimental data, numerical results and the present study…….……115
Fig 6-2 Comparison between the experimental data, numerical results and the present tudy…….……..115
Fig 6-3 Effects of particle exit diameter on the cyclone pressure drop……..118
Fig 6-4 Effects of particle exit diameter on the cyclone cut size diameter….119
Fig 6-5 Grade efficiency performance of the cyclone……120
Fig 6-6 Temperature variation for desorption and adsorption……121
Fig 6-7 Pressure variation for desorption and adsorption……...122
Fig 6-8 Variation for adsorbate mass for desorption and adsorption……..122
Fig 6-9 Temperature profile in the first 60 s along (a) desorber during desorption process (b) adsorber during adsorption process……124
Fig 6-10 Temperature profile within the second 60 s along (a) desorber during desorption process (b) adsorber during adsorption process….125
Fig 6-11 Temperature profile after the first 60 s along (a) desorber during desorption process (b) adsorber during adsorption process……127
Fig 6-12 Pressure profile in the first 60 s along (a) desorber during

desorption process (b) adsorber during adsorption process……...129
Fig 6-13 Pressure profile within the second 60 s along (a) desorber during desorption process (b) adsorber during adsorption process……130
Fig 6-14 Pressure profile after the first 60 s along (a) desorber during desorption process (b) adsorber during adsorption process……132
Fig 6-15 Adsorption quantity profile in the first 60 s along (a) desorber during desorption process (b) adsorber during adsorption process….133
Fig 6-16 Adsorption quantity profile within the second 60 s along (a) desorber during desorption process (b) adsorber during adsorption process…….135
Fig 6-17 Adsorption quantity profile after the first 60 s along (a) desorber during desorption process (b) adsorber during adsorption process….137
Fig 6-18 System performance for various cycle times……...139
Fig 6-19 System performance for various desiccant flow velocities……..140
Fig 6-20 System performance for various desorber bed temperatures……...141
Fig 6-21 System performance for various adsorber bed temperatures……...142

List of Tables

Table 2-1 Comparison of different cooling technologies…….28

Table 3-1 Summary of reviewed works on development history of adsorption cooling technology……..…58

Table 5-1 Cyclone geometry and dimensions……..…….90

Table 5-2 Simulation Data for cyclone…….91

Table 5-3 Particle feed size distribution……...95

Table 5-4 System and operating parameters for the adsorption refrigeration unit simulation……...……..100

Table 6-1 Cyclone Simulation results…….112

Chapter 1: Introduction

1.1 Background

The production of cold (refrigeration) has multifarious applications in a considerable number of fields of human life. The storage of food products and medicines, especially immunisation vaccines, are important applications of cold. Many agricultural products, such as, fruits, vegetables, meat, milk, fish etc., can be maintained in fresh conditions for significantly longer periods of time if they can be stored and maintained at low temperatures. In addition, vaccines require refrigeration during transportation to remain effective. Food preservation is not only a health issue but also an economic one because a substantial proportion of the harvest including dairy products is lost annually in the rural areas of the developing countries, where the fresh farm products are produced, due to lack of refrigeration systems. Consequently, there is always an unexplainable gap between the harvest and the off-harvest seasons. Therefore, the vital role played by refrigeration in efforts to improve the quality of rural economy and health care can never be overemphasized.

In spite of these indisputable roles played by refrigeration in human life, the prevailing trends in the field have a deep engineering interest and automation with the aim of addressing two major problems [1].

i. The increase in global consumption of limited primary energy and
ii. The effect of refrigerants on the environment such as global warming and ozone depletion.

1.1.1 The increase in global consumption of limited primary energy (Energy crisis in Developing Countries)

The International Institute of Refrigeration in Paris has estimated that approximately 15% of all the electricity produced in the whole world is employed for refrigeration and air-conditioning processes of various kinds, and the energy consumption for air-conditioning systems has been estimated to be 45% of the whole households and commercial buildings [2].

Energy problem has always been focused on since the global energy crisis broke out in the 1970s [3]**.** In spite of the 1990s wave of globalization that prompted developing countries to liberalize and privatize their energy industry to finance the required investment for generating energy supplies for development, it is now clear that only a handful of developing countries were able to attract capital and grow rapidly. Also, in the initial years of the twenty-first century, energy black-outs due to shortages of energy supplies for fuel development persisted. While the total number of people without electricity has fallen by less than 500 million since 1990, over 1.6 billion people in the developing world (accounting for over 40 per cent of the population in Africa and South Asia in 2004) still have no access to electricity. In 2004, over 2 billion people in developing countries continued to use traditional biomass for cooking heating [4].

As depicted in Fig. 1.1, in spite of the slower rates of population growth, the current global population of about 8 billion is expected to reach 8.5 billion in 2030, 9.7 billion in 2050 and 10.4 billion in 2100 according to the latest projections by the United Nations population division [5]. With roughly 81

million people being added to the world's population every year, it is not unexpected that this upward trend in the world population size would continue.

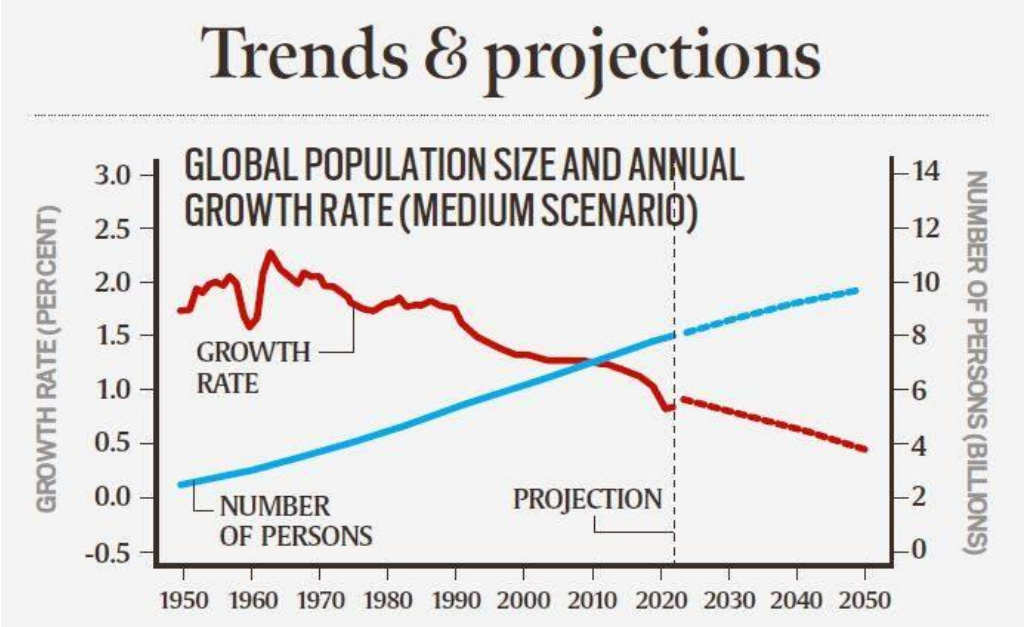


Fig 1-1 United Nations 2022 World population growth projection [6]

The share of population living in developing regions will increase from 77% to 85% in 2030 and to 90% in 2050. The number of people lacking access to commercial energy will continue to grow in the developing world [4].

The majority of the citizens of the developing countries dwell in rural areas where there is difficult terrain, lack of transportation infrastructure and no easy access to refined fossil fuel and electricity grids. Most of these communities are located at long distance from the nearest common connection point of a utility grid system. Some of them have very low population density, characterized by low level of education, and low load density usually identified by very short periods of peak load. These rural dwellers rely on the usage of standalone diesel generators for meeting their electricity needs. However, several constraints like high cost of fuel, maintenance cost and irregular

delivery of fuel due to bad or flooded roads (especially during the rainy season) affect the reliability of operation of the diesel generators.

1.1.2 Ecological consideration for refrigerant choice

Conventional vapour compression refrigeration machines consume a lot of electrical energy, leading to depletion of precious fossil fuel resources and production of greenhouse gases. Refrigerants, used in these systems, also contribute to greenhouse gas emission. Some of the refrigerants, like chloro-fluoro-carbons (CFCs) and hydro-chloro-fluoro-carbons (HCFCs), also cause depletion of stratospheric ozone layer [2].

Economizing energy, environmental protection and sustainable development are all the main themes of the contemporary world in the 21st century. In order to protect the ozonosphere and the ecological environment, the treaty system of ozone layer protection made of: Vienna Convention for Protection of the Ozone Layer (1985), Montreal Protocol on Substances Depleting the Ozone Layer (1987) and five amendments of Montreal Protocol has provided the schedule to reduce the use of CFCs. However, the situation deterioration still continues. According to the newly observation of NASA, the holes in the ozonosphere over the North and South Poles has surprisingly enlarged to about 28,300,000 km^2 since they were first observed to be 24,000,000 km^2 in 1994. This unprecedented growth speed of the holes in the ozonosphere indicates that depleting of ozone has not been effectively controlled. The utilization of CFCs is being restricted more severely [3].

Therefore, the consequence of many international protocols (Montreal Protocol, Kyoto Protocol, and Sustainable Development Goals - SDGs) have

made the improvement of the primary energy utilization ratio and environmental consideration exigent tasks for Researchers in the choice and design of refrigeration systems. Equally, this unabated electricity crisis and the need to reduce the greenhouse gases should be the major drivers for pursuing the renewable energy options in meeting the refrigeration needs of the rural communities of developing nations [7].

1.2 Need for alternative refrigeration system in rural areas of developing countries

A large proportion of the people in developing countries live in remote locations where grid electricity coverage is sparse or unavailable. Cooling applications such as food and medicine preservation in such areas, therefore, requires alternative refrigeration system.

Besides the merit of energy saving accredited to alternative energy sources, one of the essential targets of the United Nation Sustainable Development Goals (SDGs) is to completely abolish the non-renewable energy sources by 2030 and consequently achieving a reduction of CO_2 emissions.

In considering the world average emission factor, Hadj et al. [8] showed that using a renewable energy powered-refrigeration system instead of an equivalent conventional vapour-compression freezer could save 2.1 kWh of energy per day which corresponds to 1365g of CO_2 emission prevented from being released into the atmosphere.

Hence, it is becoming more imperative to look for efficient and sustainable alternative energy technology in meeting the growing refrigeration needs in the rural areas of developing countries.

1.3 Research aims and objectives

1.3.1 Research aims

This research overall imperative is to develop a novel energy efficient adsorption refrigeration system for application in rural areas of developing countries. As depicted in Fig 1-2, the novel arrangement of the solid desiccant cooling system is aimed to address the issues of intermittency, adsorbent deterioration, refrigerant leakage, poor heat transfer, and mechanical complexities in the existing adsorption systems. These have been identified as a major research gap through an extensive review of literature covering the development trends in adsorption refrigeration technology as presented in this work.

1.3.2 Research objectives

The following are the main objectives of this research:

i. Conduct a wide and extensive literature review to understand the advantages, limitations and current direction of research on adsorption refrigeration system.
ii. Investigate a novel design configuration of solid desiccant cooling/heating system which would be able to address those identified limitations of the existing adsorption systems.
iii. Define the operating parameters of the novel candidate system including mechanical arrangement, types of materials and operation mode.
iv. Mathematical formulation and computer modelling of key performance indices of the system.

v. Conduct a parametric analysis using the developed computer model to evaluate the effects of various design and operational parameters on the CFAR system thermal performance with the purpose of predicting how it would change during its practical use.

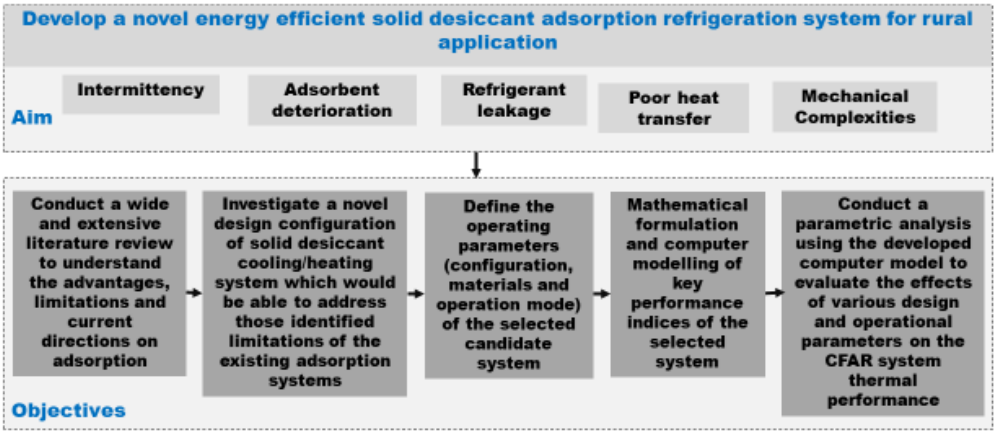


Fig 1-2 Research aims and objectives

1.4 Research methodology

The stepwise research methodology carried out in order to achieve the aims and objectives of this work as shown in Fig 1-3 is presented as follows:

1.4.1 Review of Literature

An overview of adsorption technology detailing all aspects of existing passive cooling/heating technology focusing on adsorption systems is provided. In addition, specific review of the development trend in adsorption technology in order to evaluate the working principles, configuration, advantages and limitations of each solid desiccant cooling/heating system is presented.

This literature review provides a commending grasp of the field of study which is consequently instrumental in identifying a research gap (the issues of: intermittency, adsorbent deterioration, refrigerant leakage, poor heat transfer,

and mechanical complexities in the existing adsorption systems) and some innovations resulting in this current research. Therefore, it is apparent that to advance adsorption technology, novel solutions are sought to overcome the above limitations. In this work, the following are the main ideas behind designing a new system: overcoming cooling intermittency by circulating/moving the solid adsorbent, simplifying mechanical complexities by reducing the number of switching valves, joints etc., improving the heat transfer mechanism by incorporating a fluidised adsorbent bed, improve thermal performance through the use of localised heat source and heat sink.

Additionally, a review of the mathematical models which are generally used to simulate adsorption cooling/heating systems is presented.

Lastly, the review of gas-solid cyclone separator (a mechanism for circulating the solid desiccant) is also provided.

1.4.2 Design, investigation and evaluation of the various possible alternative configurations of solid desiccant cooling/heating systems to evaluate the credits and limitations of each

A detailed design, study, investigation and evaluation of the various possible alternative configurations of adsorption cooling/heating systems that will be able to fill those identified research gaps are presented in succession. The possible alternative configurations discovered in succession are as follow:

i. Design arrangement 1: Adsorption-partial resorption out-of-phase configuration.
ii. Design arrangement 2: The rotary desiccant wheel configuration.
iii. Design arrangement 3: Desiccant-circulator-aided fluidised adsorbent bed.

iv. Design arrangement 4: Circulating Fluidised Adsorption Refrigeration (CFAR) System.

1.4.3 Design and definition of the broad characteristics of a novel system

Consequent to the detailed evaluation of the various possible alternative configurations of solid desiccant cooling/heating systems, the design arrangement 4 (circulating fluidised adsorption refrigeration (CFAR) system) appears as the most preferred in filling those identified research gaps. Therefore, its broad characteristics in terms of configuration, materials, mode of operation and performance are presented.

1.4.4 Computer modelling of the novel design to investigate its performance parameters

This objective was further broken down into two: (I) The theoretical analysis/model formulation for the separation circuit (cyclone) and the mathematical formulations for the modelling of the heat and mass transfer of the adsorption cooling/heating circuit. (II) The performance of the separation circuit (cyclone) was investigated by writing a computer code using MATLAB software to determine the speed of adsorbent flow. Subsequently, from the discretised governing equations of energy and mass conservation combined with the associated boundary conditions and the adsorbent flow speed already determined, a computer code using MATLAB software was developed to determine the system performance parameters.

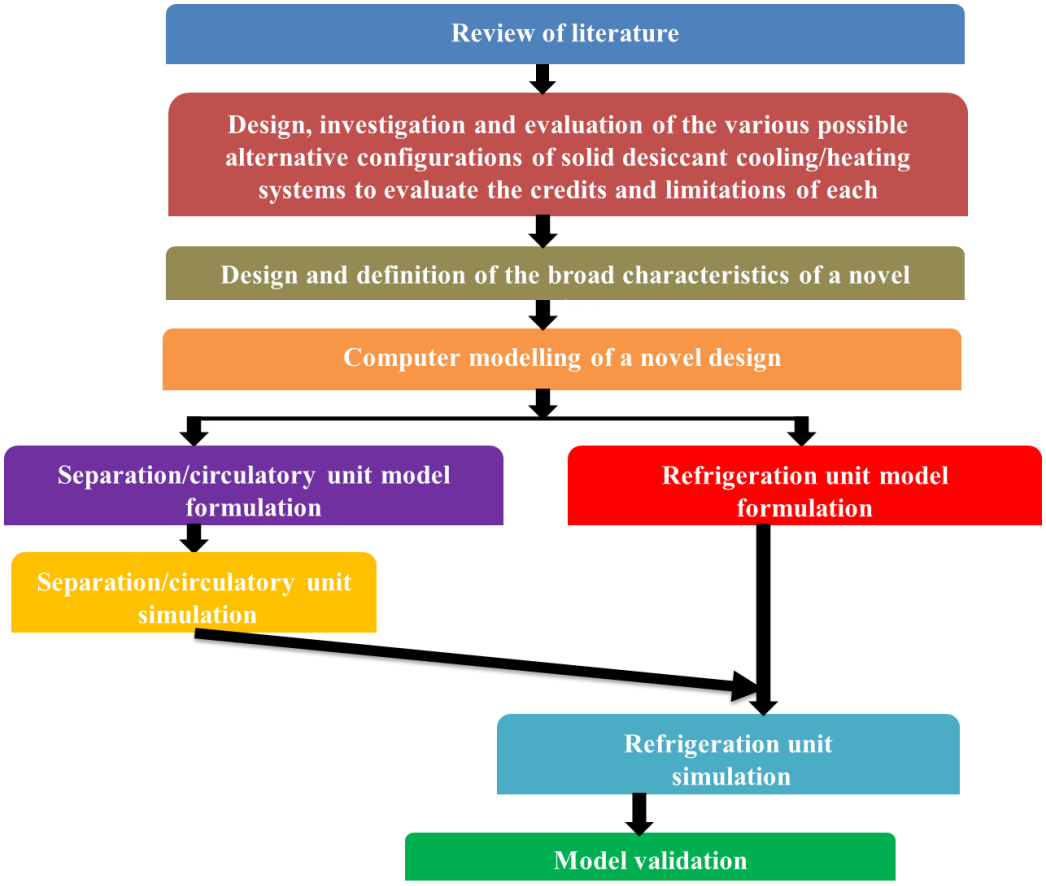


Fig 1-3 System configuration flowchart

1.5 Problem Statements

1.5.1 Adsorption deterioration

Just as absorbents (liquid desiccants) are so germane to absorption refrigeration systems, so are adsorbents (solid desiccants) to adsorption refrigeration systems. Hence, adsorption deterioration of the adsorbent impacts the widespread utilization of adsorption refrigeration. Besides the problems of poor heat and mass transfer and others as identified above, the adsorption deterioration of the adsorbent is also vital to the development and applications of the adsorption refrigeration technology [3, 9].

Solid adsorbents are used in both adsorption refrigeration and open cycle desiccant dehumidification applications. However, unlike in a rotary solid

desiccant dehumidifier where the adsorbent can be repeatedly used for many years, in a vacuum condition as we have in adsorption refrigeration system, the adsorption capacity of the adsorbent severely diminishes after a short period of utilization due to the: more frequent switching, larger pressure difference and faster speed between adsorption and desorption. The intense energy exchange on adsorbents micropores changes the surface microstructure which eventually impacts the adsorption capacity adversely.

To this end, this research is aimed at solving these crucial bottlenecks that make the system not yet competitive with the convectional vapour compression system.

1.6 Thesis Layout

This thesis is structured into 7 chapters:

Chapter 1 covers the general background of the indisputable roles played by refrigeration in human life. Also covered in this chapter is the global needs (with focus on rural areas of developing countries) for alternative refrigeration systems. Chapter one also includes the research aims and objectives, the research methodology, problem statements and the novelty of the research.

Chapter 2 presents an overview of refrigeration technologies covering the general classification of various types of cooling technologies focusing the theory, working principle and the performance of each. Furthermore, an extensive review (including: adsorption refrigeration cycle, choice of adsorbent, adsorbent general requirements, selection of working pairs, advantages etc.) is presented on adsorption refrigeration technology being the focal domain of this study.

Chapter 3 presents a comprehensive plethora of the development trend in adsorption cooling technology ranging through its allied technologies and cycles which are basic/intermittent and advanced/continuous cycles. Also presented is the analysis of the reviewed works on adsorption cooling technology.

Chapter 4 presents the design, investigation and evaluation of the various possible alternative configurations of adsorption solid desiccant cooling/heating systems to ascertain which configuration has the best potential to fill the identified research gaps and thus meet the aims of this research study. Also well covered in chapter 4 are: the CFAR system description, components, its operational principles and its design considerations.

Chapter 5 presents the detailed design processes of the CFAR system configuration which include: the mathematical modelling of the CFAR system including: the model formulation for the separation circuit, the numerical modelling process for the adsorption refrigeration circuit. The CFAR system performance indices also presented.

Chapter 6 analyses and discusses the results of the numerical simulation carried out on both the circulatory/separation unit (cyclone) and the adsorption refrigeration unit. The results of the parametric analyses carried out on both the cyclone and the adsorption refrigeration units as well as the model validation are also presented.

Chapter 7 concludes the research findings and highlights the novelties and the main contributions of this CFAR system. In addition, recommendations and suggestions for any future works are as well presented.

Chapter 2: Overview of Refrigeration/cooling Technologies

2.1 Classification of cooling technologies

Cooling technologies can be classified in many ways based on temperature, refrigerant type, thermodynamic cycle, driving energy sources, etc. An example of classification of cooling technologies is shown in Fig 2-1 which classifies cooling technologies as electricity-driven cooling systems and thermally-driven cooling systems. The electricity-driven technologies include the conventional vapor compression refrigeration (VCR) driven by grid electricity or by Photovoltaic (PV) modules and cooling by thermoelectric cooler (TEC) modules. The thermally-driven cooling technologies which can be operated by low grade energy sources such as waste heat, solar, etc. are divided into two categories: the thermal-sorption cooling technologies and the thermal-mechanical cooling technologies. Thermal-sorption cooling technologies include closed-type cycles (absorption and adsorption cycles) and open-type cycles (solid and liquid desiccant systems). The thermal-mechanical cooling technologies primarily include the ejector systems, the organic Rankine cycle (ORC) systems and the newly introduced thermal mechanical compressor (TMC-VRC) technologies [10].

In this work, the focus is on cooling technologies that can be operated using low grade energy sources such as solar, waste heat, etc.

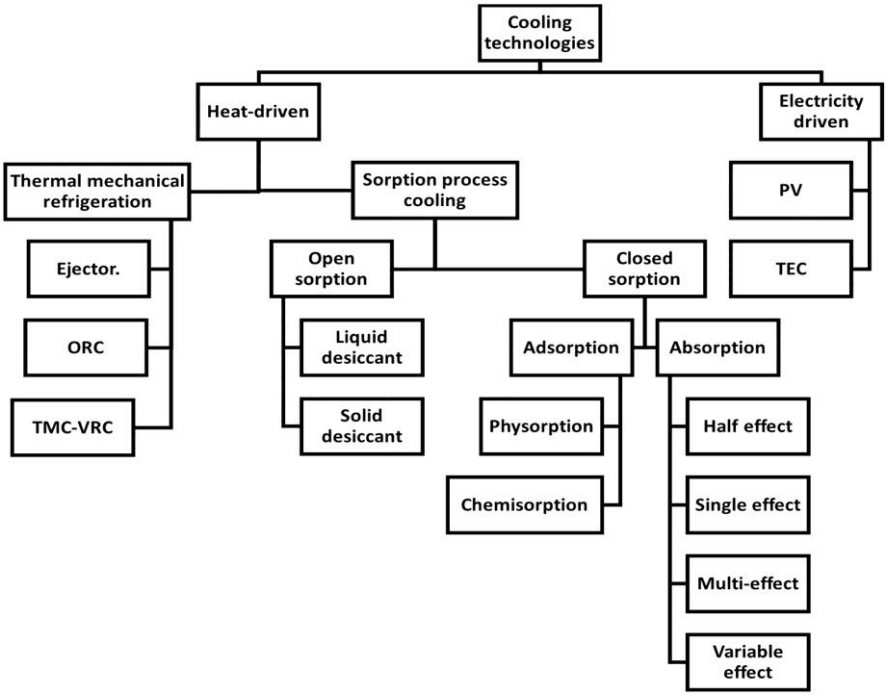


Fig 2-1 Classification of cooling technologies [10]

2.2 Types of cooling technology

There are many types of cooling systems used for various applications in refrigeration processes and space air conditioning both in commercial and domestic buildings.

2.2.1 Ejector refrigeration technology

The structure of a typical ejector is represented in Fig 2-2a while Fig 2-2b shows the schematic representation of a basic ejector refrigeration system showing its various components.

Ejector refrigeration is a thermally driven technology that has been used for cooling applications for many years. In their present state of development, they have a much lower COP than vapour compression systems but offer advantages of simplicity and no moving parts [11].

The ejector (a thermally-driven compressor) generally consists of: three chambers (suction, mixing and diffuser chambers), nozzle and three ports (primary flow entrance, secondary flow entrance, and mixed flow outlet). The main flow enters the nozzle with high pressure and temperature. Through the converging part of the nozzle, its velocity increases up to a sonic value at the nozzle throat with pressure being decreased while a further pressure decrease and velocity increase up to supersonic velocity occurs at the divergent part of the nozzle. Meanwhile, the primary flow forms a partial vacuum at the nozzle outlet plane in order to suck the secondary flow as it enters the suction chamber with increasing velocity and decreasing pressure [10].

Consequently, both flows start the mixing in the suction chamber and become completely mixed in the mixing chamber (MC) inside which the back-pressure (BP) resistance causes a shock resulting in sharp pressure increase and a corresponding decreased velocity. A further pressure increase occurs in the diffuser. The mixed flow enters the condenser with high pressure and leaves in liquid phase. A portion of the liquid is pumped to the high pressure generator to be evaporated and re-directed to the main inlet of the ejector. The other portion of the liquid expands through the expansion valve (EV) and flows to the evaporator to perform the cooling effect and re-directs to the secondary ejector inlet to begin another cycle [10].

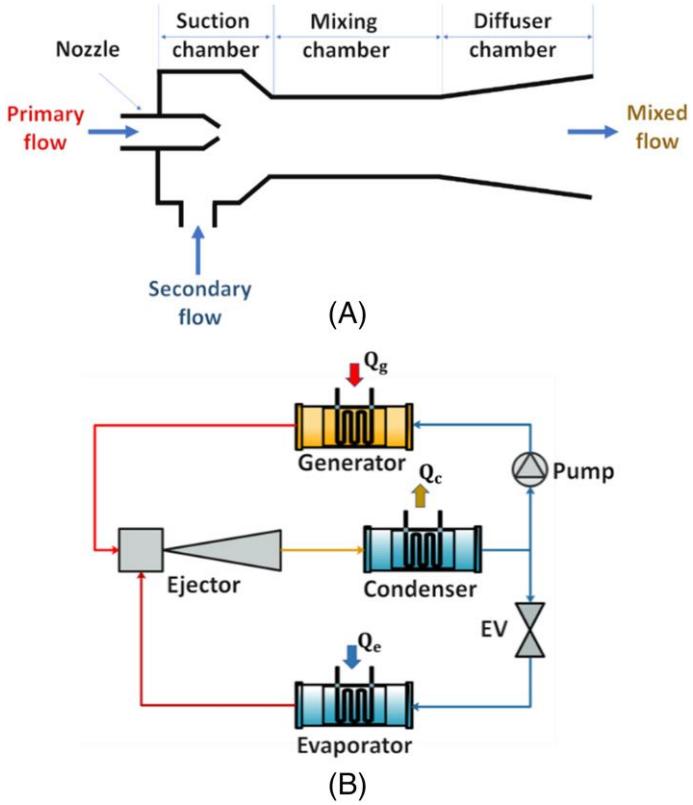


Fig 2-2 (A) Representation of ejector structure (B) Schematic diagram of a basic ejector refrigeration system [10]

In spite of the huge achievement recorded in developing this technology with cooling capacities as high as 60,000 kW, there are still issues like low COP, unavailability of off-the-shelf systems which could help to facilitate selection for particular applications and lastly, lack of access to performance data from commercial applications [11]. All these, have negatively impacted the wide application of this technology when compared to the conventional vapour compression cooling technology and other thermally driven technologies.

2.2.2 Vapour-compression refrigeration technology

The standard vapour compression refrigeration (VCR) technology (Fig 2-3) can be driven by grid electricity or by Photovoltaic (PV) modules. The operation of VCR by electricity strongly increases the consumption of

electricity and thus makes it not useful for people in the rural areas of developing countries. Besides, it uses non-natural working fluids like CFCs, HCFCs and HFCs which are directly responsible for ozone depletion and/or global warming.

With the exception of the energy-supply sub-system, PV-powered refrigeration is similar in most respects to any other vapour compression refrigeration system. The energy supply in the system is provided by an array of solar cells which convert the incident solar radiation to electricity. The latter is used to drive the compressor and the excess charges a battery system for use at periods of low or no insolation [12]. Although PV refrigerators are more commercially successful among the thermal refrigeration technologies, they have the disadvantages of high cost and low possibility of manufacture in many developing countries [13].

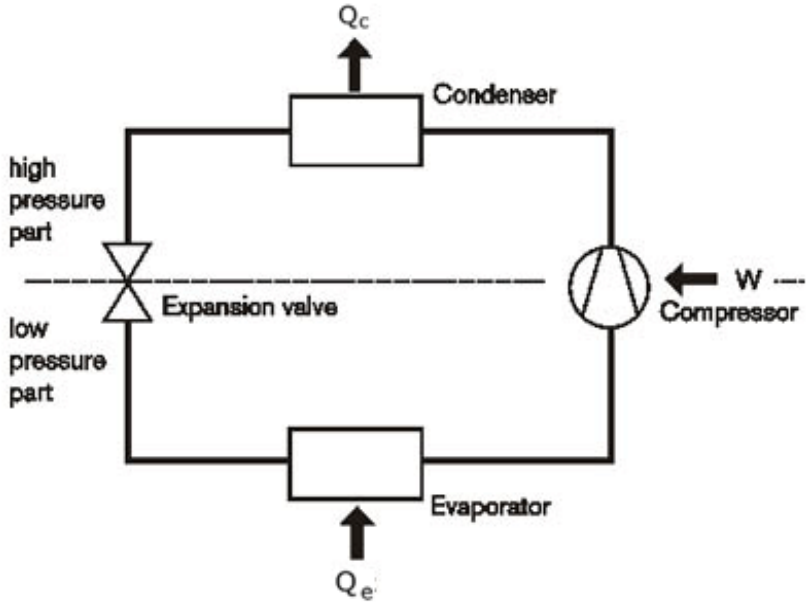


Fig 2-3 Schematic diagram of a vapour compression refrigeration system

2.2.3 Absorption refrigeration technology

Absorption is the process in which a substance assimilates from one state into a different state. These two states create a strong attraction to make a strong solution or mixture [14]. Absorption machines use a liquid–gas working pair. The absorbent exhibits a strong potential to absorb the vapour phase of the refrigerant [2]. Fig 2-4 shows the schematic diagram of a basic close absorption refrigeration thermodynamic (pressure-temperature) cycle which comprises absorber, generator, condenser and evaporator all connected in a loop.

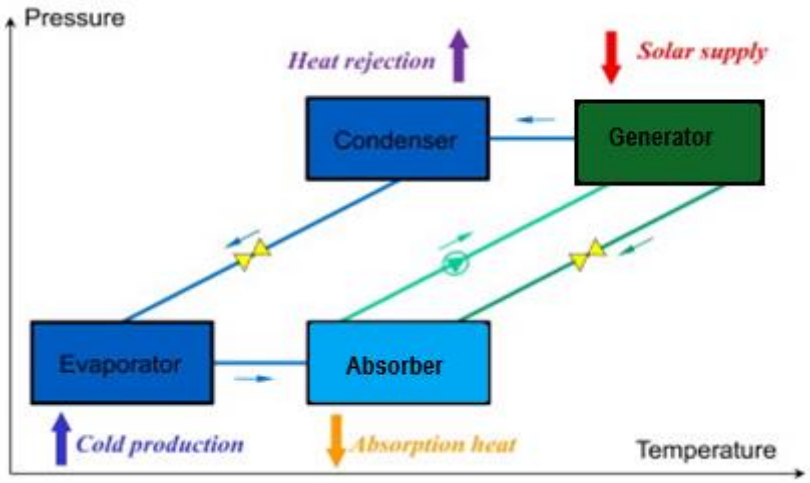


Fig 2-4 Schematic diagram of a basic absorption refrigeration cycle [15].
Note that desorber was replaced by generator in this work.

On the basis of the operating system temperature range, number of generators and solution heat exchangers used, absorption systems may be classified as single effect, double effect, and multiple effect absorption refrigeration systems. Fig 2-5 shows a single-effect absorption refrigeration system in which the vapor from the evaporator enters the absorber, where it gets absorbed by the weak solution while heat of absorption is also extracted or removed. The strong solution formed in the absorber enters the solution heat exchanger at

generator pressure. The solution heat exchanger adds heat to the solution before entering the generator. In the generator, boiling takes place leading to the separation of the weak solution from absorbed vapor. The weak solution returns to the absorber while the vapor refrigerant flows into the condenser [16]. The condenser condenses the refrigerant by rejecting the heat and then the cooled liquid refrigerant is expanded by the evaporator, and the cycle is completed [14].

The refrigerant side of the absorption system essentially works under the same principle as the vapour compression system. However, the mechanical compressor used in the vapour compression cycle is replaced by the thermal compressor in the absorption system. The thermal compressor consists of the absorber, the generator, the solution pump, and the expansion valve. The attractive feature of the absorption system is that any types of heat source, including solar heat and waste heat, can be utilized [14].

The working fluid pairs to be used in absorption refrigeration units must be selected on the bases of their suitability under the conditions of their thermodynamic properties, chemical and thermal stability, and toxicity. Examples of pairs and applications that have been extensively developed are: ammonia/water used in air conditioning and refrigeration in which ammonia is a refrigerant and water is a solvent; ammonia/hydrogen used in domestic refrigerators; aqua-Lithium bromide solution used in domestic and commercial air conditioners [17].

This technology, among all other heat driven sorption cooling technologies, has successfully established itself as a commercially available technology. However, it is found to be more suitable for larger applications because of the

disadvantages of high cost and low possibility of manufacture in many developing countries. More efficient double-effect and triple-effect absorption systems require a huge enhancement, which makes the systems unnecessarily complex and costly [2].

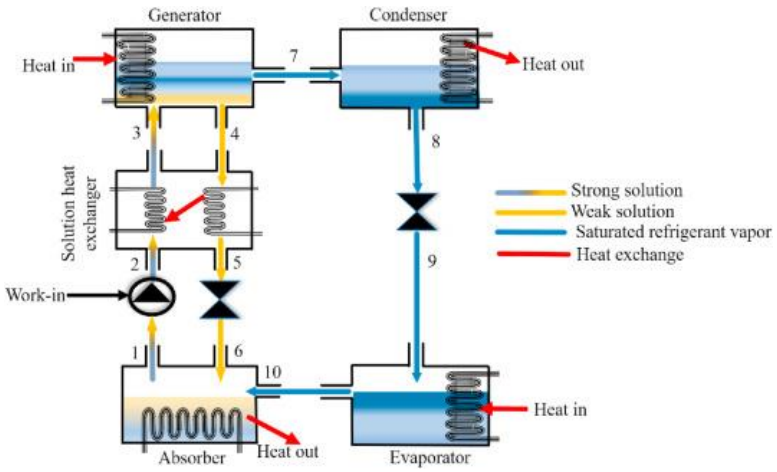


Fig 2-5 Schematic diagram of a single-effect absorption refrigeration system [16]

2.2.4 Run-around Solid Desiccant for Dehumidification

[18] developed a model to investigate into the heat and moisture transfer between supply and exhaust air streams for a run-around system shown in Fig 2-6, in which the coupling materials are coated solid desiccant particles (silica gel) that are transported between two exchangers. In the energy recovery closed loop system, the solid desiccant particles which exit the exhaust air exchanger are conveyed to the inlet of the supply air exchanger. Similarly, the outlet particles that flow from the supply exchanger are conveyed to the inlet of the exhaust air exchanger. He verified the accuracy of his model by comparing the simulations results with well-known theoretical solutions for a single cross flow heat exchanger and a liquid coupled run-around system. A difference less than 1% over a range of operating conditions was found

The model was also verified by modifying the boundary conditions to represent a counter flow energy wheel and the calculated sensible, latent, and total effectiveness values showed good correlations with data in the literature. Comparison between the solid desiccant and salt solution run-around system effectiveness also revealed a good agreement.

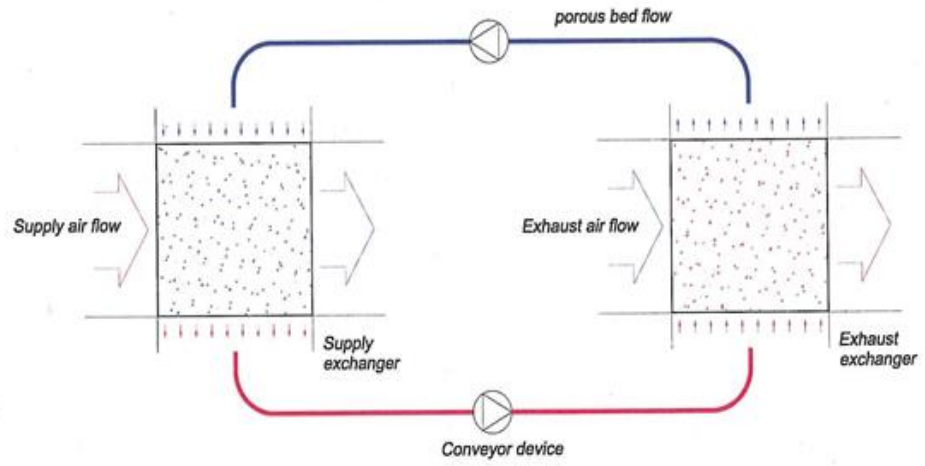


Fig 2-6 Schematic diagram of a run-around system with moving solid desiccant [18]

2.2.5 Organic Rankine Cycle refrigeration technology

Organic Rankine cycle consists of two different loops which are the power loop (consisting of a boiler, expander, condenser, and pump) and the cooling loop (consisting of an evaporator, compressor, condenser, and expansion valve. There are two possible configurations for the components of this technology. The first is to use both the power and the cooling loops separately while the expander of the power loop and the compressor of the cooling loop are coupled mechanically as shown in Fig 2-7. Another possibility is to integrate the power loop into the cooling loop resulting in an expander-compressor hybrid with one condenser working for both loops.

Basically, the operation of organic Rankine cycle is explained as follows: the high-pressure organic fluid inside the boiler absorbs the heat from a low-temperature heat source and evaporates. The resulting vapour from the evaporation process then enters the expander and produces mechanical power which in return is used to power the compressor of the cooling loop. The low-pressure vapor from the expander enters the condenser of the power loop and its being condensed into a saturated liquid by rejecting heat to a heat sink. The pressure of the liquid is being increased by the aid of a pump and then enters into a higher-pressure boiler (which is being heated by a low-temperature heat source) to begin another power cycle. The operation of the cooling loop of this technology is the same as that of the conventional vapour compression refrigeration cycle.

This technology operates with an organic working fluid that has a low boiling temperature. Usually, it operates in the temperature range of (60 °C -350 °C). The power rating of the organic Rankine cycle ranges from micro-scale (1-5 kW) to large scale (50-300 MW). Compared to steam Rankine cycle, this technology has a smaller evaporator that could use versatile heat sources (such as solar, geothermal, and waste heat). Also, the expander has a simpler design. However, the expander efficiency is still low relative to the efficiency of today's steam turbines [10].

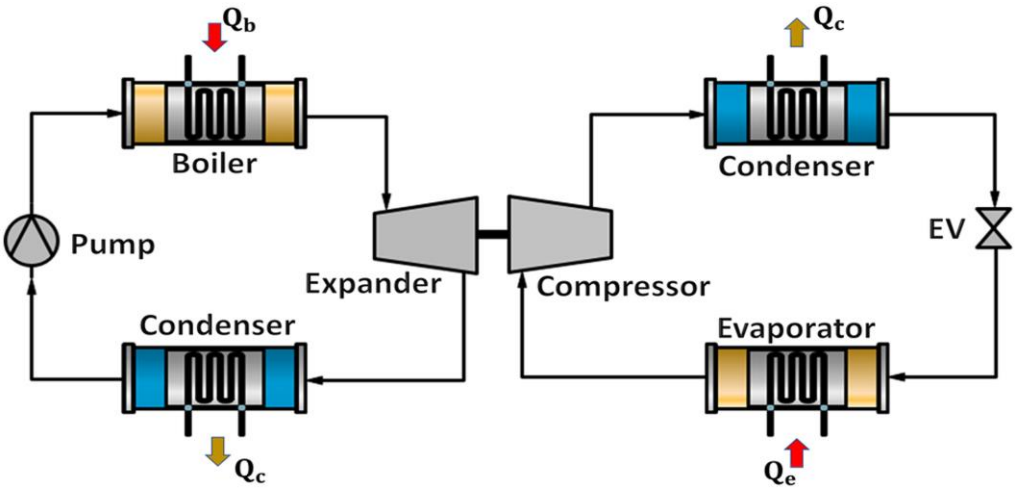


Fig 2-7 Schematic diagram of an organic Rankine cycle refrigeration system [10]

2.2.6 Adsorption refrigeration technology

2.2.6.1 Principle of Adsorption Refrigeration

Adsorption is the general phenomenon resulting from the interaction between a solid (adsorbent) and a fluid (adsorbate). An adsorption refrigeration system utilizes the phenomenon of physical adsorption between the refrigerant and a solid adsorbent. Hence, most of the adsorption refrigeration systems deploy physical adsorption [19]. Adsorption refrigeration does not use any mechanical energy, but only heat energy (solar, waste etc.). It is, in principle, similar to vapour compression system except that a thermal compressor operating as heat input instead of the conventional compressor is employed. Thus, eliminating the need of electrical energy to perform the compression process. The operation of adsorption refrigeration system is dependent on adsorption/desorption characteristics of the typical adsorbent/adsorbate pair. Generally, the mathematical models which are used to simulate adsorption cooling systems can be grouped into lumped parameter model, heat and mass transfer model, and thermodynamic model.

2.2.6.2 Basic Adsorption Refrigeration Cycle

The main components of the basic adsorption system as shown in Fig 2-8 are:

(1) Thermal compressor for adsorption and desorption of refrigerant.

(2) Condenser

(3) Expansion valve

(4) Evaporator

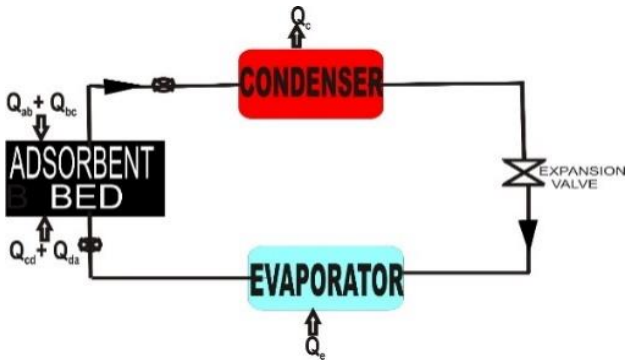


Fig 2-8 Schematic diagram of basic adsorption refrigeration system

The adsorbent is packed in the adsorbent bed in a way that allows absorption of heat energy at a particular temperature in compliance with its condensing pressure. A basic adsorption cycle is a succession of four thermodynamic processes explained with Fig 2-9 as shown below:

(i) Isosteric heating and Pressurization (a-b)

During this process, the bed absorbs heat thereby increasing the adsorbent's temperature from T_a to T_b which initiates a pressure increase from P_e to P_c but the mass of the adsorbed refrigerant remains constant at the maximum value X_{max}. This process is equivalent to compression in vapour compression cycle.

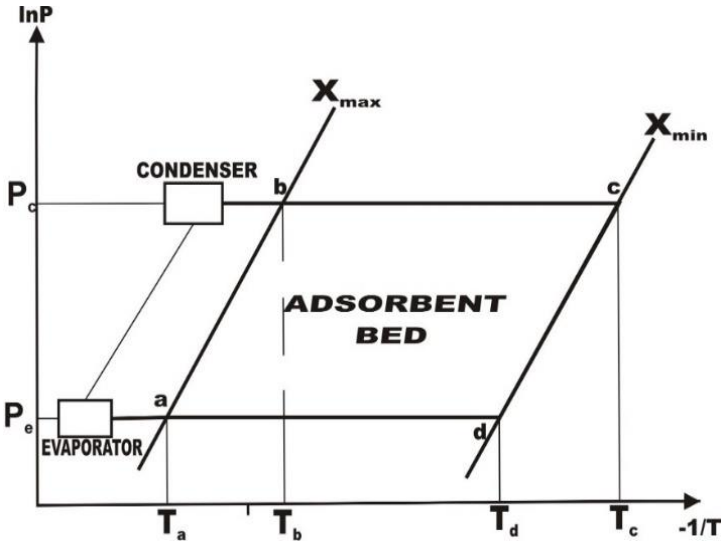


Fig 2-9 Thermodynamic cycle of the basic adsorption system

(ii) Heating, Isobaric desorption and condensation (b-c)

The raising of the bed pressure to P_c opens the valve between it and the condenser and thus connects them together and the progressive heating of the bed (from T_b to T_c) initiates desorption of refrigerant vapour which is liquefied in the condenser. This is equivalent to condensation in compression cycles. This process ends as the adsorbent reaches its maximum regeneration temperature T_c and the adsorbate content reduces to the minimum value X_{min}.

(iii) Isosteric cooling and depressurization (c-d)

During this process, the bed cools down from T_c to T_d which initiates a pressure decrease from P_c to P_e and the valve connecting the condenser to the evaporator opens allowing the liquid refrigerant mass at constant at the minimum value X_{min} to flow into the evaporator. This process is equivalent to expansion in vapour compression cycle.

(iv) Cooling, Isobaric adsorption and evaporation (d-a)

During this process, the liquid refrigerant in the evaporator begins to evaporate by gaining heat energy from the load in the evaporator and gets adsorbed by the adsorbent in the bed thereby producing cooling. This is equivalent to evaporation in compression cycles.

2.2.6.3 Adsorbents general requirements

The choice of adsorbent for a particular application often involves a considerable compromise on different criteria but the most important general factors are [19-21]:

i. High abrasion resistance i.e. non deterioration with usage;
ii. High thermal stability;
iii. Small pore diameters, which result in higher exposed surface area per unit weight, and hence high surface capacity for adsorption/desorption;
iv. A distinct pore structure which enables fast transport of the gaseous vapors;
v. Low specific heat;
vi. Good thermal conductivity, to shorten cycle time;
vii. Non-toxic and non-corrosive;
viii. Chemically and physically compatible with the chosen refrigerant; and
ix. Must be cost effective and widely available.

2.2.6.4 Choice of Adsorbate

For an effective performance, the adsorbate must meet the following requirements: [19, 21]

i. Small molecular size for better adsorption;
ii. High latent heat per unit volume;

iii. High thermal conductivity;

iv. Good thermal stability with the adsorbent in the operating temperature range;

v. Low viscosity and low specific heat;

vi. Low toxicity and must not be inflammable and corrosive;

vii. Low saturation pressures (slightly above atmospheric pressure) at normal operating temperature;

viii. Must be environment friendly.

2.2.6.5 General selection of working pair

Generally, there are several possible adsorbent–adsorbate working pairs that can be used in adsorption refrigeration systems. The selection should involve a cautious effort since the optimal performance of a typical system is highly dependent on the chosen working pair. The proper selection depends on the temperature of the heat source, the desired characteristics of the refrigeration system, the properties of the working pair constituents, the affinity between them, cost, availability and environmental impact.

The most commonly used working pairs are: silica-gel/water; activated-carbon/methanol; activated-carbon/ammonia; zeolite/water; activated-carbon granular and fibre adsorbent, metal chloride/ammonia; and composite adsorbent/ammonia [14]. The selection and choice of adsorption pair for this present work, which is based on the design considerations of the particular system in this current work, is presented in details in chapter four of this work.

2.2.6.6 Important advantages of the adsorption refrigeration technology

Adsorption refrigeration technology is briefly compared with other cooling technologies in Table 2.1.

Table 2-1 Comparison of different cooling technologies

Cooling Technology	Heat source temperature °C	COP	Main benefits	Main limitations
Electricity driven cooling (Photovoltaic, thermoelectric cooler)	-	3.0-3.45	Flexible and reliable	High cost
Absorption	85-220	0.7-1.25	High cooling capacities	Limited operating temperature
Desiccant	60-95	0.3-0.51	Low operating temperatures	Complex control, crystallization risk
Organic Rankine cycle (ORC)	100-300	0.1-0.75	A mature technology	Not economical at temperatures lower than 100ºC
Ejector	60-160	0.1-0.62	Simple, high capacity	Not flexible
Thermo-mechanical refrigeration (TMR)	60-100	-	Simple, flexible	Low cooling capacities
Adsorption	60-165	0.3-0.7	Less corrosion at high temperatures	Expensive and bulky systems

Source: [10]

This technology has been confined to lab research worldwide despite the many advantages it has, including the following [22] **:**

i. It is environmentally friendly since it does not contain any hazardous material for environment such as CFCs.
ii. It can operate with thermal driving energy sources such as waste heat, solar, and geothermal energies, etc. That is, it can work with low temperature driving energy sources.
iii. It requires small quantity of electrical energy to drive auxiliary equipment.

iv. It does not suffer from crystallisation and corrosion problems due to the working pairs normally used.

Hence, adsorption refrigeration technology appears as a good alternative to replace (or integrate) the traditional refrigeration systems by more environmentally friendly systems, which can be powered by renewable energy sources and contribute to a sustainable development, meeting the current international directives and demands [21].

2.3 Summary

This chapter provided an overview of refrigeration technologies covering the general classification of various types of cooling technologies focusing the theory, working principle and the performance of each.

Ejector refrigeration is a thermally driven technology that has been used for cooling applications for many years. However, in their present state of development, they have a much lower COP than the convectional vapour compression systems. However, the standard vapour compression refrigeration technology is driven by electricity which strongly increases the consumption of electricity and thus makes it not useful for people in the rural areas of developing countries. Besides, it uses non-natural working fluids which are directly responsible for global warming.

Photovoltaic (PV) refrigeration technology, except for the energy-supply sub-system, is similar in most respects to any other vapour compression refrigeration technology. The energy supply in the former is provided by an array of solar cells which convert the

incident solar radiation to electricity. Although PV refrigerators are more commercially successful among the thermal refrigeration technologies, they have the disadvantages of high cost and low possibility of manufacture.

Absorption refrigeration technology which uses a liquid–gas working pair has successfully established itself as a commercially available technology among all other heat driven sorption cooling technologies. However, it is found to be more suitable for larger applications.

Presented also in this chapter is a run-around solid desiccant system for dehumidification which investigated into the heat and moisture transfer between supply and exhaust air streams for a run-around system in which the coupling materials were coated solid desiccant particles (silica gel) transported between two exchangers.

Furthermore, an extensive review (including: adsorption refrigeration cycle, choice of adsorbent, adsorbent general requirements, selection of working pairs, and advantages etc.) is presented on adsorption refrigeration technology being the focal domain of this study.

Hence, adsorption refrigeration technology has been noted as a good alternative to replace (or integrate) the traditional refrigeration technologies by more environmentally friendly systems, which can be powered by renewable energy sources and contribute to a sustainable development, meeting the current international directives and demands.

Chapter 3: Development Trend in Adsorption Cooling Technology

3.1 Development history of adsorption cooling technology

The first record of adsorption refrigeration phenomenon finds its origin in Faraday's laboratory in 1848 where the possibility of generating cooling capacity when silver chloride adsorbed ammonia was discovered. Then, G.E. Hulse in 1920, proposed a refrigeration system in which silica gel/sulphur dioxide working pair was used for food storage in a train. History has it that this system which was powered by the combustion of propane and cooled down by the convection heat transfer of air could have its lowest refrigerating temperature reaching 12℃.

Between 1940 and 1945, an adsorption refrigeration system, with calcium chloride/ammonia working pair, driven by steam at 100 ℃ was used for food storage application on a train from London to Liverpool. Contrastingly from the 1930s, there was a sudden emergence of new technologies such as Freon discovery and the successful development of the totally closed compressor which appreciably improved the efficiency of the convectional compression refrigeration system. Consequently, adsorption refrigeration technology couldn't compete with the highly efficient CFCs system. Hence, it was not being considered by researchers for a long time not until the occurrence of the 1970s energy crisis which offered a great chance for the development of adsorption refrigeration technology, mainly because of the fact that it is driven by a low-grade heat source such as waste heat/solar energy.

In the 1990s, the colossal increase in environmental pollution and the shortcomings of the CFCs system were being recognized worldwide as the

major causes of the ozonosphere depletion and greenhouse warming problems. Hence, green refrigeration technologies, such as adsorption which is a thermal powered refrigeration technology, regained its recognition by academics globally. Not until about 1992, most of the works produced on adsorption refrigeration was mostly about the theoretical analysis and simulation of different cycles, especially about how the cycle parameters influenced the performances. For the system design, the heat and mass transfer intensification attracted a great deal of attention. The first sorption conference held in Paris in the year 1992 favoured this technology to gain more worldwide attention [23]. Since then, the key research aspects of this technology are uniformly being recognized by worldwide researchers because numerous new ideas such as, evaluation of adsorption and properties of the working pairs, development of predictive models of their behaviours under different conditions and the development and study of different cycles, are being put forward on how to improve the adsorption refrigeration performance in order to overcome its current technical and economic issues [19, 23].

3.2 A review of development trends

Based on working principle, adsorption refrigeration cycles can be divided into just two classifications which are intermittent and continuous cycles but going through the transitional development history of adsorption refrigeration as well as the study status of scholars globally, adsorption refrigeration cycles can be broadly classified as shown below in Fig 3-1.

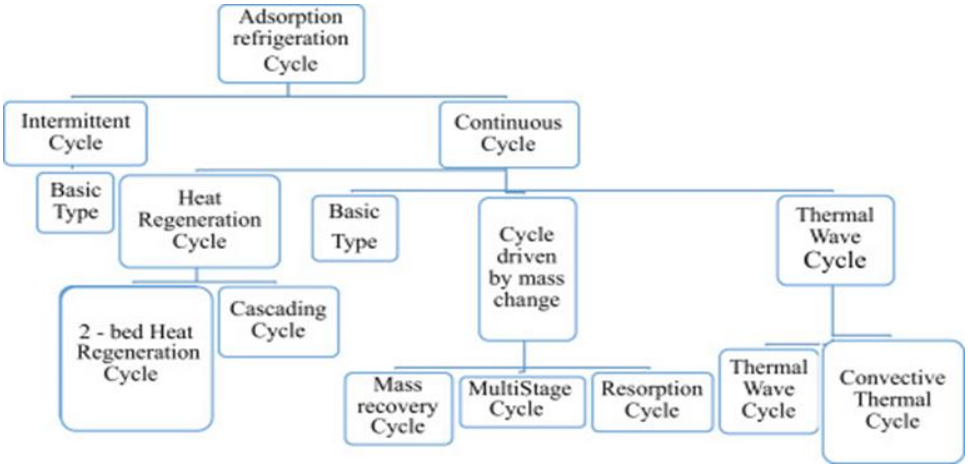


Fig 3-1 Classification of adsorption refrigeration cycle based on development history [23]

3.2.1 Basic or Intermittent cycles

The earliest adsorption refrigeration cycle, called the basic cycle, is the simple and reliable single-bed intermittent cycle mostly used in the solar powered refrigerator.

This basic cycle has been researched extensively since 1986 when Pons and Guilleminot [24] experimented and built a solar-powered ice maker in Orsay. The system, using activated carbon-methanol pair was able to produce 30–35 kg of ice per sunny day at a net solar COP of 0.12. In that same year, Sakoda and Suzuki [25] developed a quantitative model for the simultaneous transport of heat and adsorbate in the operation of a closed-type solar-powered adsorption cooling system. The system COPs based on various operating conditions were estimated by numerical simulation on the basis of the model. The structures of the adsorbers were also optimized in order to achieve larger COP.

Some years later, Tan et al.[26] designed a solar adsorption ice maker with active carbon-methanol pair for experimental study. The system had the capacity of producing 4 kg of ice per day with a solar COP range of 0.1-0.123. In that year, an on-the-site experimental flat plate solar collector-powered refrigerator producing 4 kg of ice per day with a net solar COP range of 0.08-0.12 was successfully developed [27, 28].

Critoph et al. [29], carried out a research to evaluate the best of three available configurations : single glazing, double glazing and single glazing with transparent insulation material (TIM). The experimental results showed that the single glazing configuration was the best of the three. The collector efficiency was between 47% and 36% from sunrise to midday with a generating temperature of about 100 ℃. The authors concluded that the use of a TIM is not recommended as it only adds to the cost of the collector without due return in COP or collector efficiency.

Sumathy and Zhongfu [30] designed and built a solar-driven refrigerator with a flat plate collector exposed area of 0.92 m^2 producing 4-5 kg of ice daily at a solar COP of about 0.1 to 0.12.

Boubakri et al. [31] presented an experimentally validated solar adsorptive ice maker model capable of reaching a COP of 0.19 with an estimated ice production of about 11.5 kg/m^2 when the machine operates at the optimum physical and meteorological conditions. Just about some years after, with the expectation of reducing its weight and cost simultaneously, they [32, 33] proposed a novel concept of the machine having a single heat exchanger acting alternatively as the condenser and evaporator. The mathematical model

showed the possibility of daily ice production exceeding 5.2 kg, with a COP of more than 0.14, an interesting value comparable to COP of 0.08–0.2 usually obtained for systems operating with separate condenser and evaporator operating under the same meteorological conditions or technologies.

Leite and Daguenet [34] presented a model based on instantaneous heat and mass transfers in each one of the components of an adsorption solar cooling system which was powered by a static solar collector covered by Transparent Insulation Material (TIM). The average net solar COP was 0.13 corresponding to 7–10 kg/day of ice production per m^2 of solar collector with solar irradiations range of 20-23 MJ/m^2. The TIM cover's system proved to be about 40% more efficient than the single cover solar system.

Li et al. [35] conducted an experimental study on the dynamic performance of a flat-plate solar ice maker. The results showed that the machine could produce 7–10 kg of ice while receiving 28–30 MJ of radiation energy with a collector area of 1.5 m^2.

Buchter et al. [36] developed a refrigerator with a 2 m^2 single glazed solar collector furnished with ventilation dampers to aid night cooling of the adsorbent bed. The system was producing ice of 5 ℃ during day time at a COP ranging between 0.09 and 0.13. In this same year, Li et al. [37] presented the simulation result on the evacuated tube adsorber of a solar refrigerator. The system was capable of working at a COP higher than 0.25 theoretically while the optimal thickness of adsorbent was about 15 mm when the largest COP was considered.

Anyanwu [38] presented a detailed review of classifications of adsorption solar refrigeration cycles based on the adsorbates utilized. The performances of those refrigeration cycles, drawn from actual field testing experiences, together with the techno-economic constraints that affect the technology popularization and their suggested possible solutions, were also reported.

Anyanwu and Ezekwe [13] designed, constructed and tested a prototype of a solar-powered adsorption refrigerator of flat plate collector of 1.2 m^2 effective exposed area using activated carbon-methanol. The refrigerator yielded evaporator temperatures ranging over 1.0–8.5 ℃ from water initially in the temperature range 24–28 ℃ with the maximum daily useful cooling produced being 266.8 kJ/m^2.

A solar powered adsorption refrigerator using activated carbon AC35-methanol was designed, constructed and tested by Lemmini and Errougani [39, 40]. Experimental results showed that such refrigerator unit could have a solar COP range of 5-8% for an irradiation range of 12,000-27,000 kJ/m^2. In order to predict the performance of this refrigerator and to avoid unnecessary experimental costs, Anyanwu and Ogueke [41, 42] carried out further studies relating to transient simulation models. The models found to be satisfactorily validated were employed for the optimisation of the refrigerator with improvements in the ranges of 29–38% and 26–35% respectively for COP and condensate yield.

Saha et al. [43] presented a methodology capable of determining the minimum desorption temperature required to operate an adsorption refrigeration system. On testing the methodology with three systems, it was concluded that waste

heat as low as 60 ℃ can operate such systems which makes them good energy conservation devices.

The experimental result of the performance analysis carried out by Liete et al. [44] on three thermodynamic cycles (each with a different weather condition) of a solar adsorptive icemaker revealed that with the evaporating temperature of -4.6 ℃, the maximum regenerating temperatures were 100.1, 87.3 and 92.7 ℃, with an ice production of 6.05, 2.10 and 0 kg/m^2 respectively for cycles of clear sky, partially cloudy and overcast nights, with the COP of 0.085.

Gonzalez et al. [45, 46] developed a numerical model for optimising an experimental prototype of a solar-powered adsorption chiller with a 0.55 m^2 compound parabolic concentrator (CPC) collector. While the solar COP range was 0.078-0.096, the average gross cold production was 2.2 MJ/m^2 per day.

Maggio et al. [47] proposed a theoretical model to estimate the performance of a solar adsorption ice-maker with 1.5 m^2 flat plate solar collector using a novel composite adsorbent of lithium chloride in silica gel pores and methanol as adsorbate. The maximum observed net solar COP was 0.33 with maximum daily ice production of 20 kg/m^2. Such performance was noted to be higher than those obtained using commercial activated carbon.

Hassan et al. [48] introduced a theoretical simulation model for a tubular solar adsorption refrigerating system using activated carbon–methanol. The system having a $1m^2$ flat plate collector was having a solar COP and a specific cooling power of 0.211 and 2.326 respectively.

A solar powered zeolite-water adsorption refrigerator using two CPC solar collectors of total area of 1.029 m^2 having a COP range of 0.838 - 1.48 was developed by Omisanya et al. [49].

About 99% satisfactory agreement was recorded between the results obtained from literature and those from direct and inverse artificial neural network(respectively ANN and ANNi) models developed in order to predict the optimal COP of a solar assisted adsorption refrigeration using carbon-methanol [50].

Abu-Hamedah et al. [51] developed a model of a solar adsorption refrigeration unit powered through a 3.7 m^2 parabolic trough solar collector (PTC) using olive waste-methanol pair. The highest gross COP obtained was 0.75 with a lowest temperature of 4 ℃ in the refrigerated space.

Omisanya et al. [52] presented a comparison between the results of the experiment and the simulation of a solar (zeolite 4 A and water) adsorption refrigerator using Trnsys and Matlab Softwares. The system was able to achieve a solar COP of 0.0133.

A solar powered adsorption refrigeration system was designed, constructed and tested by Anjorin and Bello [53]. The system utilized granular 70% CaCl2 + 10% activated carbon + 20% CaSO4 / NH3 as an adsorbent/adsorbate pair. The refrigerator has an overall COP range of 0.021 - 0.033 with daily ice production range of 0.49–0.63 kg/m^2.

The experimental result of a laboratory test performed on a built adsorption refrigerator prototype by Fatih et al. [54] revealed an evaporator temperature

more than 3 ℃, condensing temperature up to 37 ℃ and a COP of about 0.07 under the laboratory working conditions.

A solar adsorption refrigerator system with silica gel-water using reflecting surface technique for heat transfer enhancement in adsorbent bed was built and tested by Bouzeffour et al. [55]. A minimum evaporator temperature of 5 ℃ and maximum solar COP of 0.09 were achieved.

Hadj et al. [8] theoretically studied the operating and performance parameters of a solar-driven steady-temperature adsorption refrigeration system. Comparative study between different types of activated carbon revealed an optimal COP of 0.73 with 18740.5 kJ as total energy input corresponding to a total daily ice production of 13.65 kg at −3 ℃ for the stone coal based system.

Though the basic cycles are simple and reliable but the early research work pointed out that they needed to be improved in many ways due to the bottlenecks of low COP, low SCP and especially the intermittent refrigeration production. Therefore, in order to improve the efficiency and practicability of the basic cycle, different advanced adsorption refrigeration cycles are being proposed by various researchers and companies with their thermal performances being studied and analysed.

3.2.2 Advanced or continuous cycles

For the continuous refrigeration cycles, there are generally two or more beds operating to achieve alternate cycles of adsorption and desorption in order to produce continuous refrigeration output [15, 19, 23]. Following is the plethora of the development trend of such cycles:

3.2.2.1 Heat recovery adsorption refrigeration cycle

This concept was first introduced into the adsorption refrigeration system for improving COP based on the principle of recoverer. The heat recoverer used in the adsorption systems is the adsorbent bed itself [19]. This principle could be applied in adsorption cooling system with two or more adsorbent beds. After switching of beds between adsorption and desorption, the adsorber to be cooled (for adsorption) transfers its heat to the adsorber to be heated (for desorption) through a heat transfer fluid circulating in a closed loop. This heat includes sensible heat as well as the heat of adsorption. Heat recovery leads to higher COP [2]. According to the corresponding research, heat recovery can improve COP by 25% [3].

A quasi-continuous adsorption refrigeration system with heat recovery whose schematic diagram is depicted in Fig 3-2 was experimentally investigated by Wang et al. [56, 57]. While cooling-adsorption-evaporation is being carried in adsorber 1, adsorber 2 connected to the condenser is heated to obtain heating-desorption-condensation. The operation phase can be changed, and the intermediary will be a short time heat recovery process. The result showed that the system COP was increased by about 25% when compared with one adsorber basic cycle system. Miles et al. [58] used this technique to enhance the COP of his experimental activated carbon/ammonia solar refrigeration system up to 0.8.

Jones [59, 60] suggested an improvement by installing more adsorbers into the system. As compared to the basic cycle, heat recovery in this process is only effective if the heat transfer fluid temperature leaving the adsorbers is sufficiently high [59, 60]. Simulation results have shown that the maximum

value of the COP depends on the number of adsorbers and desorbers installed. He later extended the analysis to a system containing six adsorbers and six desorbers at the same test temperature conditions and discovered that it was possible to obtain COP as high as 1.16.

Multi-beds can be also adopted to recover more heat which subsequently increases the COP further, but it should be noted that the practical operation of the system becomes questionable due to increased system complexity [61, 62].

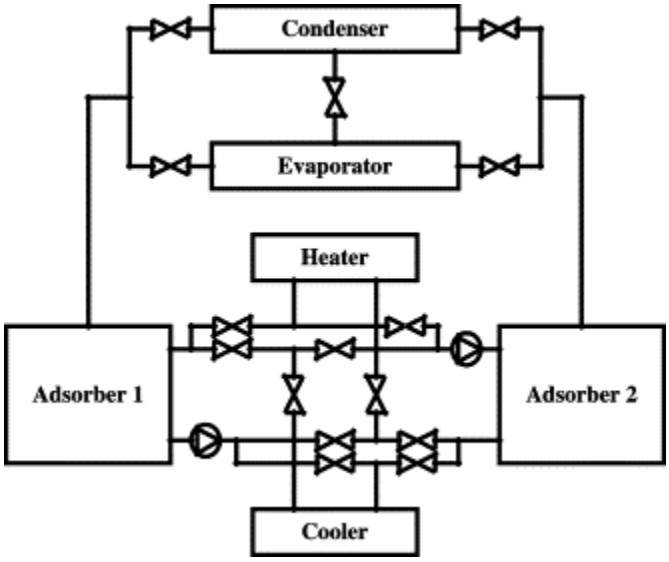


Fig 3-2 Schematic diagram of heat recovery two-bed adsorption refrigeration system [56, 57]

3.2.2.2 Heat and mass recovery adsorption refrigeration cycle

Ordinarily, after switching between adsorption and desorption and just before heat recovery, the mass channels between the high pressure desorber and the low pressure adsorber are connected to each other. This initiates further desorption (by pressure reduction) and adsorption (by pressure increase) in the desorber and the adsorber respectively. This process is called mass recovery [2, 3, 19, 63]. Mass recovery increases the cyclic adsorption capacity and the SCP

is improved correspondingly and hence the refrigerating effect [2, 19]. Usually, the commonest trend is to have mass recovery and the heat recovery combined simultaneously into the heat and mass recovery cycle. If the durations of the heat recovery and the mass recovery are optimally handled, then the heat and mass recovery cycle will correspondingly increase both COP and SCP [2, 3]. This is one of the most commonly and successfully used cycles in the recent time. According to Wang [56], mass recovery is very effective in combining with heat recovery cycle and can raise the system COP by more than 10%.

Fig 3-3 (a) and (b) respectively show schematically the principle of the mass recovery cycle and thermodynamic property diagram of heat and mass recovery.

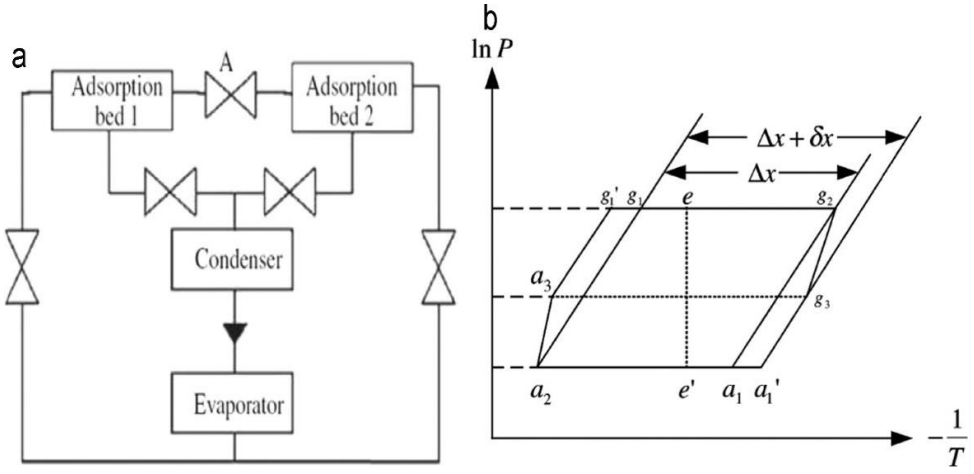


Fig 3-3 (a) Principle of mass recovery (b)Diagram of heat and mass recovery cycle[23]

The result of an analytical study done on a two-bed, silica gel-water adsorption refrigeration system with mass recovery showed that the cooling capacity of such a cycle is superior to that of conventional cycle and that mass recovery process is more effective for low regenerating temperature [63].

Liu et al. [64] developed a novel silica gel–water adsorption refrigeration system noted for its: no refrigerant valves, two adsorbers, two condensers and two evaporators novelty. The experiment results demonstrated that the chiller first prototype had a cooling capacity of 2–7.3 kW with COP of 0.2–0.42 at different evaporating temperatures; while a COP over 0.5 and cooling capacity of 9 kW was achieved at evaporating temperature of 13 ℃ for the second prototype. This concept was further improved around that same year as Wang et al. [65, 66] developed a chiller consisting of three vacuum chambers: two adsorption/desorption (or evaporation/condensation) vacuum chambers and one heat pipe working vacuum chamber as the evaporator. With that configuration, the chiller with a COP of 0.38 was able to attain a cooling capacity of 6 kW with 17.6 ℃ chilled water outlet temperature.

An adsorption refrigeration of 10–200 kW driven by a heat source of 65 ℃ and operating on the principle of heat and mass recovery process was successfully developed in 2009 by Shanghai Jiao Tong University (SJTU), China [19].

A numerical study of a continuous PTC powered-adsorption refrigeration system working on heat and mass recovery principle was done by Fadar et al. [67]. The study results had put in evidence that the system was capable of a SCP of the order of 104 W/kg, a cooling COP of 0.43, a daily useful cooling of 2515 kJ per 0.8 m^2 of collector area, while its gross solar COP could reach 0.18.

Baiju and Muraleedharan [68] conducted a performance study on a continuous two stage solar hybrid adsorption refrigeration system using activated carbon-methanol. The system was producing a cooling effect of 60.75 W and 79.87 W

with a mean cycle COP of 0.196 and 0.335 during daytime and night respectively.

3.2.2.3 Thermal wave adsorption refrigeration cycle

The basic principle, as shown in Fig 3-4, is using a single heating and cooling fluid circuit to connect two adsorbent beds, the cooler and the heater. The fluid circuit could transfer the released heat from adsorption bed to the desorption bed, and to recover the adsorption heat for the improvement of the system energy efficiency. The thermal wave means the temperature of the fluid drops or rises rapidly in the adsorbent beds, forming a large temperature difference which is essential for heat transfer between them.

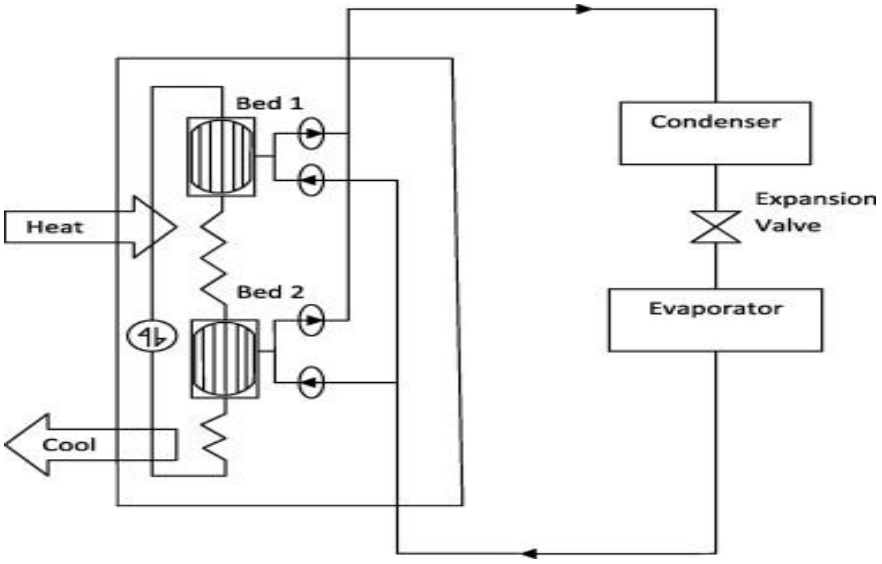


Fig 3-4 Schematic diagram of a thermal wave cycle [61]

This concept was first proposed by Shelton et al. [69, 70]. The imperative of designing this was to optimally use exothermic heat in order to reduce the heat required from the external heat source for desorption process and thereby providing efficiency gain [19]. The authors, based on their analysis, proved that over 80% of the heat required for desorption process was made available

from the bed being cooled without violating the second law of thermodynamics. This could substantially reduce the energy input cost. The efficiency of the system with thermal wave cycle was found to be quite insensitive to the cycle's heat input and output temperatures.

A solid-sorption heat-pump system based on thermal wave adsorption refrigeration cycle using activated carbon-ammonia was designed, built and tested by Miles and Shelton [71]. The experimental results showed that a cooling seasonal COP of 0.76 and a heating seasonal COP of 1.21 were obtained.

A four bed regenerative adsorption thermal wave based heat pump using carbon/ammonia analysed by Jones [72] was able to give a cooling COP of 1.0 4 bed system and a heating COP of 1.9.

Amar et al. [73] investigated the effects of various operating parameters on the performance of an adsorptive thermal wave regenerative heat pump. Though the system was capable of achieving a numerical COP value greater than unity but it was slightly higher for air conditioning application purposes as concluded in Spinner's model [74].

Sun et al. [75] numerically investigated adsorptive heat pump systems with thermal wave heat regeneration under uniform-pressure conditions in order to estimate the variation in COP due to decrease in thermal conductivity. A drop in the COP from 0.87 to 0.21 was observed when the apparent thermal conductivity was decreased from 100 to 0.25 W/m-K.

Chahbani et al. [76] presented an analysis of intraparticle mass transfer limitations on the performance of cooling machines with thermal wave heat regeneration technology. With the bed thermal conductivity varying from 0.1 to 10.0 W/m-K, a COP range of 0.27-0.89 was obtained. Whereas the SCP ranged from 73.0 to 182.0 W/kg.

However, for efficient running of a thermal wave cycle, large temperature drop and lift are respectively required in the desorber and adsorber. The cycle also needs good bed heat transfer properties which are difficult to get from low thermal conductivity adsorbent materials [2]. Therefore, it can be concluded that thermal wave cycle is better for the system COP but not for SCP [3].

3.2.2.4 Convective thermal wave adsorption refrigeration cycle

Critoph [77, 78] in an effort to improve the performance of thermal wave cycle, rather than heating the bed directly as in thermal wave cycle, initiated the heating/cooling of the thermal fluid by packing two inert beds with non-reactive particles. The first half of the proposed convective thermal wave cycle is shown in Fig 3-5. With 5 ℃ evaporating temperature, 40 ℃ condensing temperature, 200 ℃ desorption temperature and the heat regeneration rate of 0.8, a theoretical COP of 0.90 was predicted. This system has the advantages of being cost effective as compared to conventional heat exchangers, high COP values and good energy efficiency.

Lai [79], in his interesting effort to enhance the performance of convective thermal wave adsorption refrigeration cycle, proposed a different cycle configuration called Periodic Reversal Forced Convective cycle. However, controlling the flow rate of the refrigerant vapour and the high vacuum under

which the gas recycle pump works are two technical issues to be solved to make the cycle practicable.

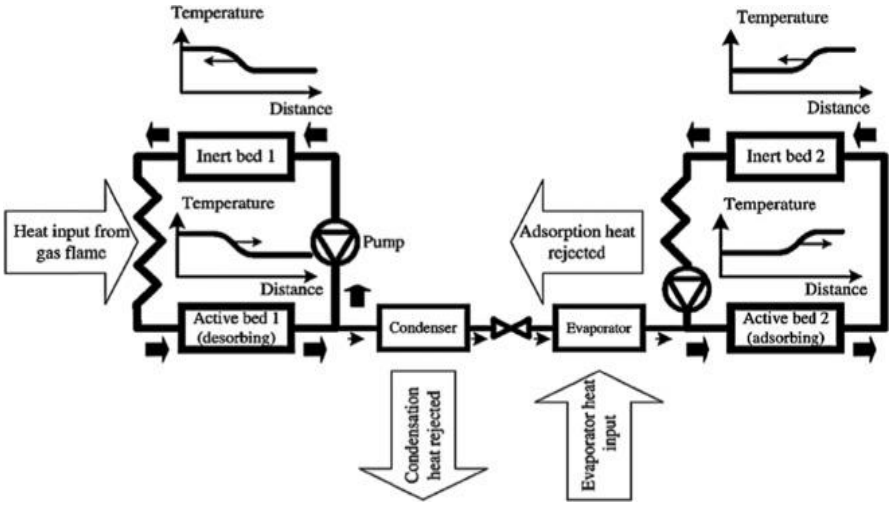


Fig 3-5 Adsorption refrigeration system with convective thermal wave cycle [78]

3.2.2.5 Cascaded Cycle

In cascading cycles, different operating temperatures of different working pairs are utilised. The sub-cycle of high and low temperature working pairs is driven by the high and low temperature heat source respectively. These are applied when there exists a huge temperature gradient between the heat source and the evaporator [3, 19].

Douss and Meunier [80] experimented on a cascading adsorptive cycle consisting of two adsorbers: zeolite-water at high temperature stage and an intermittent active carbon-methanol at low temperature. Experimental cooling COP was found to be 1.06, which was far more than the COP of an intermittent cycle and more than the COP of a two adsorber zeolite water cycle under similar operating conditions.

For cascade cycle to be applicable in the practical systems, its reliability and complexity should be studied further [3].

3.2.2.6 Multi bed and multi stage Cycle

All the cycles discussed above are single stage and so cannot effectively utilize high temperature heat sources and as well do not perform optimally at very low temperatures. The basic idea is to perform desorption–condensation processes and adsorption–evaporation processes at different temperature/pressure levels by using the same working pair [19].

Saha et al. [81] proposed the design and experimental prototype of a two-stage non-regenerative adsorption chiller with silica gel–water pair. With a 55 ℃ driving source in combination with a heat sink at 30 ℃, the chiller's COP was found to be 0.36.

An innovative three-bed adsorption cycle in parallel flow configuration of the heat transfer fluids was proposed by Saha et al. [82]. The simulation result demonstrates that, while optimum COP values are obtained with 30 ℃ cooling water and driving source temperatures range of 80-90 ℃ , optimum cooling capacity values are obtained for adsorption–desorption cycle time between 180 and 300 seconds with a fixed pre-heating or pre-cooling cycle time. It is also proved that waste heat recovery efficiency of the three-bed system is about 35% higher than that of the two-bed system.

A study was conducted by Shu et al. [83] on combined system consisting of an adsorption–absorption cascading multi-effect refrigeration cycle. The system

consists of a high temperature stage of solid adsorption unit with zeolite-water and a low temperature stage of double effect absorption unit with LiBr–water. The working principle of this cycle is demonstrated with Fig 3-6. The work showed that the cycle COP can be greatly improved by efficient energy recovery and utilization within the system.

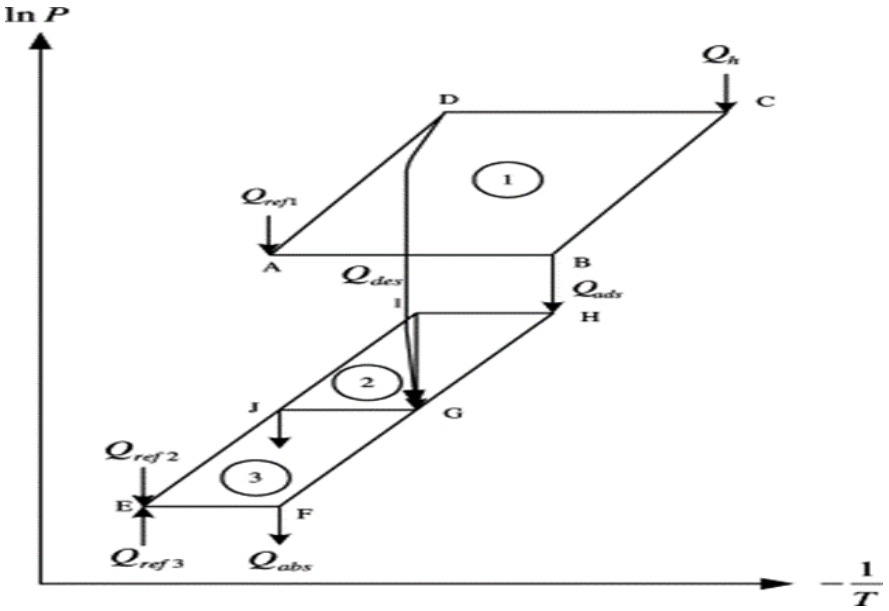


Fig 3-6 Adsorption–absorption cascading multi-effect refrigeration cycle: (1) adsorption cycle; (2) high pressure absorption cycle and (3) low pressure absorption cycle [61]

Saha et al. [84, 85] developed a three-stage adsorption chiller capable of operating at about 50 ℃ waste heat with a cooling water temperature of 30 ℃. The experimental result showed that the cooling capacity is maximized with adsorption/desorption cycle times between 200 and 360 seconds. The COP, on the other hand, increases uniformly with cycle time due to less frequent temperature switching of the adsorber/desorber. However, the simulated COP only agrees with the experimental one qualitatively and not quantitatively.

Saha et al. [86] designed a dual-mode, multi-stage, multi-bed silica gel–water adsorption system which can be powered by solar/waste heat of 40-95℃. The system is capable of operating in the first mode with the driving source of 60-95 ℃, and in the second mode (whose work is similar to an advanced three-stage adsorption chiller) with the available driving source of 40-60 ℃. The limitation in this operational mode is its poor efficiency in terms of cooling capacity and COP. Simulation results showed that the optimum COP ranges for the three-stage mode are obtained at driving source of 50-55 ℃ and 80-85℃ in single-stage mode.

Critoph [87] gave the analytical performance prediction of a continuous multi-bed regenerative adsorption system consisting of 32 simple tubular adsorption modules. The systems using those advanced cycles are very complex and the performance is much low so that these cycles are not used in the practical system at present [3].

3.2.2.7 Fluidised bed technology

Wang et al. [88] designed a fluidized-bed adsorber/desorber which can be used in the adsorption refrigeration system instead of the conventional fixed-bed. The experimental result showed that the fluidized adsorbent could enhance the heat and mass transfer either in adsorption or desorption with nearly no change of the adsorbent micropores. Hence, it was concluded that with the new approach, the poor heat and mass transfer in the conventional fixed-bed can be overcome and the system SCP can be appreciably improved with considerably reduced cycle time. The only drawback is that extra

electricity is required to run the blower needed for fluidisation which makes the technology only suitable for large refrigerating load applications.

3.2.2.8 Constant temperature Adsorption Refrigeration (CTAR) Cycle

Still in the quest to mitigate intermittency issue in adsorption refrigeration systems, Hassan et al. [89] proposed a novel and continuous solar-driven adsorption refrigeration (CO-SAR) system (Fig 3-7 and Fig 3-8), capable of providing cold continuously along the 24 hours of the day and whose working principle was based on constant temperature adsorption refrigeration cycle.

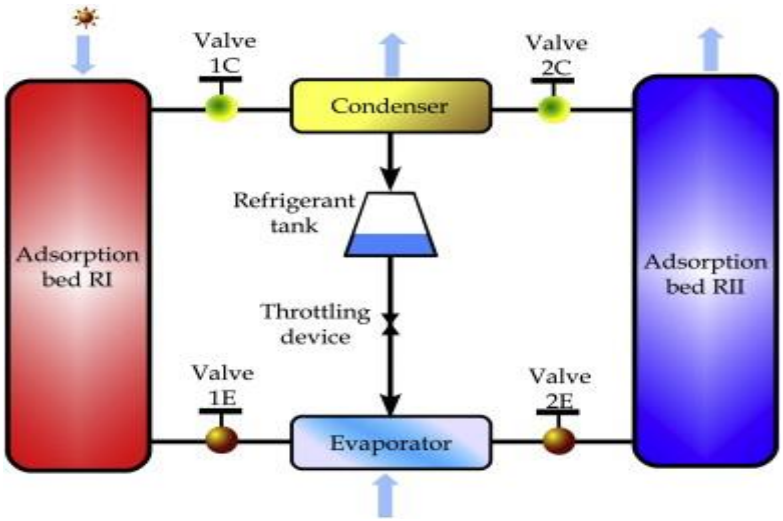


Fig 3-7 Schematic diagram of the constant temperature adsorption cooling cycle [89]

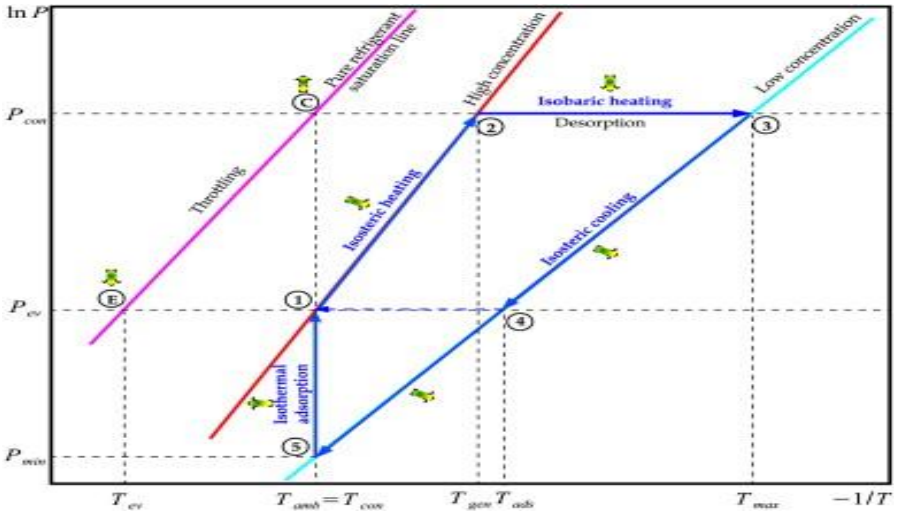


Fig 3-8 Clapeyron diagram for the constant temperature adsorption cooling cycle [89]

Hassan and Mohamad [90] further applied this principle to their proposed system shown in Fig 3-9. An activated carbon–methanol water chiller modelled after the operation of the novel cycle was found to produce a daily mass of 2.63 kg cold water at 0 ℃ from water at 25 ℃ per kg of adsorbent with a cooling COP of 0.66.

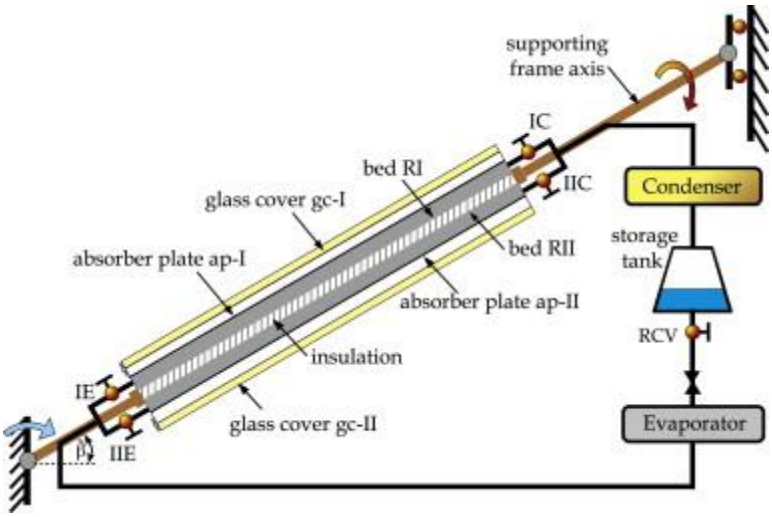


Fig 3-9 Schematic diagram of the proposed CO-SAR system [90]

This same Hassan group [91] studied this system further by carrying out a dynamic analysis on the CTAR cycle. The obtained results demonstrated that,

the idealization of the constant temperature adsorption process in the theoretical CTAR cycle was not far from the real situation and could be approached.

3.2.2.9 Hybrid systems

In order to make the adsorption cooling system competitive in the market, various investigations have been conducted by researchers on hybrid systems which use the basic adsorption cycle for heat and cold production or in combination with other types of refrigeration systems.

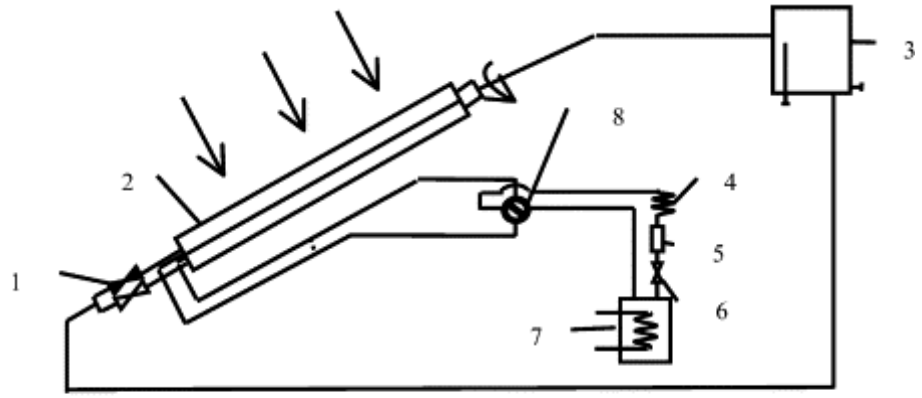
The first hybrid adsorption heating and cooling system was developed by Tchernev [92]. The system, having zeolite-water pair, was able to achieve space heating in winter and also air conditioning purposes.

A hybrid system of solar powered water heater and adsorption ice maker using activated carbon-methanol was proposed and developed by Wang et al.[93]. It was experimentally verified that the hybrid system was capable of heating 60 kg water to about 90 ℃ as well as producing ice at 10 kg per day with a 2 m^2 solar collector having a COP of 0.144. This was later improved by Wang [94] by including a second tank which served as hot water reservoir. The same research group developed few more models, each time having better heating efficiency than the previous [19].

Odesola and Oluleye [1] presented the description and thermodynamic analysis of a hybrid system of solar-powered heater and adsorption ice maker. The simulation results revealed the ability of the system with the COP of 0.62 to heat 50 kg water to about 96 ℃ and also producing 7.2 kg ice per day with a 2 m^2 evacuated vacuum-tube-type solar collector.

Zhang and Wang [95] also developed a simulation model of a hybrid heating and cooling solar adsorption system (Fig 3-10) capable of reaching a mean heating COP of 0.34 and cooling COP of 0.18 while furnishing 30 kg hot water of 47.8 ℃.

The modelling and simulation of a solar powered adsorption refrigeration system using flat plate solar collector, with activated carbon/methanol pair was undertaken by Suleiman et al. [96]. The results revealed that the system was having a solar COP of 0.02 and a heating efficiency of 0.46.



1—water valve 2—hybrid bed array 3—water tank 4—condenser
5—liquid receiver 6—throttle valve 7—evaporator 8—rotary valve

Fig 3-10 Schematic representation of Continuous hybrid adsorption refrigeration system [95]

A conventional mechanical compression was supplemented by thermal compression with the aid of a string of adsorption compressors with activated carbon-HFC 134a pair by Banker et al. [97]. This group realised that almost 40% energy saving is possible by carrying out a portion of the compression in a thermal compressor as compared to when the entire compression is carried out in a single-stage mechanical compressor.

With the intention to utilise the low grade thermal energy to drive a refrigeration system that is capable of cooling some critical electronic components, Banker et al. [98, 99] studied various stages of the laboratory model of a thermally driven adsorption refrigeration unit with three specimens of varying achievable packing densities. It was concluded that packing density of the adsorber plays a major role in the performance of the system and that two stage thermal compression will be a viable proposition when either, the heat source temperature is low or adsorption characteristics are weak or adequate packing densities are difficult to realize.

A simulation study of a hybrid multi-bed adsorption chiller cum desalination system was carried out by Mitra et al. [100, 101] to investigate the system performance. The result showed a realistic minimum desorption temperature range of 46-52 ℃ when chilled water inlet temperature was reduced from 24 ℃ to 11.5 ℃. According to the result, the system throughput [specific cooling capacity (SCC) and specific daily water production (SDWP)] had a direct relationship with both the cycle time and the heat source temperature unlike the COP which was having a monotonic function of both the cycle time and heat source. The authors hence concluded that, optimized cycle time allocation is suitable for maximizing cooling and potable water production whilst longer cycle time is preferable for higher COP. A model, which could qualitatively predict the fluctuating inter-stage pressure during the mass transfer between two stages, was later presented which was an advancement over the earlier models.

3.3 Analysis of reviewed works on development history of adsorption cooling technology

Energy economy, nature conservation and sustainability remain the focal points of the global world. Due to the increase in the global consumption of limited primary energy and the ecological consideration for refrigerants choice, adsorption cooling technology has been the subject of extensive research for cooling applications due to its merits which are not limited to low energy intensity, use of low grade heat sources and being eco-friendly thereby meeting the current global regulations.

Table 3-1 summarised the reviewed studies on the comprehensive plethora of the development trend in adsorption cooling technology ranging from the basic cycles to the advanced cycles as presented in this work. The summary spans through the allied technologies, cycle types, methodology, adsorption working pairs, heat source, applications and the related performance parameters.

Even though the results of the reviewed studies summarised below might not be directly compared to one another because they were obtained under different operating conditions, they can still be taken as a reference point to what can be expected from such reviewed systems.

Hence, from the reviewed studies, it seems the performance of the basic cycle can no longer be significantly improved. Regarding the advanced cycles, although higher performances seemed to have been recorded about them, it can be noted from the below summary that, in spite of the numberless attempts made by various researchers to improve their performances and as well maintain their presence in the market, they appears not yet ready to compete

with the traditional vapour compression cooling systems due to identified technical and economic limitations like low COP, high initial cost, poor heat management, large volume and weight, operating conditional variations and automatic control which seem difficult to overcome. Honestly, most of the advanced cycles are just theoretically studied or on laboratory scale. They are often being limited by the issue of low COP and they usually require a continuously circulating cooling/heating medium and too many valves to operate uninterruptedly. However, the heat and mass recovery cycle is one of the easiest cycles used in practical applications.

Therefore, the concept of the configuration in this work with its pertinent potentials (including continuous cold production, eradication of the issue of unnecessary load on the evaporator, maximum optimization of both adsorption and desorption processes due to the spatial separation of both desorber and adsorber, absence of thermal stress induction in the bed as heat source and heat sink heat exchangers are localised) is intended to overcome some of the above bottlenecks often encountered by adsorption cooling technology.

Table 3-1 Summary of reviewed works on development history of adsorption cooling technology

Cycle type	Methodology	Working pair	Performance parameter	Application	Heat source	Reference
Basic / Intermittent	Exp.	Activated carbon-methanol	M_{ice}: 30–35 kg/day SCOP:0.12	Ice maker	Solar-powered	Pons & Guilleminot [24]
	Sim. and exp.	Silica-gel–Water	SCOP: 0.2	-	Solar-powered	Sakoda & Suzuki [25]
	Exp.	Activated carbon-methanol	M_{ice}: 4 kg/day SCOP:0.1-0.123	Ice maker	Solar-powered	Tan et al. [26]
	Exp.	Activated carbon-methanol	M_{ice}: 4 kg/day SCOP: 0.08-0.12	Refrigerator	Solar-powered	Boubakri et al. [27, 28]
	Exp.	Activated carbon-ammonia	η_c: 36% - 47%	Refrigerator	Solar-powered	Critoph et al. [29]
	Exp.	Activated carbon-methanol	M_{ice}: 4-5 kg/day SCOP: 0.1 to 0.12	Refrigerator	Solar-powered	Sumathy & Zhongfu [30]
	Sim. + exp.	Activated carbon-methanol	M_{ice}: 11.5 kg/m^2 COP: 0.19	Ice maker	Solar-powered	Boubakri et al. [31]
	Exp.	Activated carbon-methanol	M_{ice}: >5.2 kg/day COP: >0.14	Ice maker	Solar-powered	Boubakri [32, 33]
	Sim.	Activated carbon-methanol	M_{ice}: 7–10 kg/day SCOP: 0.13	Ice maker	Solar-powered	Leite & Daguenet [34]
	Exp.	Activated carbon-methanol	M_{ice}: 7–10 kg	Ice maker	Solar-powered	Li et al. [35]
	Exp.	Activated carbon-methanol	COP: 0.09-0.13	Refrigerator	Solar-powered	Buchter et al. [36]
	Sim.	Zeolite–water	COP: 0.17-0.31	Refrigerator	Solar-powered	Li et al. [37]

	Exp.	Activated carbon-methanol	COP: 0.02 η_c : 16.4%	Refrigerator	Solar-powered	Anyanwu & Ezekwe [13]
	Exp.	Activated carbon AC35-methanol	SCOP: 0.05-0.08	Refrigerator	Solar-powered	Lemmini & Errougani [39, 40]
	Sim.	Activated carbon AC35-methanol	SCOP: 0.29–0.38	Refrigerator	Solar-powered	Anyanwu & Ogueke [41, 42]
	Theo.	Silica gel- water; Activated carbon-ethanol; Activated carbon-HFC134a	-	Refrigerator	Waste heat	Saha et al. [43]
	Exp.	Activated carbon-methanol	M_{ice}: 0-6.05 kg/m^2 SCOP: 0.085	Ice maker	Solar-powered	Liete et al. [44]
	Exp. + Sim.	Activated carbon-methanol	COP: 0.078-0.096	Chiller	Solar-powered	Gonzalez et al. [45, 46]
	Sim.	Lithium chloride in silica gel pores-methanol	M_{ice}: 20 kg/m^2 SCOP: 0.33	Ice maker	Solar-powered	Maggio et al. [47]
	Sim.	Activated carbon-methanol	SCOP: 0.211 SCP: 2.326	Refrigerator	Solar-powered	Hassan et al. [48]
	Exp.	Zeolite-water	COP: 0.838 - 1.48	Refrigerator	Solar-powered	Omisanya et al. [49]
	Sim.	Activated carbon-methanol	-	Refrigerator	Solar-powered	Laidi & Hanini [50]
	Sim.	Olive waste-methanol	COP: 0.75	Refrigerator	Solar-powered	Abu-Hamedah et al. [51]
	Exp. + Sim.	Zeolite 4A -water	SCOP: 0.0133.	Refrigerator	Solar-powered	Omisanya et al. [52]
	Exp.	$CaCl_2$ + activated carbon + CaSO4 - NH3	M_{ice}: 0.49–0.63 COP: 0.021 - 0.033	Refrigerator	Solar-powered	Anjorin & Bello [53]
	Exp.	Silica gel-water	COP: 0.07	Refrigerator	Iodine-tungsten lamp	Fatih et al. [54]

	Exp.	Silica gel-water	SCOP: 0.09	Refrigerator	Solar-powered	Bouzeffour et al. [55]
	Theo	Activated carbon-methanol	COP: 0.73	Refrigerator	Solar-powered	Hadj et al. [8]
Advanced / Continuous						
Heat recovery ARC	Exp.	Activated carbon-methanol	M_{ice}: 5–7 kg/day M_{ice}: 5.2 kg/day	Ice maker Refrigerator	Solar-powered; Waste heat	Wang et al. [56, 57]
	Exp.	Activated carbon-ammonia	COP: 0.8	Refrigerator	Solar-powered	Miles et al. [58]
	Exp.	Activated carbon-ammonia	COP: > 1.16	Refrigerator	-	Jones [59, 60]
Heat and mass recovery ARC	Exp. + Theo.	Activated carbon-methanol	COP: > 0.5	Cooler	-	Wang [56]
	Sim.	Silica gel-water	-	Refrigerator	Waste heat	Akahira et al. [63]
	Exp.	Silica gel-water	Cooling capacity: 2–9 kW; COP: 0.2- over 0.5	Water chiller	Electric heater	Liu et al. [64]
	Sim. + Exp.	Silica gel-water	Cooling capacity: 6 kW COP: 0.38	Chiller	-	Wang et al. [65, 66]
	Sim. + Exp.	Activated carbon-methanol	COP: > 0.6	Air-conditioner	Waste heat	Wang [57]
	Sim.	Activated carbon-ammonia	SCP: 104 W/kg; Cooling COP: 0.43; SCOP: 0.18	Refrigerator	Solar-powered	Fadar et al. [67]
	Exp.	Activated carbon-methanol	Cooling effect: 60.75 W-79.87 W	Refrigerator	Solar-powered	Baiju & Muraleedharan [68]

			Mean cycle COP: 0.196 (day), 0.335 (night)			
Thermal wave ARC	Exp.	Activated carbon/ammonia	COP (cooling): 0.76, COP (heating): 1.21	Heat pump	Electric HXF heater	Miles & Shelton [71]
	-	Carbon/ammonia	COP (cooling): 1.0 COP (heating): 1.9	Heat pump	Heater	Jones [72]
	Sim.	Zeolite NaX-water; Activated carbon AXZI-ammonia	SCP: 200 W/kg COP: >1	Heat pump	-	Amar et al. [73]
	Sim.	Zeolite NaX -water	0.87 – 0.21	Heat pump	Heater	Sun et al. [75]
	Sim.	Carbon-ammonia	SCP: 73.0-182.0 W/kg; COP: 0.27- 0.89	Heat pump	Heater	Chahbani et al. [76]
Convective thermal wave ARC	Sim. + Exp.	Carbon-ammonia	COP: 0.90	Cooler	-	Critoph [77, 78]
	Sim.	Zeolite 13X-water	SCP: 125 W/kg COP (cooling): 1.0 COP; COP (heating): 1.9	-	-	Lai [79]
Cascaded Cycle	Exp.	Zeolite-water @ high temperature; Active carbon-methanol @ low temperature	COP: 1.06	Heat pump	Boiler	Douss & Meunier [80]
Multi bed and multi stage	Exp.	Silica gel–water	COP: 0.36	Chiller	Solar/waste heat	Saha et al. [81]
	Sim.	Silica gel–water	COP: 0.38 T_{cw}: 6 °C	Chiller	Waste heat	Saha et al. [82]

Cycle	-	Zeolite-water, LiBr–water	-	Refrigerator	Waste heat	Shu et al. [83]
	Sim. + Exp.	Silica gel–water	CC: up to 2.4 kW COP: up to 0.2	Chiller	Waste heat	Saha et al. [84, 85]
	Sim.	Silica gel–water	CC: up to 7 kW COP: up to 0.55	Chiller	Solar/waste heat	Saha et al. [86]
	Sim.	Active carbon-ammonia	COP (cooling): 0.60; COP (heating): 1.52; CC: 291 W; SCP: 142 W/kg	Refrigerator/heat pump	Heater	Critoph [87]
Fluidised bed technology	Exp.	Activated carbon-R134a	-	Refrigerator	Boiler, blower	Wang et al. [88]
Constant temperature ARC	Sim.	Activated carbon-methanol	M_{ice}: 0.64-0.75 kg/day COP: 0.6	Refrigerator	Solar- powered	Hassan et al. [89]
	Sim.	Activated carbon-methanol	M_{cw}: 2.63kg COP: 0.66	Chiiler	Solar- powered	Hassan & Mohamad [90]
	Sim.	Activated carbon-methanol	COP: 0.61-0.66	Refrigerator	Solar- powered	Hassan et al. [91]
Hybrid systems	Exp.	Zeolite-water	-	Air conditioner + refrigerator	Solar- powered	Tchernev [102]
	Exp.	Activated carbon-methanol	M_{ice}: 10 kg/day; COP: 0.144; heating 60 kg water to about 90 ℃	Water heater + Ice-maker	Solar- powered	Wang et al. [93]
	Sim.	Activated carbon-methanol	M_{ice}: 7.2 kg/day; heating 50 kg water to	Water heater + Ice-maker	Solar- powered	Odesola & Oluleye [1]

			about 96 ℃; COP: 0.62			
	Sim.	Activated carbon-methanol	30 kg hot water of 47.8 ℃; COP (cooling): 0.18; COP (heating): 0.34	Water heater + Ice-maker	Solar- powered	Zhang & Wang [95]
	Sim.	Activated carbon-methanol	SCOP: 0.02 η_h: 0.46	Water heater + Refrigerator	Solar- powered	Suleiman et al. [96]
	Sim.	Activated carbon-HFC 134a	COP: 0.07-0.11	Refrigerator	Waste heat	Banker et al. [97]
	Sim. + Exp.	Activated carbon-HFC 134a	COP: 0.04	Refrigerator	Solar/waste heat	Banker et al. [98, 99]
	Sim.	Silica gel-water	SCC: 2-7 Rton/tonne of silica gel; SDWP: 0.3–0.9 m^3/day/ tonne of silica gel; COP: 0.05-0.26	Cooler + desalinator		Mitra et al. [100, 101]

Sim: Simulation; Exp: Experiment; Theo: Theoretical; SCOP: Solar coefficient of performance; M_{ice}: mass of ice; η_c : collector efficiency; SCP: Specific cooling power; ARC: Adsorption refrigeration cycle; T_{cw}: Chilled water temperature; CC: Cooling capacity; M_{cw}: Mass of chilled water, η_h : Heating efficiency; SCC: Specific cooling capacity; SDWP: Specific desalinated water production

3.4 Summary

A comprehensive plethora of the development trend in adsorption cooling technology ranging through its allied technologies and cycles and has been extensively presented in this chapter. From the development history, adsorption refrigeration cycles, based on working principle, can be divided into two classifications which are basic or intermittent and advanced or continuous cycles.

The basic cycles are the earliest ones which consist of simple and single-bed intermittent cycle mostly used in the solar powered refrigerator. In order to produce continuous refrigeration output, unlike in the case of the basis cycles whose refrigeration outputs are intermittent, the advanced cycles generally make use of two or more beds operating to achieve alternate cycles of adsorption and desorption.

Furthermore, going through the transitional development history as well as the study status of scholars globally, the advanced adsorption refrigeration cycles have been developed into: heat recovery cycle, heat and mass recovery cycle, thermal wave cycle, convective thermal wave cycle, cascaded cycle, multi bed and multi stage cycle, fluidised bed technology, constant temperature cycle and hybrid systems. These are all presented in this chapter.

Chapter 4: Alternative Adsorption refrigeration system design configurations

4.1 Introduction

This section covers adsorption system designs in view to enhancing current technology with several innovative approaches have been proposed to address the technology's limitations including operation mode, mechanical complexities and poor heat transfer processes. Currently, the adsorption systems operate intermittently or using double bed adsorption system which suffers from mechanical complexities and low reliability. In addition, the use of static adsorbent beds affects negatively heat transfer due to low thermal conductivity of the porous materials.

Further design challenges to be addressed are adsorption capacity deterioration through refrigerant leakage and materials degradation after many cycles of operation.

These advancements collectively mark a significant leap forward in the evolution of adsorption cooling technology, propelling it closer to widespread adoption and mainstream implementation.

In this chapter, an outline of different designs and discuss of the merits and limitations of each alternative configuration for adsorption solid desiccant cooling/heating systems is presented. The discussion centres on assessing each configuration's strengths and weaknesses and identify the most promising option that effectively addresses the research gaps identified earlier. Through this systematic evaluation, we can determine which configuration aligns best with the research objectives and demonstrates the most potential for fulfilling the identified research gaps.

The main design innovation considered in this work relates to the way in which the solid desiccant is circulated hermitically between the heat source and heat sink.

4.2 Proposed adsorption design arrangements

The following discuss the configuration of four main designs:

4.2.1 Design arrangement 1: Adsorption-partial resorption out-of-phase configuration

Working principle: A simplified schematic of the arrangement is shown in Fig 4-1, this arrangement consists of two adsorbent beds, a refrigerant receiver, a condenser and an evaporator. In this arrangement, it is envisaged that the adsorber and disorber operate out of phase but continuously by combining the two processes. As the pressure of the desorber is being raised to that of condenser due to heating, desorption of the adsorbate is being initiated. The desorbed high pressure gaseous adsorbate enters the condenser through one-way valve, DC, and is liquefied and collected into the receiver. This adsorbate passes through the throttling device and enters the evaporator as a low pressure liquid adsorbate. Later, it begins to boil due to heat gain from the evaporator load and consequently, as the adsorber pressure reaches that of the evaporator, it gets adsorbed through one-way valve, AE, by the adsorbent in the adsorber thereby producing cooling in the evaporator. This absorbate later get re-absorbed into the desorber for another cycle. It is envisaged that part of the boiling adsorbate would move back to the desorber through one-way valve, DE, through diffusion process.

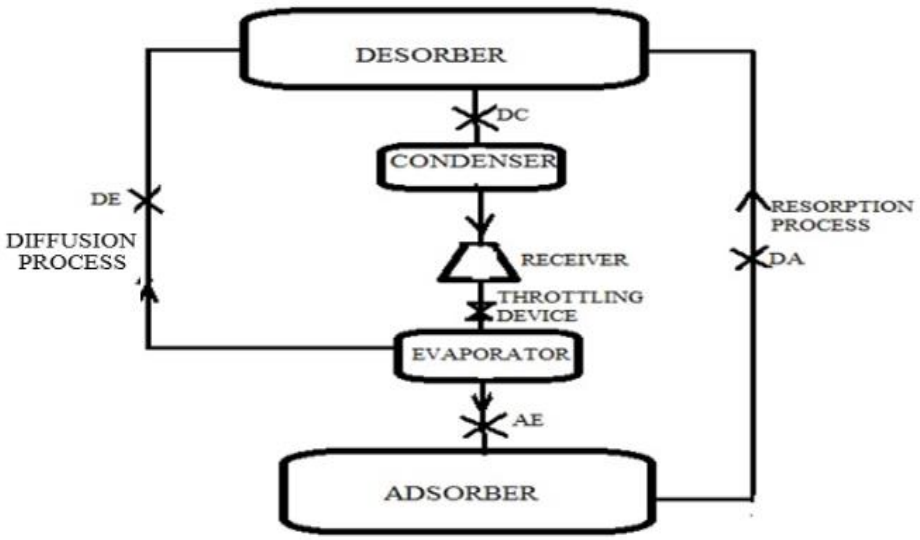


Fig 4-1 Schematic of proposed design arrangement 1

Merits and limitations: The integration of adsorption and resorption processes in a single system is a significant advantage as this approach allows for improved energy utilization and enhanced system performance. This combination ensures a continuous and cyclic operation, optimizing the overall cooling/heating process. In addition, the utilization of separate beds for adsorption and desorption, without substituting their functions, is important in ensuring effective heat transfers as they are dedicated to their respective roles. This leads to stable and reliable system performance, avoiding potential issues that might arise from bed substitution during the cooling/heating cycle. The described configuration, though, is still mechanically complex as isolation of different processes and components will require opening and closing many valves which are prone to premature failure and fluid leakage. Importantly, the major drawback of this design is that there will be partial resorption process of the adsorbate into the desorber. This is because heating of the adsorber is still needed to regenerate. Hence, the desorber and the adsorber are not totally out of phase.

4.2.2 Design arrangement 2: The rotary desiccant wheel configuration

Working principle: Fig 4-2 illustrates a configuration where a desiccant wheel is divided into two sections: the adsorbing and desorbing sections. In this setup, the low-pressure and low-temperature adsorbate vapour from the evaporator is introduced into the adsorption section of the system. The transfer of the adsorbate releases heat during the adsorption process. The continuous rotation of the desiccant wheel allows the saturated section of adsorber to enter the desorption section and release the absorbate and the equivalent disrobed section to enter the adsorption section again, creating a full cycle of adsorption and desorption.

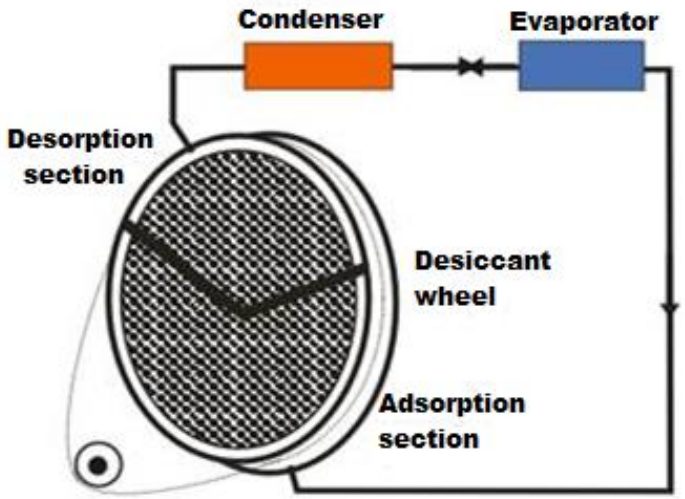


Fig 4-2 Schematic of proposed design arrangement 2

The desorbed adsorbate then enters the condenser, where it is cooled and its temperature is subsequently reduced. The high pressure adsorbate enters the evaporator through an expansion valve reducing its pressure and temperature which allows it to absorb heat from the evaporator. The low-pressure adsorbate vapour from the evaporator, in turn, re-enters the adsorption section, initiating

another adsorption cycle. While this arrangement offers design merits, it also presents certain limitations.

Merits and limitations: The proposed design arrangement presents several noteworthy credits that improve energy performance. For example, the integration of a rotary adsorbent bed enables continuous and uninterrupted adsorption and desorption processes, enhancing the overall system performance. It also eliminates the need for complex valves for refrigerant and hot/cold fluid, simplifying the system's mechanical components. Equally, the self-regenerating capability of the system eliminates the need for a circulating heating or cooling medium, streamlining the design and reducing energy consumption. Additionally, the continuous adsorption and desorption processes ensure a consistent and stable cooling output with low-energy continuous wheel rotation mechanism which contributes to improved energy efficiency.

On the other hand, one of the major likely drawbacks is sealing issues. That is, separating the low pressure region from the high pressure one. In addition, since the system is anticipated to be self-regenerating, there will be a high demand for thorough insulation and airproofing in order for the energy released at the adsorption section of the wheel to be optimally retrieved at the desorption section. Another likely drawback is the use of external transmission equipment for the rotation of the adsorbent wheel.

4.2.3 Design arrangement 3: Desiccant-circulator-aided fluidised adsorbent bed

Working principle: In this configuration, the utilization of a fluidized adsorbent bed is considered, where the solid adsorbent undergoes continuous

movement between the heat source (for heating/desorption) and the heat sink (cooling/adsorption), as depicted in Fig 4-3. This innovative approach enables an uninterrupted operation, facilitating both cooling and heating processes continuously. However, the main technical challenge is in devising a cost effective method to circulate the solid desiccant without compromising its strength and structural integrity. Overcoming this difficulty will be essential for fluidized adsorbent bed arrangement for efficient and reliable cooling and heating applications.

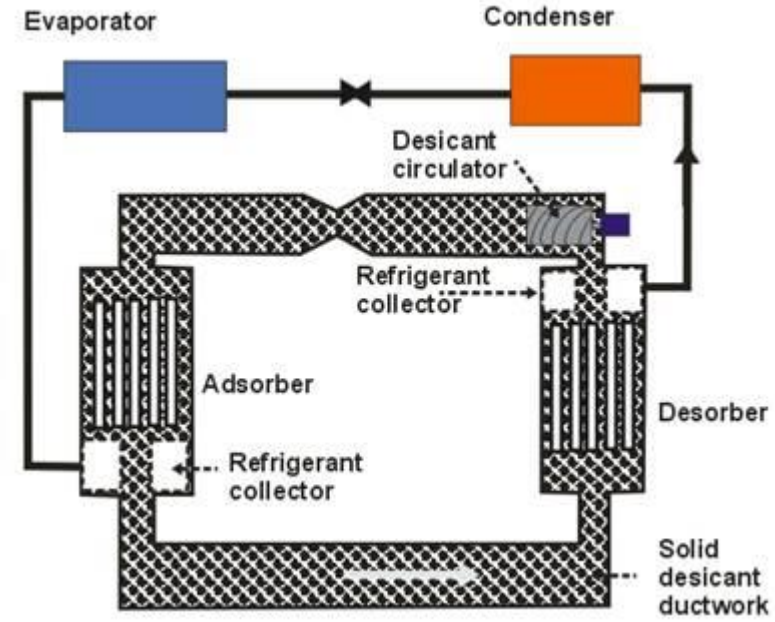


Fig 4-3 Schematic of proposed design arrangement 3

Merits and limitations: This arrangement eliminates complex use of control valves for refrigerant and hot/cold fluid flows for the adsorption and desorption process, reducing potential points of failure and increasing system reliability. In addition, the localization of the heat source and heat sink heat exchangers ensures effective heat transfer in the adsorber and desorber beds. The use of circulating motor/vane mechanism of the solid desiccant increases

the system reliability but equally, it could lead to mechanical failure and requires frequent maintenance. Moreover, this may prove challenging to sealing the refrigerant as well as achieving separation of low-pressure and high-pressure regions within the system. The continuous movement of the desiccant may lead to the possible deterioration of the desiccant materials over time through friction, necessitating careful material selection and monitoring. Lastly, there is a risk of entrainment of solid desiccant particles into the condenser/evaporator circuit, which could cause fouling of the heat exchangers and impact the system's functionality and require appropriate filtration.

4.2.4 Design arrangement 4: Circulating Fluidised Adsorption Refrigeration (CFAR) System

The moving bed concept from the previous design configuration has been retained in this design arrangement. To eliminate the migration of solid desiccant particles into the refrigerant circuit, a mechanical separation component using a cyclone is introduced. This configuration as shown in Fig 4-4 involves the continuous circulation of the fluidized adsorbate-laden-solid adsorbent by means of a cyclone.

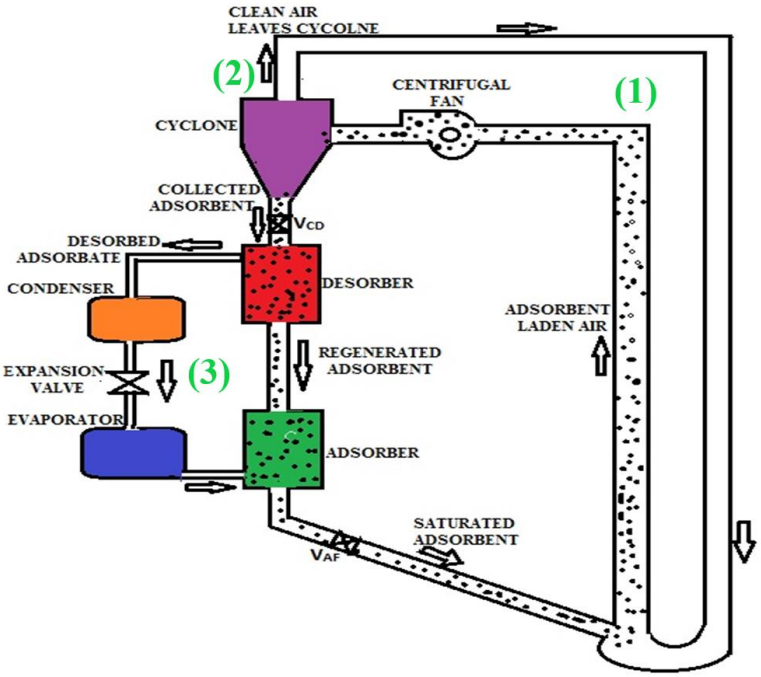


Fig 4-4 Schematic representation of the CFAR system

4.2.4.1 CFAR system Description

The system configuration offers the following advantages:

i. It is a continuous process which can produce refrigeration continuously thereby overcoming the bottleneck of intermittent cold production associated with fixed beds.

ii. Once the system is started up, concentration and temperature profiles are formed and become time invariant, which simplifies the issue of unnecessary load on the evaporator as it is with fixed beds.

iii. In contrast to conventional fixed-bed adsorbers and other continuous systems in the literature, this system does not only stand out because of its continuous cold production, but also because adsorption and desorption processes occur separately (that is, they are separated spatially) and can thus be optimized maximally.

iv. The issue of switching between beds and the use of a reversible pump in the previous works is overcome here. Hence the valves complexity and thermal stress induced in the bed by switching between heating and cooling is completely solved.

v. Heat source and heat sink heat exchanger are localised.

Its anticipated disadvantage is the necessary handling of the solids, which is not the case in fixed-beds. However, as shown in this work, the advantages that can be gained from this configuration outweigh this shortcoming.

As depicted in Fig 4-4, the system comprises three interconnected circuits that work in tandem. These circuits are: (1) the circulatory circuit (CC) that involves a low-energy consumption centrifugal fan and circulating channels (pipes), (2) the separation circuit (SC) consisting of a reverse flow cyclone separator, and (3) the refrigeration circuit (RC) which includes a desorber/regenerator, a condenser, an evaporator, an adsorber, and two 1-way valves, V_{CD} and V_{AF}. The detailed working principle of the CFAR system including its three interconnected circuits represented in Fig 4-4 is discussed in the following sections.

4.2.4.2 Operation principle and components of the system

As schematically represented in Fig 4-4, the adsorbent (already saturated with adsorbate) laden air stream, with the aid of the centrifugal fan, enters tangentially at the top of the cyclone barrel and travels downward into the lower (conical) part as it forms an outer vortex with increasing air velocity which results in a centrifugal effect on the adsorbent particles. Hence, the saturated adsorbent particles are separated from the air stream and enters into

the desorber through the collection pipe (dip leg) while the clean air flows radially inwards to form the inner vortex and then flows out of the cyclone separator into the circulating field (pipe) to be laden again by the adsorbent.

The CFAR system theoretical thermodynamic cycle is depicted in Fig 4-5 in which for a complete thermodynamic operating cycle, the saturated adsorbent enters into the desorber for the regeneration process. The heating of the saturated adsorbent which is at the ambient temperature, T_A and evaporator pressure, P_{eva} starts at point A.

The progressive heating of the desorber during process A→B to the desorption temperature, T_B, consequently raises its pressure to that of the condenser, P_{con}, the point at which the desorber is connected to the condenser. Hence, this initiates desorption of the adsorbate vapour (process C→D) which is liquefied in the condenser during process B→1(condensation). This process ends as the adsorbent reaches its maximum allowable regeneration temperature, T_c, and the adsorbate content reduces to the minimum value. The regenerated adsorbent thereafter flows into the adsorber for the cooling process, C→D and the adsorption process, D→A.

The high pressure liquid adsorbate leaves the condenser and enters through the expansion valve (process 1→2) into the evaporator as a low pressure liquid adsorbate at the evaporator pressure, P_{eva} and temperature, T_{eva}. As it gains heat energy from the load in the evaporator, it begins to boil and as soon as the adsorber pressure reaches the evaporator pressure, P_{eva}, and temperature, T_D, at point D, it then gets adsorbed by the adsorbent in the adsorber thereby producing cooling in the evaporator.

The saturated adsorbent takes its course back into the flow path of the circulating air from the cyclone and then the mixture of the duo is extracted again by the fan into the cyclone to begin another cycle.

A complete thermodynamic operating cycle of the CFAR system as illustrated in Fig 4-5 consists mainly of: The preheating and pressurization of the adsorbent process (A→B), heating and desorption process, (B→C), depressurization and cooling of the adsorbent process, (C→D), cooling and adsorption process (D→A). The pure adsorbate circuit includes sequential processes (B→1), (1→2) and (2→A) which are condensation, isenthalpic expansion (throttling) and evaporation.

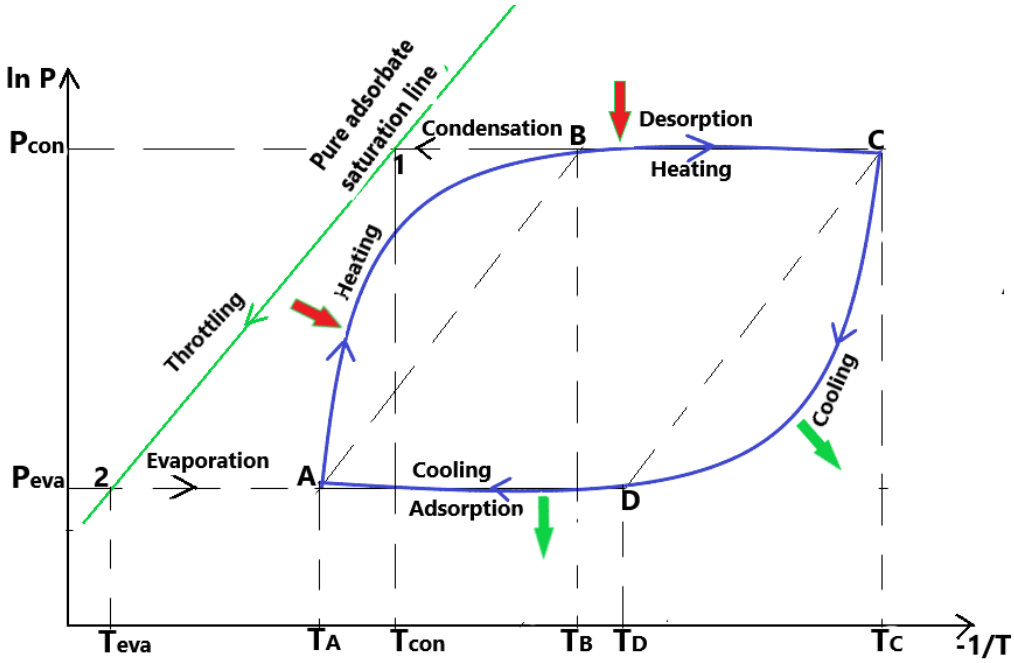


Fig 4-5 Clapeyron diagram for the CFAR cycle

4.2.4.3 Desiccant circuit

As illustrated in Fig. 4-5 and Fig. 4-6, the saturated desiccant takes its route from the cyclone into the desorber at point A to undergo the regeneration/desorption process after which it enters the adsorber with reduced

adsorbate content at point C for the adsorption process. After the completion of the adsorption process, the saturated adsorbent enters with the aid of gravity into the circulatory channels and then get fluidized by the flow path of the clean air stream which is ready to be laden by it. Finally, with the aid of the centrifugal fan, it then enters into the cyclone to begin another cycle.

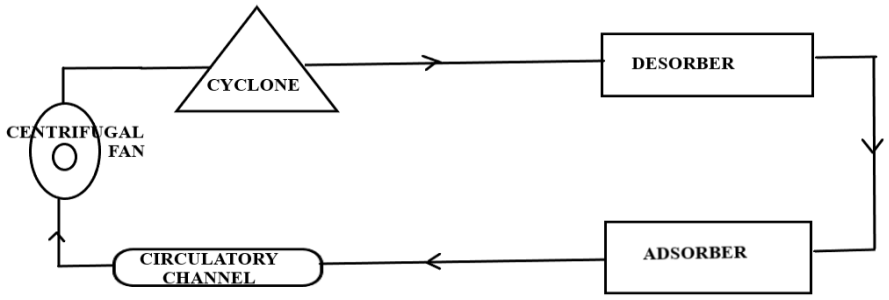


Fig 4-6 The schematic of the desiccant circuit

4.2.4.4 Refrigerant/adsorbate circuit

As illustrated in Fig. 4-5 and Fig 4-7, the circuit of the adsorbate starts from the desorber whose progressive heating initiates the desorption of the refrigerant vapour which then enters into the condenser at point B to be liquefied. The high pressure liquid adsorbate leaves the condenser and then enters into the expansion valve at point 1. It then undergoes an isenthalpic expansion which eventually makes it pressure and temperature to reduce from the condenser pressure, P_{con} and temperature T_{con} to the evaporator pressure, P_{eva} and temperature T_{eva}. The resulting adsorbate enters into the evaporator at point 2 as a low pressure liquid adsorbate which gains heat energy from the evaporator load. It begins boiling and then gets finally adsorbed by the adsorbent in the adsorber thereby producing a cooling effect. Summarily, the

pure adsorbate circuit includes sequential processes (B→1), (1→2) and (2→A) which are condensation, isenthalpic expansion (throttling) and evaporation.

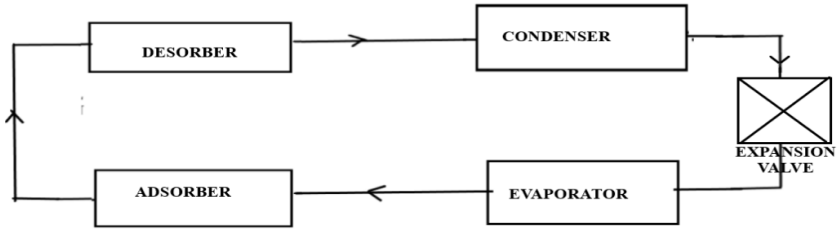


Fig 4-7 The schematic of the refrigerant circuit

4.2.4.5 Desiccant separation

A gas-solid cyclone is introduced into the system to help separate the desiccant particles (already saturated with adsorbate) from the fluid stream by an induced centrifugal force (from a centrifugal fan) which is tangentially imparted on the wall of the cyclone cylinder. This force coupled with the density gradient between the fluid and the solid desiccant particles, increases the relative settling velocity of the solid desiccant particles and thereby driving them towards the cyclone wall where they slide to the particle exit and enter into the desorber through the collection pipe (dip leg) while the clean air flows radially inwards to form the inner vortex and then flows out of the cyclone separator into the circulating field (pipe) to be laden again by the desiccants particles. This vortex cyclonic separation is demonstrated in Fig 4-8 through a typical cyclone separator.

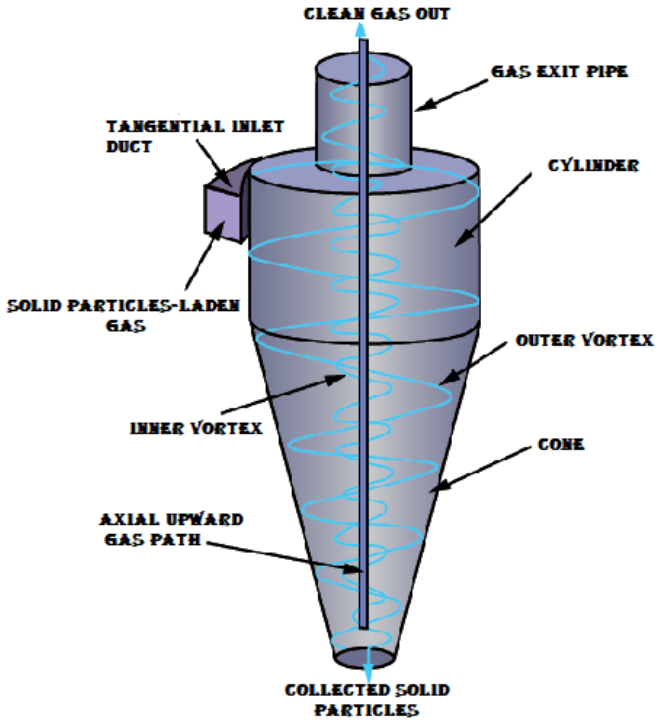


Fig 4-8 A typical cyclone separator [103]

4.2.4.6 System design considerations

(A) Choice of adsorbent (desiccant)

(i) On the basis of circulation consideration

Any adsorbent to be used in a circulating fluidized bed for a continuous circulating mode must satisfy the following primary conditions among others:

i. High attrition/abrasion resistance
ii. High adsorption capacity
iii. Highly and easily generable during multicycle use or continuous circulating mode
iv. Easily fluidizable
v. Appropriate geometric shape and size.

According to Gabelman [104], coconut-derived activated carbons are generally considered high in quality, as evidenced by their high hardness (so they

experience less attrition) low ash content, low dusting tendency, relative ease of generation and high iodine number (high adsorption capacity). Though from the experimental work of Jing and Exell [105], the Thai MD6070 granular activated carbon gave the best adsorptive properties of all the different coconut base activated carbon samples tested, but because the data of its adsorptive and thermal properties are not readily available in the literature, G32-H, a coconut based activated carbon has been chosen for this work.

(ii) On the basis of refrigeration consideration

For refrigerating applications, the adsorbent must have high adsorptive capacity at ambient temperature and low pressures and a small capacity of adsorption at high temperatures and pressures. The cooling effect, or the temperature attained in the evaporator, depends on the adsorptive capacity at small pressures. This is the property that allows the adsorbent, at a given temperature, to retain vapors from a fluid at a lower temperature. On the other hand, the more intense this property is, the higher the adsorbent regenerating temperature is. Thus, choosing the adsorbent will depend on two basic factors: (i) the temperature at which the evaporator must operate; and (ii) the regenerating temperature that the thermal source can possibly attain. [34]

(B) Choice of Adsorbate

According to [34], the choice of the adsorbate, or the working fluid, depends on three main conditions:

i. the evaporator temperature, according to the application;
ii. the latent heat of evaporation, which should be high;

iii. the molecular dimensions, which should be small enough to allow easy adsorption.

Methanol is chosen as the adsorbate in this work because:

i. it evaporates well at a temperature much below 0°C (its melting point is around −93°C);

ii. of its high latent enthalpy of vaporization, L which is ≈1200 kJ/kg at −5°C;

iii. its small molecular diameter (about $4\dot{A}$), which is easily adsorbed in microporous whose diameter is less than 20 Å.

iv. its normal boiling point (~65°C at 1 atm pressure) is much higher than room temperature,

v. of its usage safety consideration which arises from the fact that any abnormality in the machine can be detected before methanol leaks from the system. This is due to the fact that methanol normal boiling point (~65°C at 1 atm pressure) is much higher than the room temperature. Hence, its working pressure is always lower than atmospheric.

(C) Choice of adsorption pair

Zeolite–water and activated carbon–methanol are the most used adsorbent–adsorbate pairs in refrigeration systems. These two pairs have entirely different physical and chemical properties: methanol is easily desorbed from activated carbon when it is heated, while in zeolite, the water is kept much longer. Thus, the activated carbon–methanol pair is best adapted to operating cycles with small evaporating temperature variation (up to 40°C), since adsorption cycles

with the zeolite–water pair need a larger evaporating temperature change (70°C or more) to operate [106]

Another vital consideration in choosing the adsorbent is the possible catalysis of the adsorbate's dissociating reactions. For example, the methanol adsorption in zeolite is restricted to 100 °C as its maximum temperature. At higher values, the zeolite is a catalyst for the methanol → water + dimethyl ether reaction, producing a blockage of the adsorption process. For the activated carbon–methanol pair, this catalyst reaction will only occur above 150°C, which is perfectly suitable for low heat source powered-refrigeration applications [34]. Activated carbon has a significant volume of micropores of convenient size for adsorption.

Therefore, on the basis of the above considerations for both circulation and refrigeration purposes, G32-H which is a coconut-derived activated carbon has been chosen as the adsorbent for this work because of its low desorption temperature and low desorption heat while methanol is chosen as the adsorbate.

4.2.4.7 Theoretical Analysis for the separation circuit

Cyclonic separation is a means of separating different liquid phases (different liquid densities), or, separating solid particles from a gas stream. There are two main designs of cyclone separator, these are the gas-solid cyclone separator and hydrocyclone. Gas-solid cyclone separators are used to remove entrained solid particles from a gas stream while hydrocyclones are used for separating fluids of different densities [107]. Since this present study is concerned about

gas-solid cyclone separator, hence the necessity for a brief review on it before presenting is model formulation.

(i) Gas-solid cyclone separator

Cyclones have been used to remove particulates from gas streams since the middle of the nineteenth century [108].

Cyclones are important devices to control the performance of circulating fluidized beds (CFB) and ensure their stable operation; heat-carrying and/or solid particles being circulated in a CFB should be efficiently separated from gas at a reduced pressure loss during separation [109]. Large recirculation cyclones with high concentrations of particulate solids have gained considerable importance in the field of CFB technology [110].

In a coal-burning power plant utilizing a circulating fluidized bed (CFB) system, cyclones are installed in order to separate solids as efficiently as possible from the exhaust gas and circulate them back to the combustor. In these plants, the solids in the circulating mass are about 90% fly ash of 5 to 500 μm particle size, about 5 to 10% partly burned coal of nearly the same size but lower density, and only about 1 % very fine lime particles of 1 to 15 μm [111]. The solids circulation rate is about 10 times the mass of the feed coal, and the unburnable part of the coal is about 3 to 10%. The solids circulate back to the combustor about 15 to 50 times or more. In petrochemical reactors, the necessary catalyst has to be recirculated to the fluidized bed or a riser [112].

(ii) Advantages of cyclone

The selection of a cyclone separators offers many benefits including simple and reliable component which is easy to integrate into the system.

Furthermore, cyclones are of low capital cost and provide a cost-effective and low maintenance solution for separation of solids. Because they have no moving parts, cyclones are of compact size and have low maintenance needs, reducing the risk of wear and ensuring long-term reliability. Additionally, cyclones exhibit relative power economy, contributing to energy efficiency in the overall system operation. Their flexibility in handling extreme operating conditions is advantageous, as they can be constructed from various refractory and highly corrosion-resistant materials to cater to specific purposes. As indicated by Muschelknautz [113], cyclones can be employed in processes demanding high temperatures, high pressures, and substantial solid loads, such as handling 30 kg solids per kg of gas. Lastly, one of the major benefits of cyclone separators is the ability to reuse separated particles.

(iii) Classification of gas-solid cyclone separator

Gas-solid cyclone separators are generally classified based on their: (i) gas inlet and dust discharge configuration (ii) gas handling capacity and dust removal efficiency and (iii) arrangement.

On the basis of gas inlet and outlet configurations, cyclone can be classified as involute (tangential entry reverse flow cyclone shown in Fig 4-9a), and vane axial (axial entry cyclone shown in Fig 4-9b), types. The only difference between the two is the method of introducing the gas into the cylindrical shell in order to impact sufficient spinning motion. The involute cyclones have a distinctive and easily recognized form and are widely used in power and cement plants, feed mills and many other process industries. Vane axial cyclone units are commonly used in multi cyclone configuration, as they

provide higher efficiencies. In either case, the operation depends on the tendency (inertial) to move in a straight line when the direction of the gas stream is changed. The centrifugal force due to a high rate of spin flings the dust particles to the outer wall of the cylinder and cone. The particles then slide down the wall into the storage hopper. The cleaned air reverses its downward spiral and forms a smaller ascending spiral. A vortex finder tube extending downward into the cylinder aids in directing the inner vortex out of the device. The dust collected is trapped in a collection bin at the base of the cyclone where a rotary valve prevents re-entrainment [114].

When classified by gas handling and collection efficiency, cyclones are typically divided into three types: high efficiency, conventional (medium efficiency) and high through put (low efficiency) cyclones. Though cyclone collectors are designed for many applications, the three cyclone types have the same basic design. Different levels of collection efficiency and operation are achieved by varying the standard cyclone dimensions [103]. For high-efficiency cyclones, the inlet is higher thereby imparting a higher centrifugal force. They are generally less than 1 feet in diameter and have long cones. Heavy particles reach the wall with much smaller angular movement whereas lighter ones travel through much greater angles to reach the wall thereby requiring longer cones [115]. When collection efficiency (80-95 percent) is a primary consideration in cyclone selection, the high-efficiency single cyclone is commonly used. A unit of this type is usually smaller in diameter than others, providing a greater separating force for the same velocity and shorter distance for particles to migrate before reaching the cyclone walls [114].

Furthermore, cyclones are also classified as parallel or series based on arrangement basis. The former is used when very large gas volumes are to be handled and high collection efficiencies are needed while the latter is used when high separation efficiency and higher flow rates of carrier gas are encountered or when it is required to protect a smaller higher efficiency cyclone from large abrasive particles [114].

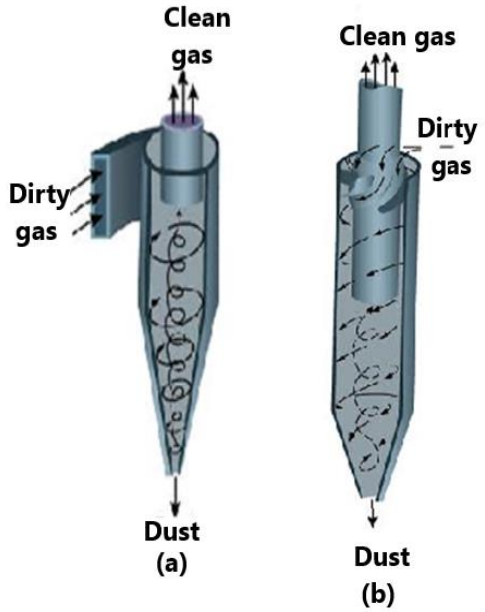


Fig 4-9 Cyclone classification based on gas inlet and dust discharge configuration [103]



Fig 4-10 Cyclones installed for industrial applications [116]

Shown in Fig 4-10 are some cyclones installed for industrial applications for the collection of heavier solid particles.

4.3 Summary

This chapter presented the design, investigation and evaluation of the various possible alternative configurations of adsorption solid desiccant cooling/heating systems in order to evaluate the credits and limitations of each and then ascertain which configuration has the best potential in filling the identified research gaps.

In the quest to meet the aims of this research study, four possible configurations were proposed. The first possible design arrangement is the adsorption-partial resorption out-of-phase configuration. In this configuration, the adsorber and the desorber operate out of phase but continuously. Hence, there is possibility of continuous cold production as there is no substitution of beds. However, there will be partial resorption process as heating is still needed for the considerable mass of the adsorbate to be fully reabsorbed into the desorber.

The rotary desiccant wheel configuration is the second proposed design arrangement in which a desiccant wheel is split into adsorbing and desorbing sections which is anticipated to be self-regenerating. Though the arrangement also appears to have some design merits including continuous cold production, elimination of complex valves for refrigerant and hot/cold fluid circulation but these are far outweighed by its limitations which have been identified as the use of external transmission equipment for the rotation of the adsorbent bed (wheel), insulation and sealing issues.

Another proposed design arrangement is the desiccant-aided fluidised adsorbent bed in which the solid adsorbent will be continuously moved between the heat source (heating/desorption) and the heat sink (cooling/adsorption). This configuration is envisaged to also allow a continuous cold production but the main difficulties are: sealing issues and possibility of circulating the solid desiccant under friction forces without affecting strength and structure integrity.

After a thorough investigation and critical evaluation, a fourth design arrangement called CFAR system was proposed. This configuration which involves the circulation of the fluidized adsorbate-laden-solid adsorbent by means of a cyclone has been identified to have the best potential in filling those identified research gaps because of its laudable credits over others.

Also well covered in this chapter are the CFAR system description and components, its operational principles, its design considerations covering the choice of adsorption pair based on both circulation and refrigeration considerations, and the theoretical basis for the separation unit ranging from: the overview of the solid cyclone separator, the types, the working principles, the classifications and the pertinent benefits of cyclone separator which have favoured its application in this work. Finally, on the basis of some vital design considerations, G32-H, a coconut-derived activated carbon has been chosen as the adsorbent for this work because of its low desorption temperature and low desorption heat while methanol is chosen as the adsorbate.

Chapter 5: Design and mathematical modelling of the proposed circulating fluidised adsorption refrigeration system configuration

5.1 Introduction

In this work, the model formulation for the separation circuit with the circulatory unit is first carried out and this was followed by that of the refrigeration unit.

5.2 Model Formulation for the separation circuit

5.2.1 Cyclone Design

The main parameters that determine the design and performance of a reverse flow cyclone separator are: pressure drop, cut size diameter and the collection/separation efficiency.

Though several models have been developed for the estimation of these parameters, but based on the literature, the best suited model and the most practical method for modelling a tangential inlet reverse flow cyclone separator in the present time is the Muschelknautz method (MM) which has the ability to simulate reality with reasonable precision in most cases of practical interest [117]. This model is able to overcome all the drawbacks in the previous models. Hence, that has been chosen for this work.

5.2.2 Cyclone Geometry

In order to optimize the design of the cyclone for minimum possible pressure drop, the optimal cyclone geometrical ratios which was determined based on the MM model [118] by [119] and was reported to have a collection efficiency equal to the [120] cyclone, but with approximately half the pressure drop, is employed for the design of the cyclone in this work but with a little

modification to S as shown in Table 5-1. The proposed cyclone separator is schematically represented in Fig 5-1. These cyclone dimensions coupled with the parameters given in Table 5-2 are the baseline parameters for simulating and optimizing the cyclone using MATLAB programming language as presented in Appendix A.

5.2.3 Assumptions

Based on some considerations and the recommendations from [117] and [112], the basic assumptions made in modelling the cyclone are:

i. A spherical geometry is assumed for the solid adsorbent particles and their surface/volume mean diameter is taken to be in the range of 50-500μm (0.05-0.5mm).
ii. Net circulation flux of solid adsorbent is substantially between 15-1000 kg/m^2s.
iii. The motion of an adsorbent particle is not influenced by the presence of neighboring particles and their movement relative to the gas stream is given by Stokes' law.
iv. The circulating gas radial velocity is equal to zero.
v. The circulating gas flow is incompressible (constant density).
vi. Buoyancy effects are neglected.
vii. The particles tangential velocity is constant and independent of position.
viii. Particles have to reach a wall by moving across a gas stream, which retains their shapes after leaving the cyclone entry in order to be collected and there is negligible chance of being re-entrained.

ix. Cyclone is assumed to be cylindrical in shape, with Diameter d, and entrance cross-section of a by b.

Table 5-1 Cyclone geometry and dimensions

Cyclone Dimensions			
Parameter	Dimension	Ratio	Value (m)
Cyclone diameter	d	d	0.1
Cyclone inlet height	a	0.62d	0.062
Cyclone inlet width/ diameter	b	0.24d	0.024
Vortex finder diameter	d_v	0.62d	0.062
Cyclone total height	H_t	4.24d	0.424
Cylinder height	h_{cyl}	1.62d	0.162
Cone height	h_{con}	2.62d	0.262
Vortex finder height inside the cyclone	S	$S = a + \frac{d}{8}$ =0.75d	0.075
Particle exit diameter	d_{pe}	0.38d	0.038
Vortex finder height outside the cyclone	L_o	1.62d	0.162

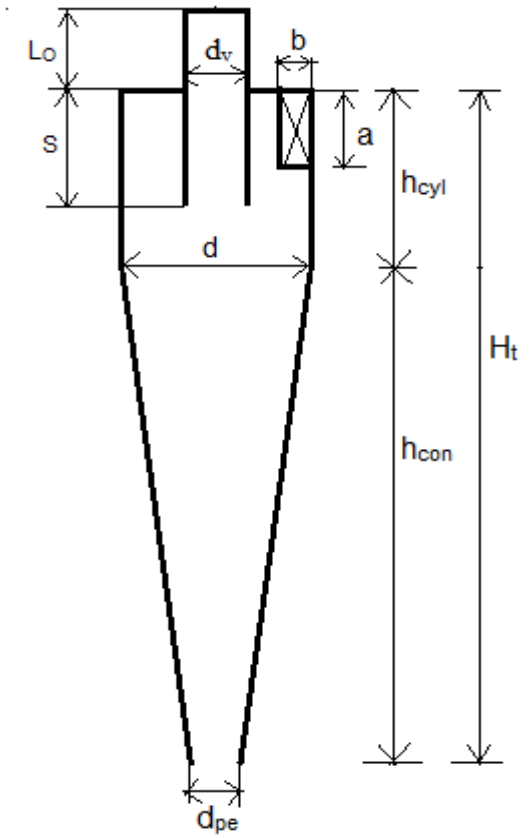


Fig 5-1 Schematic diagram of the proposed cyclone separator

Table 5-2 Simulation Data for cyclone

Parameter	Symbol	Value	Unit
Loading ratio in cyclone inlet	c_o	6	kg/kg
Gas inlet velocity	v_{in}	30	m/s
Gas density	ρ_g	1.2	kg/m^3
Adsorbent particle density	ρ_p	500	kg/m^3
Acceleration due to gravity	G	9.81	m^2/s
Absolute roughness of the inside surface of the cyclone wall	ϵ	0.046×10^{-3}	m
Incoming solid loading in cyclone inlet	c_{o_2}	$0.83c_o$	kg/m^3
Gas dynamic viscosity	μ_g	1.8×10^{-5}	Pa.s
Exponential factor	m	2	
Number of size fraction	n	20	
Mass of solid fed into the cyclone	m_{Sf}	6	kg

5.2.4 Estimation of Pressure drop, (ΔP)

Starting with the pressure drop (ΔP) across the cyclone, based on MM model, the pressure loss across a cyclone would occur primarily because of two factors namely: (a) frictional losses within the cyclone walls or the separation zone, ΔP_{wall} and (b) irreversible local losses within the vortex core due to contraction, ΔP_x . Hence, the overall pressure loss within the cyclone,

$$\Delta P = \Delta P_{wall} + \Delta P_x \quad \ldots\ldots (5.1)$$

With

$$\Delta P_{wall} = \int \frac{A_R}{0.9\dot{Q}} \frac{\rho_g}{2} \ (u_c u_x)^{1.5} \quad \ldots\ldots (5.2)$$

Where

$$\dot{Q} = v_{in} \times a \times b$$

$A_R =$ inside area of the roof + inside area of the barrel cylinder + inside area of the cone + external surface area of the vortex tube

$= A_{Roof} + A_{Barrel} + A_{Cone} + A_{Extvortex}$

$$=\pi\left[r^2 - {r_v}^2 + 2r(H_t - H_{cn}) + \left(r + r_{pe}\right)\sqrt{{H_{cn}}^2 + \left(r - r_{pe}\right)^2} + 2r_v S\right] \ldots (5.3)$$

The total frictional drag, ƒ, within the cyclone is estimated by the contributions of both the drag on the dry gas, $ƒ_{gas}$ and the additional one imposed by the moving strands of solid adsorbents present at the wall, $ƒ_{particle}$ as shown below:

$$ƒ = ƒ_{gas} + ƒ_{particle} \ldots\ldots\ldots\ldots\ldots\ldots\ldots\ldots\ldots\ldots\ldots\ldots\ldots\ldots\ldots\ldots\ldots\ldots\ldots\ldots\ldots\ldots (5.4)$$

$$ƒ_{particle} = 0.015\sqrt{c_o} \ldots\ldots\ldots\ldots\ldots\ldots\ldots\ldots\ldots\ldots\ldots\ldots\ldots\ldots\ldots\ldots\ldots\ldots\ldots\ldots\ldots\ldots (5.5)$$

$ƒ_{gas}$, the friction coefficient of the dry gas, is dependent on the cyclone size, the relative roughness (ϵ/r) and the Reynolds number (Re_c) characterizing the cyclone. Therefore,

$$ƒ_{gas} = ƒ_{sw} + ƒ_{rw} \ldots\ldots\ldots\ldots\ldots\ldots\ldots\ldots\ldots\ldots\ldots\ldots\ldots\ldots\ldots\ldots\ldots\ldots\ldots\ldots\ldots\ldots (5.6)$$

For conical-bodied cyclone

$$ƒ_{sw} = 0.323Re_c^{-0.623} \ldots\ldots\ldots\ldots\ldots\ldots\ldots\ldots\ldots\ldots\ldots\ldots\ldots\ldots\ldots\ldots\ldots\ldots\ldots\ldots\ldots\ldots (5.7)$$

$$ƒ_{rw} = \left(\log\left(\frac{1.60}{\frac{\epsilon}{r} - 0.000599}\right)^{2.38}\right)^{-2}\left(1 + \frac{2.25 \times 10^5}{Re_c^2\left(\frac{\epsilon}{r} - 0.000599\right)^{0.213}}\right)^{-1} \ldots\ldots\ldots\ldots\ldots\ldots\ldots\ldots (5.8)$$

For cylindrical-bodied cyclone

$$ƒ_{sw} = 1.51Re_c^{-1.0} \ldots\ldots\ldots\ldots\ldots\ldots\ldots\ldots\ldots\ldots\ldots\ldots\ldots\ldots\ldots\ldots\ldots\ldots\ldots\ldots\ldots\ldots (5.9)$$

$$ƒ_{rw} = \left(\log\left(\frac{1.29}{\frac{\epsilon}{r} - 0.000599}\right)^{2.59}\right)^{-2}\left(1 + \frac{2.14 \times 10^5}{Re_c^{1.64}}\right)^{-1} \ldots\ldots\ldots\ldots\ldots (5.10)$$

With the value for the relative roughness of a smooth-walled cyclone, $\frac{\epsilon}{r} \geq 0.0006$. The cyclone Reynolds number (Re_c) is given by:

$$Re_c = \frac{Re_{ge}}{4\frac{H_t}{d_v}\left(\frac{d}{d_v} - 1\right)} \dots\dots\dots\dots\dots\dots\dots\dots\dots\dots\dots\dots\dots\dots\dots\dots\dots\dots\dots (5.11)$$

with the exit pipe Reynolds number (Re_{ge}) given by:

$$Re_{ge} = \frac{\rho_g v_m d_v}{\mu_g} \dots\dots\dots\dots\dots\dots\dots\dots\dots\dots\dots\dots\dots\dots\dots\dots\dots\dots\dots\dots (5.12)$$

where $v_m = \frac{0.9\dot{Q}}{\pi(r^2 - r_{cm}^2)}$ and $r_{cm} = \sqrt{r r_v}$.

The second contribution to the overall pressure loss which is the loss in the core and in the vortex finder can be estimated by

$$\Delta P_x = \left[2 + 3\left(\frac{u_x}{v_x}\right)^{1.33} + \left(\frac{u_x}{v_x}\right)^2\right]\frac{\rho_g}{2}\, v_x^2 \dots\dots\dots\dots\dots\dots\dots\dots\dots\dots\dots\dots\dots (5.13)$$

With $v_x = \frac{\dot{Q}}{\pi r_v^2}$ and

$$u_x = u_c \frac{(r/r_v)}{\left[1 + \frac{f A_R u_c \sqrt{r/r_v}}{2\dot{Q}}\right]} \dots\dots\dots\dots\dots\dots\dots\dots\dots\dots\dots\dots\dots\dots\dots\dots\dots\dots (5.14)$$

with $u_c = \frac{v_{in} r_{in}}{\alpha r}$, and $r_{in} = (r - \frac{b}{2})$

$$\alpha = \frac{1}{\xi}\left\{1 - \sqrt{1 + 4\left[\left(\frac{\xi}{2}\right)^2 - \frac{\xi}{2}\right]\sqrt{1 - \frac{(1-\xi^2)(2\xi - \xi^2)}{1 + c_o}}}\right\} \dots\dots\dots\dots\dots (5.15)$$

where $\xi = \frac{b}{r}$

5.2.5 Estimation of the Cut size diameter, x_{50}

This is the size of the solid adsorbent particles particle that will be removed from the gas stream with 50% efficiency. It is an indicator of the size range of the solid adsorbent particles that can be collected. Particles larger than x_{50} will

be removed with a greater efficiency and smaller particles with a lower efficiency.

$$x_{50} = \sqrt{\frac{18\mu_g(0.9\dot{Q})}{2\pi(\rho_p - \rho_g)u_x^2(H_t - S)}} \quad \ldots\ldots\ldots\ldots\ldots\ldots\ldots\ldots\ldots\ldots\ldots\ldots\ldots\ldots\ldots\ldots\ldots\ldots (5.16)$$

For $Re_P < \sim 0.5$ (particle settling in the Strokes' law regime)

Where $Re_P = \frac{\rho_g u_{t50} x_{50}}{\mu_g}$ with $u_{t50} = \frac{\dot{Q}}{2\pi r_v (H_t - S)}$

For $0.5 < Re_P < 1000$ (Strokes' law not holding)

$$x_{50} = 5.18 \frac{\mu_g^{0.375} \rho_g^{0.25} u_{t50}^{0.875}}{\left[\frac{(\rho_p - \rho_g)u_x^2}{r_v}\right]^{0.625}} \quad \ldots\ldots\ldots\ldots\ldots\ldots\ldots\ldots\ldots\ldots\ldots\ldots\ldots\ldots\ldots\ldots\ldots\ldots (5.17)$$

5.2.6 Cyclone overall separation/collection efficiency, η_t

The separation characteristics of a cyclone are best described by the so-called grade-efficiency curve (GEC), which is the separation efficiency for a given feed particle size or (narrow) range of particles sizes [117]. The particle feed size distribution shown in Table 5.3 is used for this work.

Before determining the cyclone efficiency, it is imperative to first determine whether mass loading effect (saltation) occurs or not because based on MM model, the quantity of the solid adsorbents (limiting loading, c_{oL}) that the gas can hold in turbulent suspension as it enters into the cyclone is dependent on: the intermediate (that is, the median) particle size of the feed (x_{median}), the cut-point diameter (x_{50}) and to a slight extent, on the inlet loading (c_o).

$c_{oL} = 0.025 \left(\frac{x_{50}}{x_{median}}\right) (10\, c_o)^{0.15}$ for $c_o \geq 0.1$ and

$c_{oL} = 0.025 \left(\frac{x_{50}}{x_{median}}\right) (10\, c_o)^{k}$ for $c_o < 0.1$

Where $k = -0.11 - 0.10 \ln c_o$

Table 5-3 Particle feed size distribution

Particle size in range, x_i (μm)	50	100	150	200	250	300	350	400	450	500
Mass fraction W_i	0.05	0.10	0.10	0.20	0.15	0.15	0.10	0.05	0.05	0.05

If $c_o < c_{oL}$, no saltation or mass loading condition: which may be due to some factors like: low solid adsorbent loadings, c_o, a fine feed particle size distribution (that is, small x_{median}) and a large x_{50}.

$$\eta_t = \sum_{i=1}^{n} \eta_i \times W_i \quad (5.18)$$

where

$$\eta_i = \frac{1}{1 + \left(\frac{x_{50}}{x_i}\right)^m} \quad (5.19)$$

If $c_o > c_{oL}$ (saltation or mass loading condition occurs), the overall efficiency, η_t is the summation of the efficiency due to saltation in the inlet and that due to classification in the inner vortex. This implies that a proportion of the incoming adsorbent solids that is not captured in the outer vortex is thereby collected through the inner one.

$$\eta_t = \left(1 - \frac{c_{oL}}{c_o}\right) + \left(\frac{c_{oL}}{c_o}\right) \sum_{i=1}^{n} \eta_i \times W_i \quad (5.20)$$

The solid mass loading, c_o entering the cyclone inlet is estimated by:

$$Solid\ mass\ loading = \frac{mass\ of\ solid\ adsorbent\ fed\ into\ the\ cyclone}{mass\ of\ circulating\ gas\ entering\ into\ the\ cyclone}$$

$$c_o = \frac{m_{Sf}}{m_g} \quad \ldots \ldots \ldots \ldots \ldots \ldots \ldots \ldots \ldots \ldots \ldots \ldots (5.21)$$

5.2.7 Number of effective turns, Ne

The number of effective turns of a cyclone is the number of revolutions that the gas would complete while passing through the cyclone outer vortex. The model developed by [121] is used for the calculation of Ne in this work as follows:

$$Ne = \frac{1}{a}\left(h_{cyl} + \frac{h_{con}}{2}\right) \quad \ldots \ldots \ldots \ldots \ldots \ldots \ldots \ldots \ldots (5.22)$$

5.2.8 Power Requirement, P

The power (in Watts) required for the centrifugal fan is

$$P_f = \dot{Q} \times \Delta P \quad \ldots \ldots \ldots \ldots \ldots \ldots \ldots \ldots \ldots \ldots \ldots \ldots (5.23)$$

5.2.9 Solid circulating rate, $\dot{M}_{sc}$

The rate of solid adsorbent circulation or flow is

$$\dot{M}_{sc} = c_{o_2} \times \dot{Q} \quad \ldots \ldots \ldots \ldots \ldots \ldots \ldots \ldots \ldots \ldots \ldots \ldots (5.24)$$

5.2.10 Gas residence time, τ_R

For particles to be effectively collected, they must strike the wall within the amount of time that the conveying gas travels through the outer vortex. Hence,

$$\tau_R = \frac{Travelled\ distance}{Velocity} = \frac{\pi d Ne}{v_{in}} \quad \ldots \ldots \ldots \ldots \ldots \ldots \ldots (5.25)$$

5.2.11 Terminal settling velocity of solid adsorbent, u_{sc}

$$u_{sc} = \frac{b}{\tau_R} \ldots \ldots \ldots \ldots \ldots \ldots \ldots \ldots \ldots \ldots \ldots \ldots \ldots \ldots \ldots \ldots \ldots \ldots \ldots \ldots \ldots \ldots \ldots \ldots .. (5.26)$$

5.2.12 Determination of mass of solid adsorbent collected, m_c

$$Overall\ collection\ efficiency = \frac{mass\ of\ solid\ adsorbent\ collected}{mass\ of\ solid\ adsorbent\ fed\ into\ the\ cyclone}$$

$$\eta_t = \frac{m_c}{m_{Sf}} \ldots \ldots \ldots \ldots \ldots \ldots \ldots \ldots \ldots \ldots \ldots \ldots \ldots \ldots \ldots \ldots \ldots .. \ldots \ldots \ldots \ldots . (5.27)$$

Hence, the mass of the solid adsorbent collected from the cyclone particle exit is estimated by:

$$m_c = \eta_t \times m_{Sf} \ldots \ldots \ldots \ldots \ldots \ldots \ldots \ldots \ldots \ldots \ldots \ldots \ldots \ldots \ldots \ldots \ldots \ldots \ldots \ldots (5.28)$$

This collected mass is the amount entering the desorber of the RC at a velocity of u_{sc}.

5.3 Model Formulation for the Adsorption refrigeration circuit

Mathematical modelling of the adsorption refrigeration system is highly important to give an overall representation of the system performance. The mathematical models which are generally used to simulate adsorption cooling system can be grouped into three, which are: lumped parameter model, heat and mass transfer model, and thermodynamic model [62, 122-124].

In order to dynamically study the adsorption circuit of the CFAR system, there is a need to model the adsorption kinetics, mass and energy balance within it. This is based on the heat and mass transfer (distributed parameter) model.

5.3.1 Assumptions

The following simplifying assumptions were applied to develop the model:

i. The system is modeled as a one-dimensional system since the variation of the adsorbent temperature and the concentration is more dominant along the axial direction.

ii. Hysteresis in the sorption isotherm, the heats of sorption and in the adsorbent flow are negligible.

iii. Thermal and mass dispersion in the porous medium are negligible.

iv. The transport of the adsorbate within the moving adsorbent due to capillary motion is negligible.

v. The gaseous adsorbate behaves as an ideal gas.

vi. The speed and the mass flow rate of the adsorption pair stream are constant.

vii. The temperature of the heating/cooling medium is constant and hence not modelled.

viii. The local thermal equilibrium is satisfied, that is, the adsorbent and the adsorbate have the same temperature.

ix. Adsorbent particles are homogeneous, isotropic and incompressible.

x. The thermodynamic properties of most of the model parameters are considered to be constant. The adsorption equilibrium relation is, however, nonlinear.

xi. Convective mass transfer, heat losses due to radiation, viscous dissipation and the work done by pressure changes are neglected.

xii. The inlet condition of the adsorbent into adsorber is the same with its outlet condition from the desorber for any cycle in the system.

Based on the above assumptions, the isotherm, energy and mass balance equations are formulated as follows:

5.3.2 The isotherm equation

The equilibrium adsorption or desorption quantity at any state is determined by the Dubinin–Astakhov (D–A) equation [125] and [89] as given below:

$$q(T,P) = q_o exp\left[-D\left(Tln\left(\frac{P_{sat}(T)}{P}\right)\right)^n\right] \ldots\ldots\ldots\ldots\ldots\ldots\ldots\ldots\ldots\ldots\ldots\ldots\ldots (5.29)$$

Where $P_{sat} = 133.33\exp\left(A - \frac{B}{(T+C)}\right)$ P_{sat} in Pascal and T in Kelvin as given by [8].

For the pair of activated carbon-methanol considered in this study, the above adsorptive properties according to [126], thermophysical properties as reported by [127] and the values of A,B and C as given by [128] and [129] are all given in Table 5-4. Since this system is primarily aimed at solving energy problems in the rural countries of Africa, the reference-environment (ambient) conditions used in this work are set to the mean ambient conditions of Nigeria while the condenser and the evaporator pressures are set to a value which corresponds to the saturation temperature of T_C (condenser temperature) and T_E (evaporator temperature) respectively. T_C and T_E were chosen based on the general rule of thumb for an air-cooled condenser in a normal climate and for a cold room evaporator respectively with reference to the chosen ambient conditions.

5.3.3 Adsorber/Desorber configuration

The desorber/adsorber as shown in Fig 5-2 is basically of a cylindrical geometry which consists of an inner heat transfer tube containing the

heating/cooling medium and an outer tubular shell which has a vapour mesh that serves as the outlet/inlet for the adsorbate vapour at one of its side. The radial space (R-r) between the duo along their length is filled with the moving solid adsorbent particles during their transit.

Table 5-4 System and operating parameters for the adsorption refrigeration unit simulation

Parameter	**Symbol**	**Value**	**Unit**
Specific heat of adsorbent	Cp_{sc}	920	J/kgK
Specific heat of adsorbate	Cp_{ads}	2534	J/kgK
Density of adsorbent	ρ_{sc}	370	kg/m^3
Ambient temperature	T_{amb}	26.9	℃
Condenser temperature	T_C	35	℃
Evaporator temperature	T_E	15	℃
Cooling temperature	T_L	30	℃
Heating temperature	T_H	100	℃
Latent heat of vaporization of adsorbate	L_v	1102×10^3	J/kg
Maximum adsorption capacity (G32-H)	q_0	0.38	kg/kg
Adsorption parameter	D	1.94×10^{-8}	K^{-1}
Adsorption parameter	n	2.59	
Adsorption parameter	A	18.587	
Adsorption parameter	B	3626.55	
Adsorption parameter	C	-34.29	
Desorption Time	$TimeMax_{des}$	120	s
Adsorption Time	$TimeMax_{ads}$	120	s
Height of adsorber/desorber	H	0.5	m
Thermal conductivity of adsorbent	k_{sc}	0.5	$Wm^{-1}K^{-1}$
Mass of adsorbent	M_{sc}	6	kg
Activation energy	E_a	40×10^3	J/mol
Universal gas constant	R	8.3145	$J/mol\,.K$
Pre-exponential coefficient of Arrrhenius equation	D_O	3.9×10^{-2}	m^2/s
Adsorbent porosity	ε	0.7	
Heat of sorption	H_S	1900×10^3	J/kg
Adsorbent flow velocity	u_{sc}	0.49	m/s

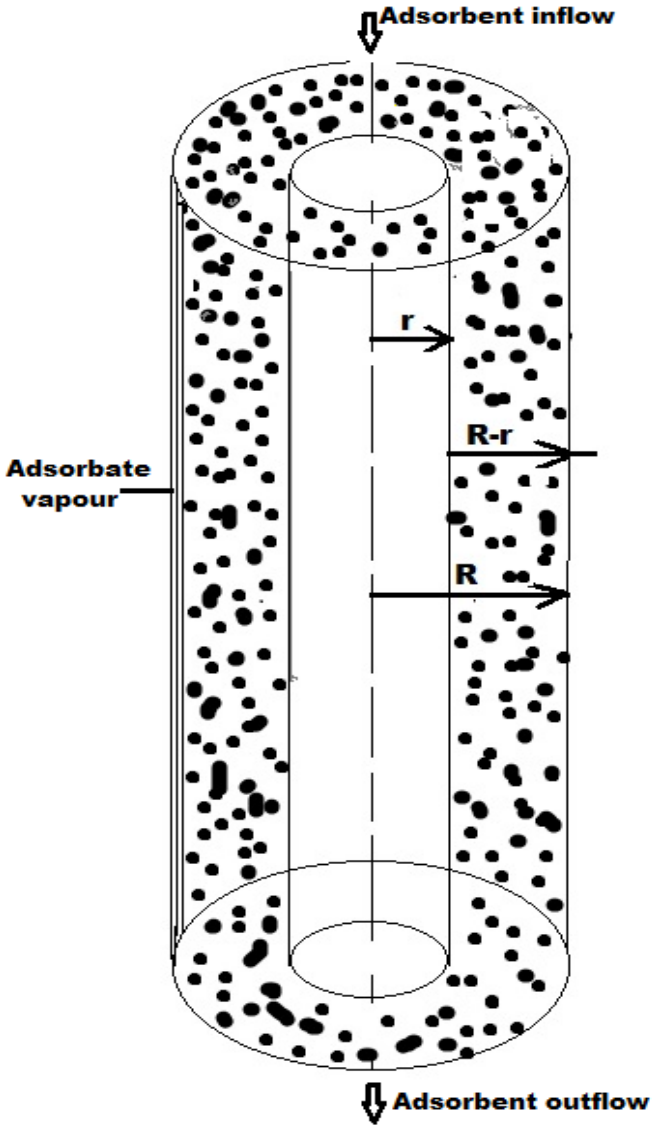


Fig 5-2 A schematic representation of the Desorber/Adsorber

5.3.4 Energy balance

Neglecting the convective heat transfer between the adsorbent and adsorbate, the energy balance for the adsorbent is:

$$\rho_{sc}\left(C_{P_{sc}} + qC_{P_{ads}}\right)\frac{\partial T_{sc}}{\partial t} + \bar{u}_{sc}\rho_{sc}\left(C_{P_{sc}} + qC_{P_{ads}}\right)\frac{\partial T_{sc}}{\partial z}$$

$$= k_{sc}(1-\varepsilon)\frac{\partial^2 T_{sc}}{\partial z^2} + \rho_{sc}H_S\frac{\partial q}{\partial t} \ldots\ldots\ldots\ldots\ldots\ldots\ldots\ldots\ldots\ldots (5.30)$$

The first term on the left-hand side (LHS) of equation (30) represents the rate of internal energy change in the adsorption pair. The second term is the convective heat transfer term, that is, the spatial energy change in the adsorption pair due to flow in the axial direction. The first term on the right-hand side (RHS) stands for conduction heat fluxes due to inflow and outflow of adsorption pair which is the diffusion term. The last term on the RHS stands for the latent heat of desorption/adsorption which is proportional to the variation in the uptake/release of adsorbent vapour. This is known as the heat source term.

5.3.5 The overall mass balance/conservation

Neglecting the influence of the vapour velocity (external mass transfer resistance) for convective mass transfer on the mass change of the adsorbate, the following equation is arrived at for the mass balance.

$$\varepsilon \frac{\partial \rho_{ads}}{\partial t} + \bar{u}_{sc} \frac{\partial \rho_{ads}}{\partial z} + (1-\varepsilon)\rho_{sc} \frac{\partial q}{\partial t} = D_S \frac{\partial^2 \rho_{ads}}{\partial z^2} \ldots\ldots\ldots\ldots\ldots\ldots\ldots\ldots (5.31)$$

The effective diffusion coefficient, D_S, can be estimated from the Arrhenius equation: $D_S = D_O exp^{\left(\frac{-E_a}{RT}\right)}$.

The first term on the LHS of equation 5.31 represents the temporal variation or accumulation in the adsorbate mass. The second term is the changes in its convective flow while the third term is the temporal adsorption changes which is the rate of adsorption. The RHS term is the axial material flow which is the diffusion term.

From the assumptions of local thermal equilibrium and the ideal gas, $\rho_{ads} = \frac{P_{ads}M_{ads}}{RT_{sc}}$ which if substituted into equation 5.31 gives equation 5.32 from which the variation of the adsorbate vapour pressure is estimated.

$$\frac{\varepsilon M_{ads}}{RT_{sc}}.\frac{\partial P_{ads}}{\partial t} + \frac{\bar{u}_{sc}M_{ads}}{RT_{sc}}.\frac{\partial P_{ads}}{\partial z} + (1-\varepsilon)\rho_{sc}\frac{\partial q}{\partial t} = \frac{D_S M_{ads}}{RT_{sc}} \ldots\ldots\ldots\ldots 5.32)$$

5.3.6 Initial and Boundary conditions

In solving equations 5.29 to 5.32, the following initial and boundary conditions are considered:

Initial conditions: The temperature, pressure and the adsorbate concentration in the axial direction are initially considered to be uniform.

$T_{sc}(z,0) = 30℃$, $q(z,0) = q_o$, $P(z,0) = P_E$

Boundary conditions: It is assumed that the conditions of the adsorbent solid particles in terms of temperature, pressure and the adsorbate concentration at the exit of the desorber and the inlet of the adsorber are uniform. Hence,

$T_{sc}(0,t) = 30℃$

$T_{sc_{Desorber_exit}} = T_{sc_{Adsorber_inlet}}$

$q_{Desorber_exit} = q_{Adsorber_inlet}$

$P_{Desorber_exit} = P_{Adsorber_inlet}$

5.3.7 Method of numerical solution

The heat and mass balance models involve a set of partial differential equations (PDEs) which are coupled through the adsorption isotherm/kinetics as well as the boundary conditions and so non-linear. As they cannot be solved

analytically, numerical simultaneous technique will be required to arrive at an approximate solution that will best predict the system. Shown in Fig 5-3 is a discretized elemental volume of the model.

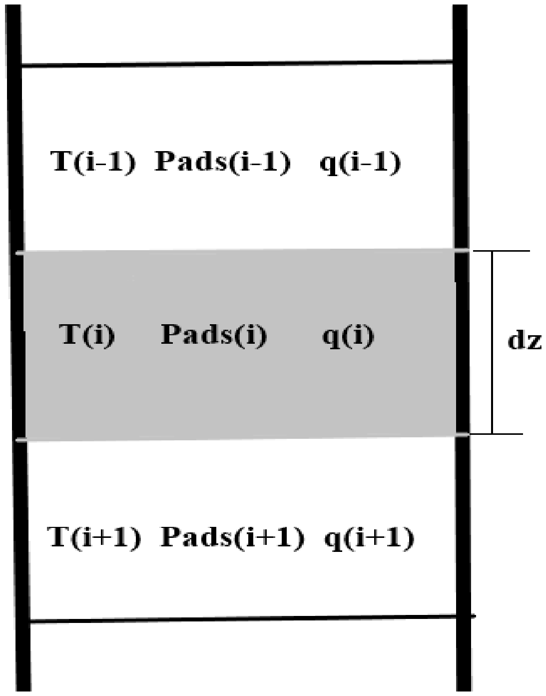


Fig 5-3 Elemental discretized volume of the model

The governing equations are approximated numerically by the explicit finite difference scheme (EFDM) with forward difference scheme in time and central difference scheme in space. The convection term is approximated by the Leap frog scheme. The System and operating parameters for this simulation are given in Table 5-4.

5.3.8 Discretization of the governing equations

The derivatives of the energy balance equation are discretized as follows:

$$\frac{\partial T_{sc}}{\partial t} = \frac{T_{sci}^{m+1} - T_{sci}^{m}}{\Delta t} \quad (5.33)$$

$$\frac{\partial T_{sc}}{\partial z} = \frac{T_{sci+1}^{m} - T_{sci-1}^{m}}{2\Delta z} \quad (5.34)$$

$$\frac{\partial^2 T_{sc}}{\partial z^2} = \frac{{T_{sci+1}}^m - 2{T_{sci}}^m + {T_{sci-1}}^m}{(\Delta z)^2} \ldots\ldots\ldots\ldots\ldots\ldots\ldots\ldots\ldots\ldots\ldots\ldots\ldots (5.35)$$

$$\frac{\partial q}{\partial t} = \frac{{q_i}^{m+1} - {q_i}^m}{\Delta t} \ldots\ldots\ldots\ldots\ldots\ldots\ldots\ldots\ldots\ldots\ldots\ldots\ldots\ldots\ldots\ldots\ldots\ldots\ldots (5.36)$$

Substituting these into (5.33), (5.34), (5.35) and (5.36) into (5.30) gives

$$\begin{aligned}&\left(\rho_{sc} C_{P_{sc}} + \rho_{sc} q C_{P_{ads}}\right) \frac{{T_{sci}}^{m+1} - {T_{sci}}^m}{\Delta t} \\ &+ \left(\bar{u}_{sc} \rho_{sc} C_{P_{sc}} + \bar{u}_{sc} \rho_{sc} q C_{P_{ads}}\right) \frac{{T_{sci+1}}^m - {T_{sci-1}}^m}{2\Delta z} \\ &= \left(k_{sc}(1-\varepsilon)\right) \frac{{T_{sci+1}}^m - 2{T_{sci}}^m + {T_{sci-1}}^m}{(\Delta z)^2} \\ &+ (\rho_{sc} H_S) \frac{{q_i}^{m+1} - {q_i}^m}{\Delta t} \ldots\ldots\ldots\ldots\ldots\ldots\ldots\ldots\ldots\ldots\ldots\ldots\ldots\ldots (5.37)\end{aligned}$$

Which is solved for ${T_{sci}}^{m+1}$ as follows

$$\begin{aligned}{T_{sci}}^{m+1} &= {T_{sci+1}}^m \left(\frac{\beta_{sc}}{{\gamma_i}^m} - \alpha_{sc}\right) + {T_{sci}}^m \left(1 - \frac{2\beta_{sc}}{{\gamma_i}^m}\right) + {T_{sci-1}}^m \left(\frac{\beta_{sc}}{{\gamma_i}^m} + \alpha_{sc}\right) \\ &+ \frac{H_S}{{\gamma_i}^m} ({q_i}^{m+1} - {q_i}^m) \ldots\ldots\ldots\ldots\ldots\ldots\ldots\ldots\ldots\ldots\ldots\ldots\ldots\ldots\ldots (5.38)\end{aligned}$$

With $\alpha_{sc} = \frac{\Delta t \bar{u}_{sc}}{2\Delta z}$, $\beta_{sc} = \frac{\Delta t K_{sc(1-\varepsilon)}}{(\Delta z)^2 \rho_{sc}}$, $\gamma = C_{P_{sc}} + {q_i}^m C_{P_{ads}}$

Conditions for stability of the numerical solution:

$1 - \frac{2\beta_{sc}}{{\gamma_i}^m} \geq 0$ implying that for a specified increment in space, the time step could be determined from $\Delta t \leq \frac{(\Delta z)^2 min(\rho_{sc} {\gamma_i}^m)}{2[max(K_{sc(1-\varepsilon)})]}$ or $\frac{\beta_{sc}}{{\gamma_i}^m} \leq \frac{1}{2}$

The derivatives of the mass balance equation are discretized as follows:

$$\frac{\partial P_{ads}}{\partial t} = \frac{{P_{adsi}}^{m+1} - {P_{adsi}}^m}{\Delta t} \ldots\ldots\ldots\ldots\ldots\ldots\ldots\ldots\ldots\ldots\ldots\ldots\ldots\ldots\ldots\ldots\ldots (5.39)$$

$$\frac{\partial P_{ads}}{\partial z} = \frac{{P_{adsi+1}}^m - {P_{adsi-1}}^m}{2\Delta z} \ldots\ldots\ldots\ldots\ldots\ldots\ldots\ldots\ldots\ldots\ldots\ldots\ldots\ldots\ldots\ldots\ldots (5.40)$$

$$\frac{\partial q}{\partial t} = \frac{{q_i}^{m+1} - {q_i}^m}{\Delta t} \ldots\ldots\ldots\ldots\ldots\ldots\ldots\ldots\ldots\ldots\ldots\ldots\ldots\ldots\ldots\ldots\ldots\ldots\ldots (5.41)$$

$$\frac{\partial^2 P_{ads}}{\partial z^2} = \frac{{P_{adsi+1}}^m - 2{P_{adsi}}^m + {P_{adsi-1}}^m}{(\Delta z)^2} \ldots\ldots\ldots\ldots\ldots\ldots\ldots\ldots\ldots\ldots\ldots (5.42)$$

Substituting (5.39), (5.40), (5.41) and (5.42) into (5.32) gives

$$\frac{\varepsilon M_{ads}}{RT_{sc}}\left(\frac{{P_{adsi}}^{m+1} - {P_{adsi}}^m}{\Delta t}\right) + \frac{\overline{u}_{sc} M_{ads}}{RT_{sc}}\left(\frac{{P_{adsi+1}}^m - {P_{adsi-1}}^m}{2\Delta z}\right) +$$

$$(1-\varepsilon)\rho_{sc}\left(\frac{{q_i}^{m+1} - {q_i}^m}{\Delta t}\right) =$$

$$\frac{D_S M_{ads}}{RT_{sc}}\left(\frac{{P_{adsi+1}}^m - 2{P_{adsi}}^m + {P_{adsi-1}}^m}{(\Delta z)^2}\right) \ldots\ldots\ldots\ldots\ldots (5.43)$$

Which is further solved for

$$\begin{aligned} {P_{adsi}}^{m+1} = {} & {P_{adsi-1}}^m(\omega + \alpha_2_{sc}) + {P_{adsi}}^m(1-2\omega) \\ & + {P_{adsi+1}}^m(\omega - \alpha_2_{sc}) \quad - \varphi . {T_{sci}}^m . {q_i}^{m+1} \\ & + \varphi . {T_{sci}}^m . {q_i}^m \ldots\ldots\ldots\ldots\ldots\ldots\ldots\ldots\ldots\ldots\ldots\ldots\ldots\ldots\ldots\ldots (5.44) \end{aligned}$$

With $\alpha_2_{sc} = \frac{\Delta t \overline{u}_{sc}}{2\varepsilon\Delta z}$, $\varphi = \frac{(1-\varepsilon)\rho_{sc} R}{\varepsilon M_{ads}}$ and $\omega = \frac{(\Delta t) D_S}{\varepsilon (\Delta z)^2}$

Conditions for stability of the numerical solution:

$\Delta t \leq \frac{(\Delta z)^2 min(\varepsilon)}{2[max(D_S)]}$ or $\omega \leq \frac{1}{2}$

5.3.9 Computer model algorithm/Solution procedure

The numerical solution involves a set of finite points, so-called nodes, at which the derived governing equations are enforced within the system domain by employing discretization process. Consequent upon the discretization of the derived governing equations with their boundary conditions as demonstrated above**,** a computer model was developed to perform the iterative process in order to determine the values of the required system dependent variables at each assigned grid. The grid distribution representing the physical system is uniform and is divided into a fixed number of nodes for each of adsorber and desorber.

The overall iterative solution procedure for the simulation is illustrated by the computer algorithm shown in Fig 5-4 which is then developed into a computer code using MATLAB programming language presented in Appendix B.

The algorithm and the iterative solution procedure are explained as follows:

i. Start simulation by resetting the computer system memory. That is, clearing all data previously stored to a variable, clearing the command window and removing all variables from the current workspace.

ii. Define the system specifications, constant properties, operating parameters and the adsorptive parameters.

iii. Calculate the effective diffusion coefficient at (T_H+T_L)/2.

iv. Initializing by preallocating values or creating arrays for the adsorbate mass, adsorbent temperature with pressure and other useful parameters.

v. Assume initial adsorbent mass, temperature and pressure distributions (m=1) for all grid points, i=1-Nz.

vi. Start iteration by setting the temperature and pressure for the desorption process and by using the adsorbent terminal settling velocity, U_sc, from the cyclone simulation as the inlet adsorbent velocity into the desorber.

vii. Set a counter for the iteration process (m=m+1) to “iterMax” iterations.

viii. Based on the assumed initial adsorbate mass, adsorbent temperature and pressure, determine the new adsorbate mass (q_i^{m+1}) from equation 5.29 for all grid points, i.

ix. Subsequently, equation (5.38) is solved to calculate the temperature distribution (${T_{sci}}^{m+1}$) for all grid points, i.

x. Based on these obtained adsorbate mass and adsorbent temperature distributions, the pressure distribution in the bed (${P_{adsi}}^{m+1}$) for all grid points, i is determined by employing equation 5.44.

xi. Repeat steps viii to x until the end of desorption cycle *(m = m_des).*

xii. Change inlet conditions to that of adsorption process.

xiii. Repeat steps viii to x until the end of adsorption cycle *(m= m_ads).*

xiv. Redo steps vi to xiii until the convergence criterion is satisfied.

xv. End simulation.

5.3.10 System performance indices

The parameters used in this present work to assess the performance of this adsorption refrigeration system are the coefficient of performance (COP) and the specific cooling power (SCP). These parameters are defined by the following equations:

The COP of the system defines its enegy performance in terms of the ratio of its output to its input. That is, the ratio of the cooling energy/refrigerating effect, Q_{ref} (J) to that of the total heat transfer to the adsorbent during the desorption process, Q_{heat} (J). This is expressed as:

$$COP = \frac{Q_{ref}}{Q_{heat}} \dots \dots \dots \dots \dots \dots \dots \dots \dots \dots \dots \dots \dots \dots \dots \dots \dots \dots \dots \dots \dots \dots (5.45)$$

$$COP = \frac{\Delta q M_{SC} L_V}{M_{sc} Cp_{sc} \left(T_{Des_outlet} - T_{Des_inlet}\right)} \dots \dots \dots \dots \dots \dots \dots \dots \dots \dots \dots (5.46)$$

where Δq is the amount of adsorbate that flows into the condenser (kg/kg dry adsorbent) which is the difference between the maximum adsorbate

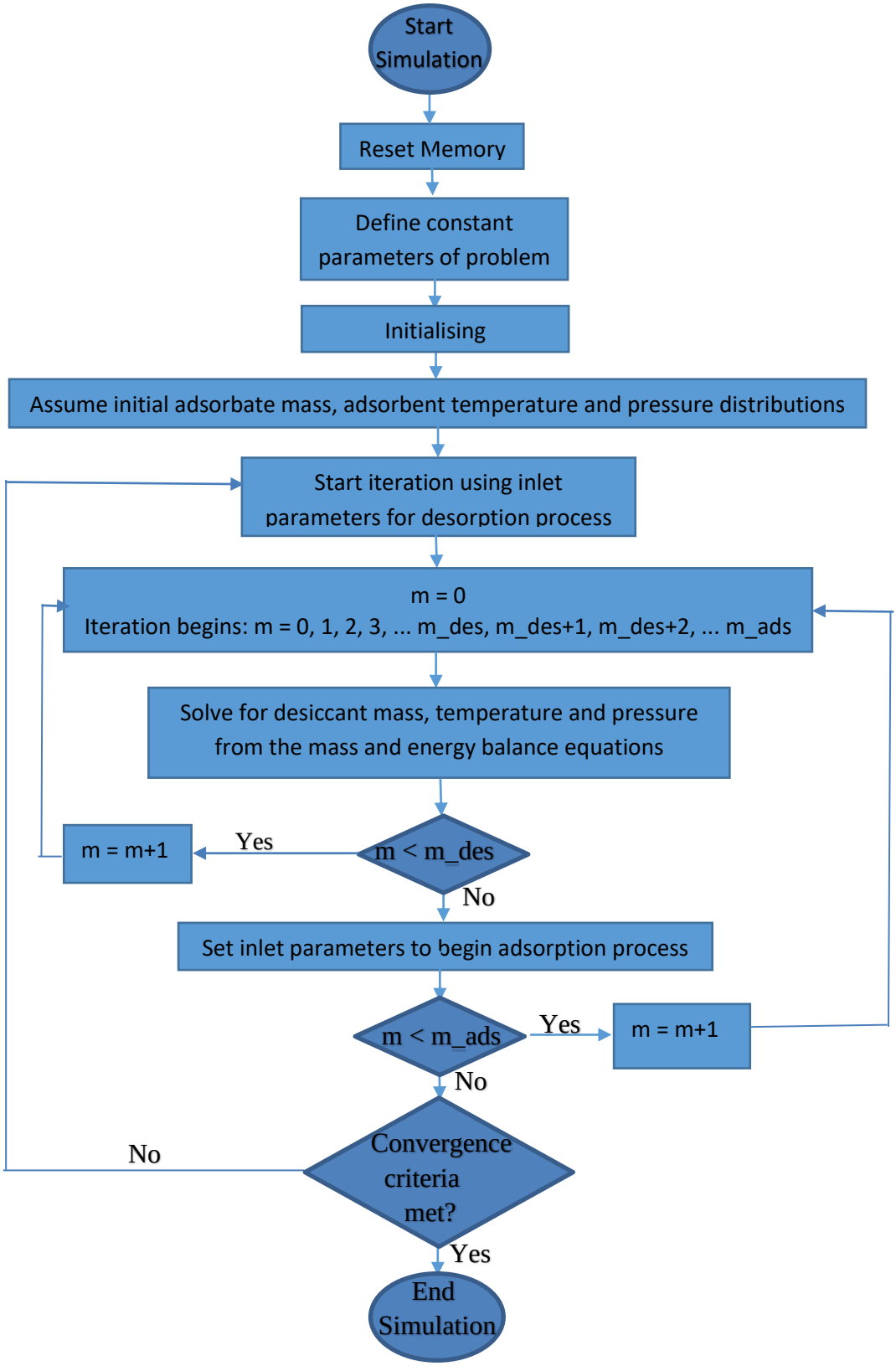


Fig 5-4 Computer Model Flowchart

concentration/concentration at desorber inlet and that at the desorber outlet, M_{sc} is the mass of adsorbent (kg), L_V is the latent heat of vaporization of adsorbate (J/kg), Cp_{sc} is the specific heat of adsorbent $(J/kg.K)$, T_{Des_outlet} and T_{Des_inlet} is the temperature at desorber outlet and desorber inlet respectively.

The SCP (W/kg dry adsorbent) is the ratio between the cooling effect/refrigerating effect Q_{ref} (J) and the cycle time (s) per unit mass (kg) of solid desiccant. This is expressed as follows:

$$SCP = \frac{Q_{ref}}{M_{sc}Cyc_time} \quad \ldots\ldots\ldots\ldots\ldots\ldots\ldots\ldots\ldots\ldots\ldots\ldots\ldots\ldots\ldots\ldots\ldots\ldots\ldots\ldots\ldots \quad (5.47)$$

where Cyc_time is the complete cycle time (for desorption and adsorption).

5.4 Summary

This chapter presents the design of a novel circulating fluidised adsorption refrigeration system configuration which offers the advantages of: continuous cold production, eradication of the issue of unnecessary load on the evaporator, maximum optimization of both adsorption and desorption processes due to the spatial separation of both desorber and adsorber, absence of thermal stress induction in the bed as heat source and heat sink heat exchangers are localised. The system consists of three different interdependent circuits which are: the circulatory circuit consisting of a low-energy consumption centrifugal (extractor) fan with the circulating channels; the separation circuit consisting of a reverse flow cyclone separator; and the refrigeration circuit consisting of a

desorber/regenerator, a condenser, an evaporator, an adsorber, and two 1-way valves.

Presented also in this chapter is the mathematical modelling of the CFAR system including: (i) the model formulation for the separation circuit ranging from cyclone geometry with its design, and (ii) model formulation/numerical modelling process for the adsorption refrigeration circuit ranging from the derivation of the governing equations of energy and mass conservation, their discretization, formation of associated boundary conditions and the iterative solution procedures (algorithm)) to simulate the operations of the adsorption refrigeration circuit of the system with its thermal performance.

This chapter also presented the system performance indices. Two performance indices were determined to assess the overall performance of the novel CFAR system: the energy performance defined by the coefficient of performance (COP) in terms of the ratio of the refrigerating effect to that of the total heat transferred to the adsorbent during the desorption process. The second is the specific cooling power (SCP) defined by the ratio between the refrigerating effect and the cycle time per unit mass of solid desiccant.

Chapter 6: Results analysis and discussion

In this chapter, the results of the numerical simulation carried out on both the circulatory/separation unit (cyclone) and the adsorption refrigeration unit are analysed and discussed.

6.1 Cyclone simulation results

The two essential performance parameters of the gas-solid cyclone separator are its separation efficiency and its pressure drop. While the former determines how much of the solid adsorbent particles fed into it are collected, the latter is an indicator of its energy consumption.

The ultimate goal of this cyclone design is to achieve optimum possible separation efficiency with the lowest possible pressure drop.

Table 6-1 shows the results from the cyclone simulation with the MATLAB code given in Appendix A.

Table 6-1 Cyclone Simulation results

Parameter	Symbol	Value	Unit
Cut size diameter	x_{50}	10.0890	μm
Gas (particle laden) volumetric flow rate	Q	0.0446	m^3/s
Overall collection efficiency	η_t	0.99	
Pressure drop	ΔP	1159	Pa
Power required for the fan	P_f	51.7392	Watts
Mass of adsorbent collected	m_c	5.94	kg
Adsorbent flow rate	$\dot{m}$	0.3227	kg/s
Cut size velocity in the inner vortex	u_{t50}	0.6557	m/s
Mean wall axial velocity	v_m	13.4615	m/s
Mean axial velocity in the vortex finder	v_x	14.7860	m/s
No of effective number of turns	N_e	4.7258	
Gas residence time	τ_R	0.0495	s
Terminal settling velocity of solid adsorbent	V_t	0.4850	m/s

The results show that the designed cyclone is an energy efficient, high efficiency one as it has an overall separation/collection efficiency of 99%. This implies that with the gas (particle laden) volumetric flow rate of 0.0446 m^3/s, 99% of the total mass of the solid adsorbent particles fed into it is being separated and enters with a flow rate of 0.3227 kg/s at a terminal settling velocity of 0.4850 m/s into the refrigeration unit for regeneration and subsequently complete the adsorption refrigeration cycle.

The design gives a particle cut size diameter of 10.09 μm which is the aerodynamic equivalent diameter (AED) of the particle that can be collected with 50% efficiency from the designed cyclone. This implies that any particle size above this can be collected with much higher efficiency. This indicator is highly in favour of the size distribution of our adsorbent solid particles.

6.1.1 Validation of the numerical model

In order to validate the obtained results, it was necessary to compare the predicted results with available published data. Simulation results of the separation unit of this present study were compared with the experimental data of Hoekstra [130], Zhao et al. [131] referenced by Jafarnezhad et al. [132] and the numerical data of El-Batsh [133]. Fig 6-1 and Fig 6-2 respectively shows the comparison of the pressure drop and separation efficiency variation at different values (5-30 m/s) of gas inlet velocity (with $d_v/d = 0.5$) obtained from the present numerical study with the above-mentioned results. It can be seen that there is a good agreement between them. It can also be observed that a cyclone pressure drop can be strongly influenced by the particle-laden gas inlet velocity as shown in Fig 6-1 that, increasing the inlet velocity increases

the pressure drop through the cyclone. The comparison figure also indicates that for a specific inlet velocity with $d_v/d = 0.5$, the pressure drop obtained from this present study has the lowest value when compared with others tested under the same condition. This is an improvement offered from this design which also confirms the validity of the model. Honestly, unlike the pressure drop, it was more difficult to determine the collection efficiency because it is dependent upon particle size distribution of the solid adsorbent incoming particles. A study comparison was performed on the cyclone collection efficiency as a function of its inlet gas velocity by varying the velocity from 10-30m/s based on the available data from the above-mentioned literature with the same test conditions. Fig 6-2 shows that for a typical size of the solid adsorbent particle tested, increasing the cyclone inlet velocity would cause a corresponding increase in the cyclone separation capability which can be traced to the increase in the centrifugal force on the solid adsorbent particles. This increase trend agrees well with other compared results both experimental and numerical.

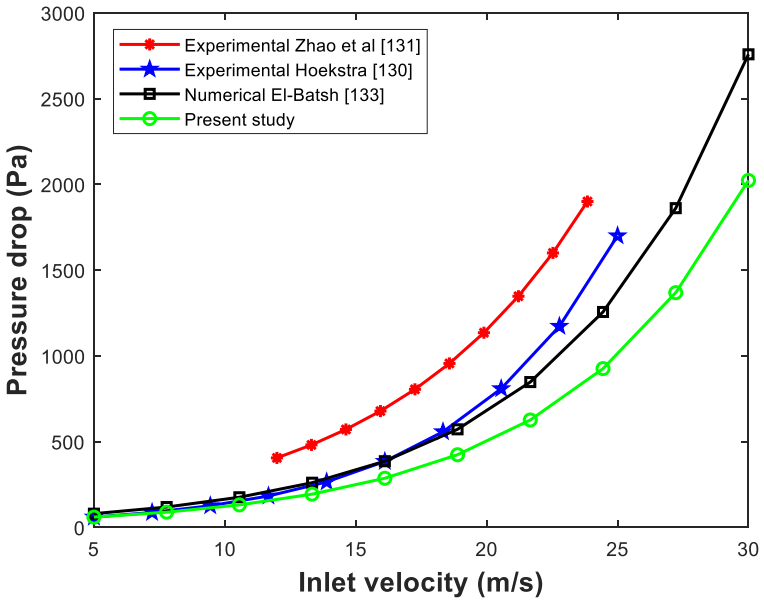


Fig 6-1 Comparison between the experimental data, numerical result and the present study

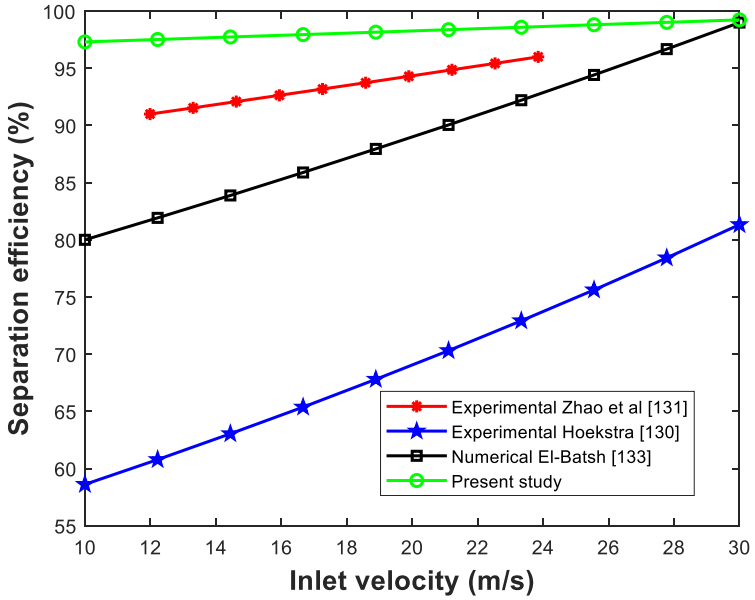


Fig 6-2 Comparison between the experimental data, numerical result and the present study

6.1.2 Effects of the cyclone operational parameters on its performance

The main operational parameters that determine the performance of a reverse flow tangential gas-solid cyclone separator are: pressure drop, cut size diameter and the collection or separation efficiency. Honestly, substantial

efforts had previously been made by researchers to investigate the influences of cyclone operational parameters on its performance criteria focusing majorly on the collection efficiency and the pressure drop of cyclone applications that involve removing a waste product (dust) from a gas but with no/less attention given to the particle exit design. However, in applications where the gases are carrying a product (like we have in this present study) rather than a waste product in which the solid loadings can be much higher such as in chemical industries, pharmaceutical industry, food processing industry, nanotechnology etc., ensuring efficient products separation and recovery from the air stream without damaging their (products) characteristics becomes so crucial. Therefore**,** for optimization purpose, it is highly imperative to focus on the design of that part of cyclone from which the products are collected by considering the effects of the particle (product, which is the adsorbent in this present study) exit diameter,d_{pe}, on the cyclone performance rather than the effect of gas exit diameter which has been broadly researched in the literature. Such is the motivation behind this section. Hence, the simulation results on the effects of the cyclone d_{pe} on the operational parameters of the cyclone performance are presented as follows:

6.1.2.1 Effects of particle exit diameter and solid loading on the cyclone pressure drop

The pressure drop of a cyclone is an indicator of its energy consumption. For the range of the Co (gas inlet solid loadings) tested which is 5-30 kg solid/kg of gas of 50 – 500 μm particles size range at the gas inlet velocity of 10m/s, as observed from Fig 6-3, there is a decreasing trend in the pressure drop as the particle exit diameter increases. Precisely, there is a notable percentage

reduction in the pressure drop up till around 0.038m particle exit diameter after which the percentage reduction becomes marginal. Even though there are no available data in the literature to validate this trend of the effect of the particle exit diameter on the pressure drop as earlier mentioned that it is one of the novelties of this study, it is worth mentioning from Fig 6-3 that there is a reduction in the pressure drop with increasing solid loading. This reduction is more significant (about 12.88% reduction) between 5 and 10 kg solid/kg of gas as it is obvious due to the wide margin between them. This reduction trend continues until after 20 kg solid/kg of gas after which the trend is almost marginal. This predicted trend in Fig 6-3 can be validated by its agreement with both available experimental and computational predictions in the literature [117, 134, 135]. The major explanation for this pressure drop decrease with increasing solid loading pointed out in the literature is that, when solid adsorbents are fed into the gas stream, there will be a rise in the cyclone wall friction due to the presence of solid adsorbent strands descending along the cyclone wall, which reduces the gas tangential velocity in the cyclone body with the resultant effect of lowering the pressure drop. Furthermore, it is obvious from the marginality trend in Fig 6-3 that the improvement (reduction) in pressure drop with increasing solid adsorbent particle loading does not continue indefinitely. There is a solid adsorbent particle loading at which the pressure drop reaches a minimum value after which it rises with any further increasing solid adsorbent particle loading. This is well in agreement with predictions in the literature [117, 135] which further validates the numerical model in this present study. Therefore, for the test conditions in this work, one

may then want to take 0.038m and 20 kg solid/kg of gas as the optimum particle exit diameter and solid adsorbent loading respectively.

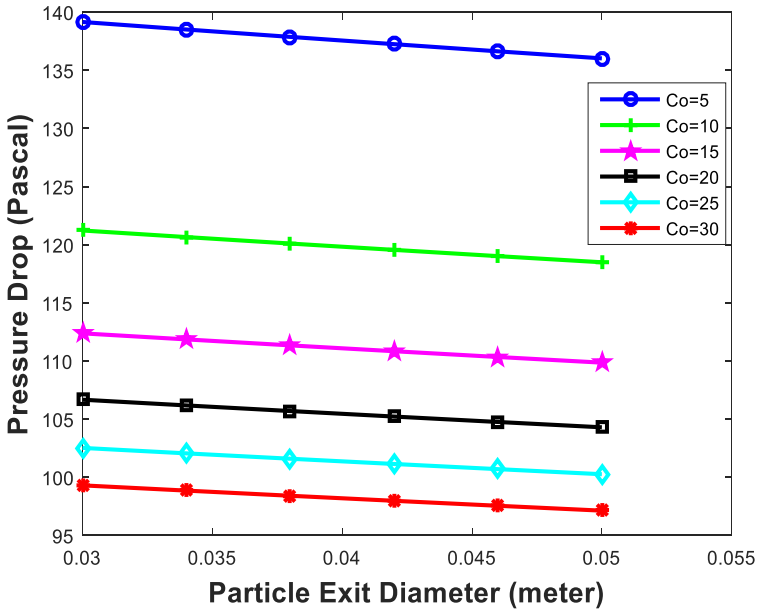


Fig 6-3 Effects of particle exit diameter on the cyclone pressure drop

6.1.2.2 Effects of particle exit diameter on the cyclone cut size diameter

The cut size diameter of a cyclone is that size of the particles that will be collected from the gas stream with 50% efficiency. It is an indicator of the size range of the solid adsorbent particles that can be collected [103]. Particles larger than x_{50} will be removed with a greater efficiency and smaller particles with a lower efficiency. With all the solid loadings (5-30 kg solid/kg of gas) of 50 – 500 μm particles size range tested at the gas inlet velocity of 10m/s, there was a direct proportionality between the cut size diameter and the particle exit diameter as shown in Fig 6-4. Though there was a corresponding increase in the cut size diameter with increasing solid loading but the increment was most significant from 5 - 10 kg solid/kg of gas (about 22.75% increment) and continued though with less % increment until 20 kg solid/kg of gas after which

the percentage increment was almost marginal which may again want to confirm 20 kg solid/kg of gas as the optimum solid loading.

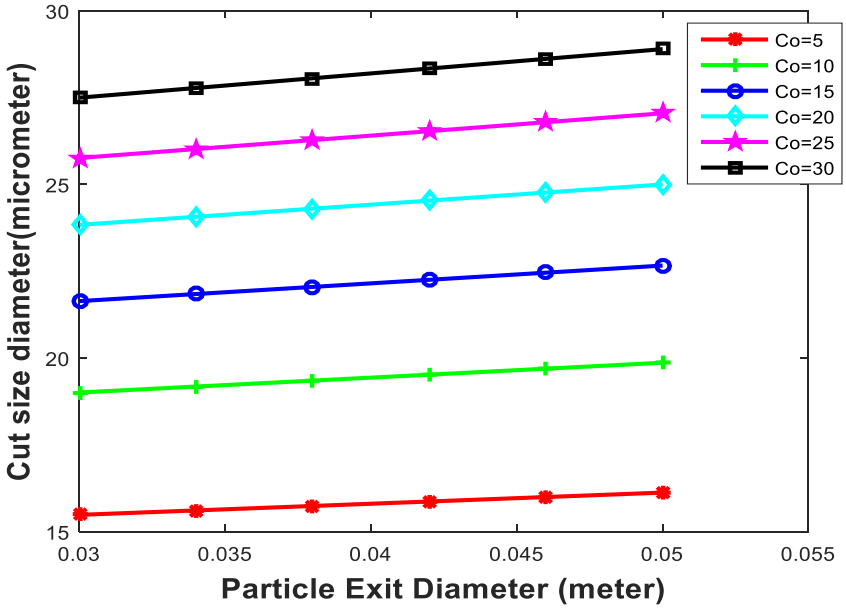


Fig 6-4 Effects of particle exit diameter on the cyclone cut size diameter

6.1.2.3 Grade efficiency performance of the cyclone

The separation/collection characteristics of a cyclone are best described by the so-called grade-efficiency curve (GEC), which is the separation efficiency for a given feed particle size or (narrow) range of particles sizes [117]. This parameter relates the percent collection efficiency of each particle within the particle size distribution (PSD) entering into the cyclone to its (particle) diameter. The grade efficiency performance of the cyclone was investigated using the optimum particle exit diameter and solid loading with all the other simulation parameters kept constant and this is presented in Fig 6-5. The shape is very much in agreement with those in the literature. Interestingly, there was no observable change in the overall separation efficiency with increasing particle exit diameter over the range of solid loadings of 50 – 500 μm particles

size range at the gas inlet velocity of 10m/s but a slight variation in the total separation efficiency was observed with particles sizes below this size range.

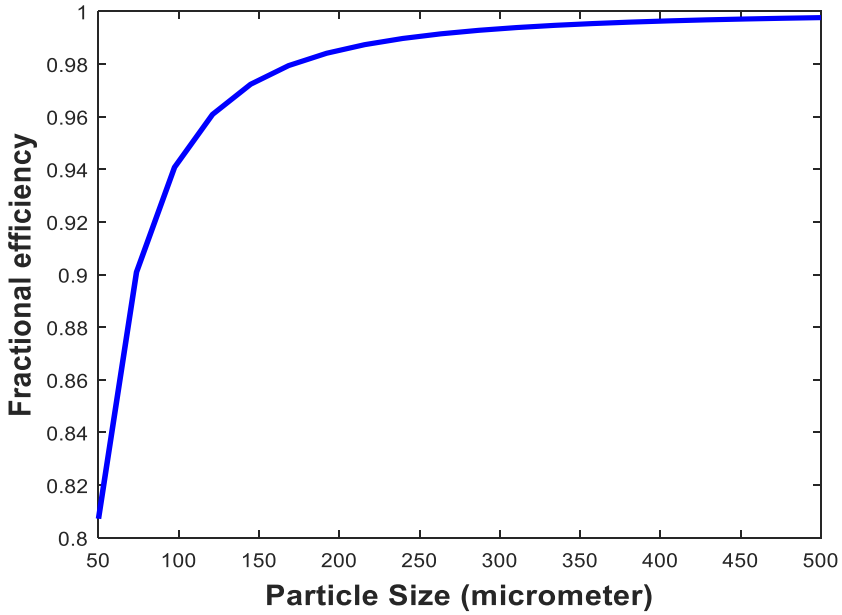


Fig 6-5 Grade efficiency performance of the cyclone

6.2 Adsorption refrigeration circuit simulation results

Based on the mathematical and numerical models coupled with the input data presented in Table 5-4 and the cyclone simulation results presented in Table 6-1, the obtained simulation results are thus presented in this section with the estimation of the overall system performance.

The simulation results show that, as the moving desiccant leaves the cyclone dipleg and enters into the refigeration unit of the system at 30 ℃ through the inlet of desorber (which is already being heated and maintained at a constant temperature of 100℃**),** its temperature and pressure as shown in Fig 6-6 and Fig 6-7 respectively, continue to increase and at a temperature of about 87 ℃, desorption of the adsorbate begins and consequently, the adsorbate

concentration in it starts decreasing from the maximum concentration of 0.38kg which indicates the start of desorption as shown in Fig 6-8. By progressively heating the desorber, more adsorbate is desorbed until it reaches its minimum concentration. The desorbed gaseous adsorbate amount flows into the condenser where it is condensed into liquid. The condensed adsorbate liquid amount is then transferred into the evaporator to initiate the cooling/refrigerating effect. During the adsorption process, it is also shown from Fig 6-6 and Fig 6-7 that the progressive cooling of the adsorber causes a reduction in both the temperature and pressure of the moving desiccant which as a result makes the adsorption quantity in the adsorber continues to increase as shown in Fig 6-8 till it reaches its initial maximum adsorption amount at the end of this cycle and beginning of the next cycle.

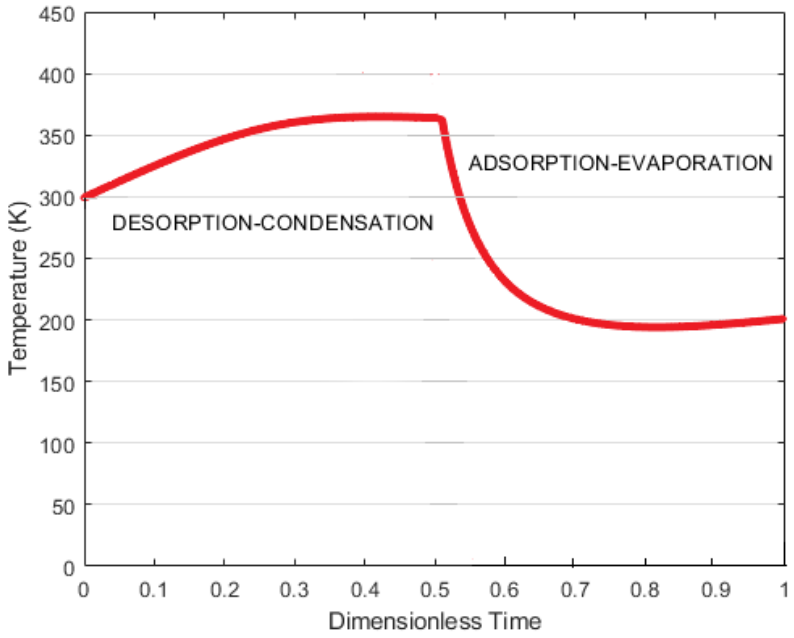


Fig 6-6 Temperature variation for desorption and adsorption

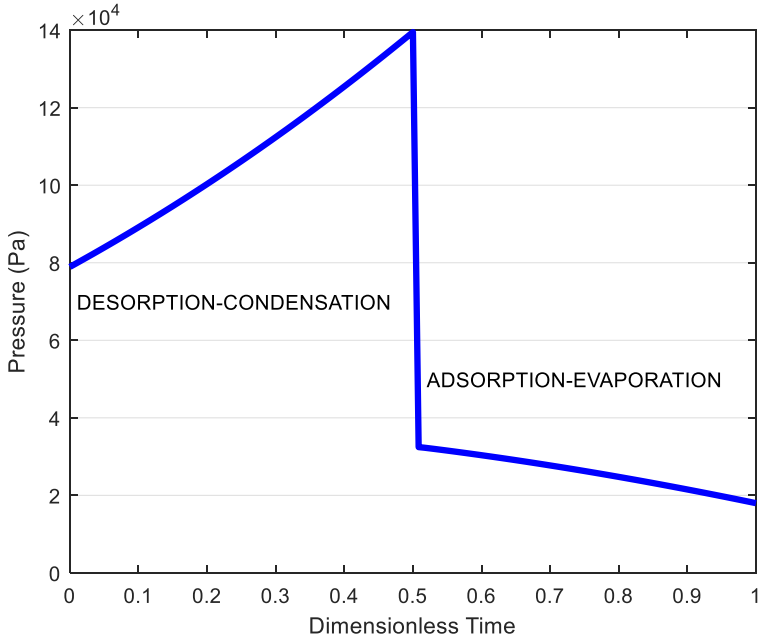


Fig 6-7 Pressure variation for desorption and adsorption

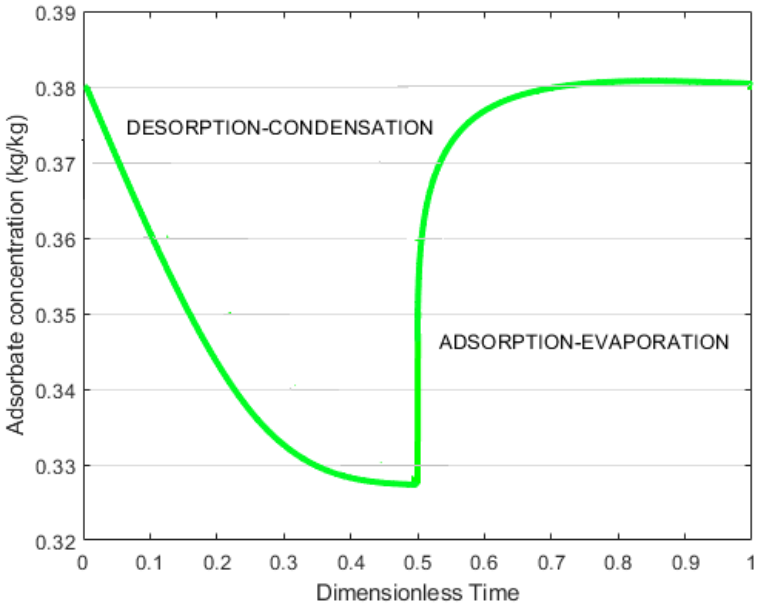
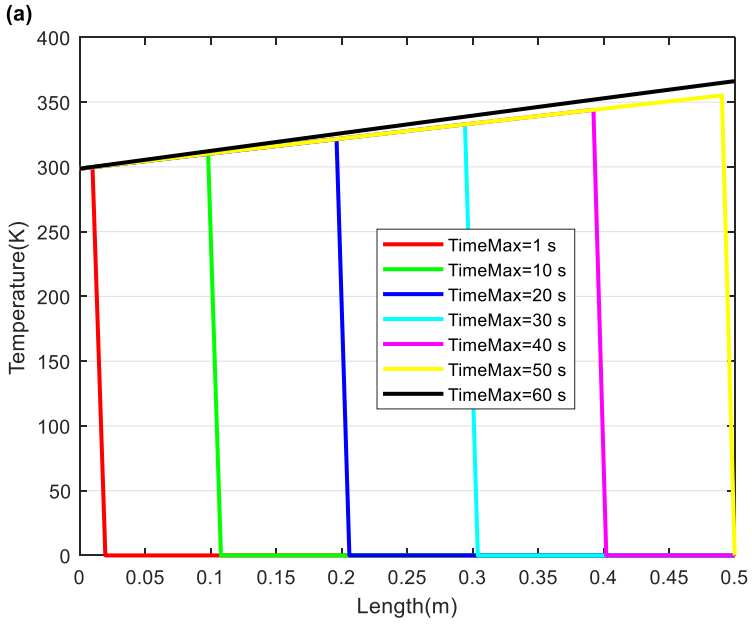


Fig 6-8 Variation for adsorbate mass for desorption and adsorption

6.2.1 Temperature profile along the desorber and adsorber

6.2.1.1 In the first 60 s

Fig 6-9 shows the temperature distribution along both desorber and the adsorber in the first 60 s of each of desorption and adsorption processes. It is obvious from Fig 6-9a that the heat energy added to the moving desiccant particles from the very first second as they enter into the desorber through its inlet for the desorption process, appears not to cause a rise in their temperature not until after 50 s. Apparently, there is an appreciably rise at 60 s in the desiccant temperature as they move from the desorber inlet to its outlet. Similar trend is observed along the adsorber as shown in Fig 6-9b where there is no regular temperature pattern until the adsorption time of 60 s where there is an observable temperature drop. Therefore, there seems to be a turbulent (irregular) temperature distribution along the desorber and the adsorber earlier than 60 s.



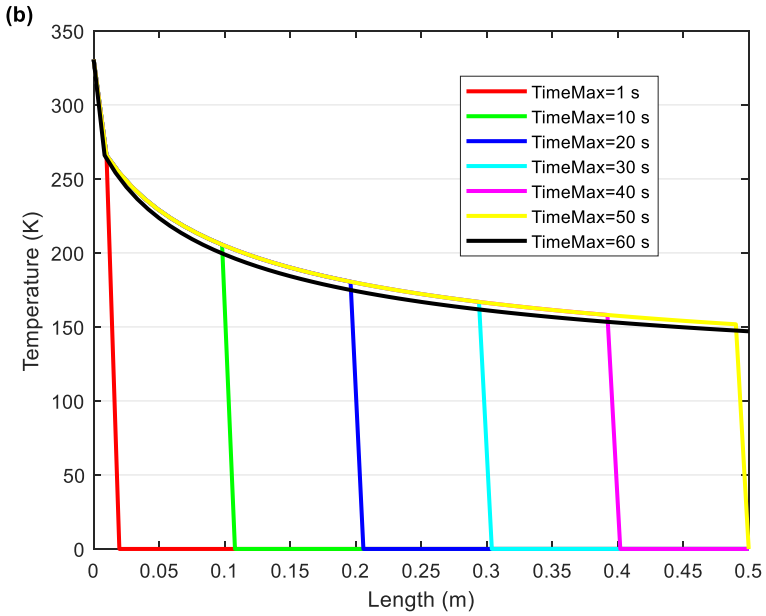


Fig 6-9 Temperature profile in the first 60 s along (a) desorber during desorption process (b) adsorber during adsorption process

6.2.1.2 Within the second 60 s

The temperature distributions obtained along the desorber and the adsorber by increasing the cycle time from 60 s to 120 s for each of desorption and adsorption processes respectively are shown in Fig 6-10. Obviously, there is more regular temperature profile this time around along both desorber and adsorber. As observed from Fig 6-10 a, for every 10 s rise in the cycle time, there is a progressive temperature increase from the start to the end of desorption process as the desiccant particles migrate from the inlet to the outlet of desorber with more significant temperature difference towards the desorber outlet.

Conversely, as observed from Fig 6-10 b, for every 10 s rise in the adsorption cycle time, there is a progressive temperature drop from the start to the end of adsorption process as the desiccant particles migrate from the inlet to the outlet

of adsorber but with less significant temperature difference towards the end of adsorption.

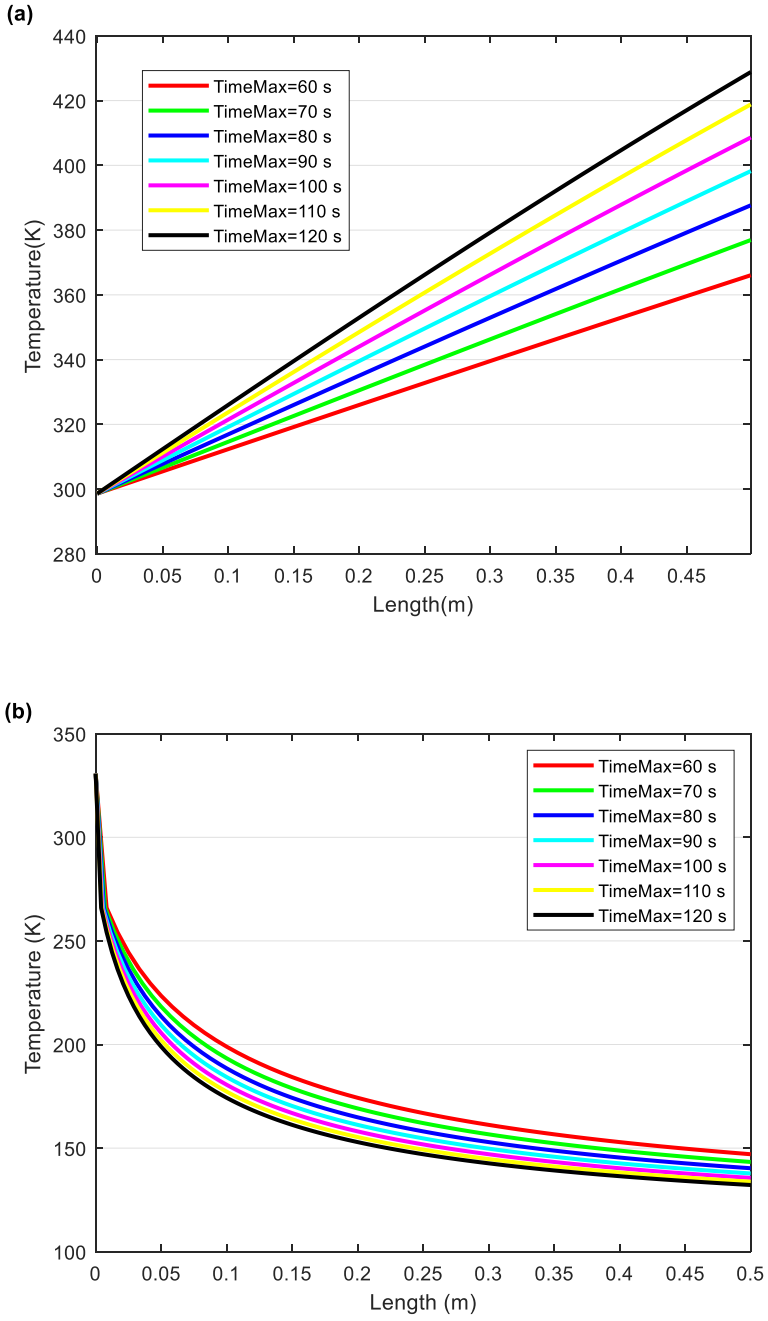


Fig 6-10 Temperature profile within the second 60 s along (a) desorber during desorption process (b) adsorber during adsorption process

6.2.1.3 After the first 60 s

Since it had been previously observed that there is a turbulent (irregular) temperature distribution along both the desorber and the adsorber for cycle time earlier than 60 s and more so that, that there appeared to be some significant temperature profile in extending the cycle time from 60 s to 120 s in the previous session as shown in Fig 6-10, it is of interest to further increase the cycle time from 60 s to 420 s for each of desorption and adsorption in order to have a comprehensive view of the temperature distributions along both desorber and adsorber respectively.

As shown in Fig 6-11a, during the progressive heating of the desiccant particles as they transit the desorber, for every 60 s increase in time, there is more significant temperature increase near the desorber outlet during the beginning of desorption process than at its inlet. However, the temperature distribution became more uniform at the end of desorption cycle.

On the other hand, during the progressive cooling of the desiccant particles as they transit the adsorber, for every 60 s increase in time as shown in Fig 6-11 b, there is more significant temperature drop at about one-third of the adsorber length throughout the adsorption period considered than at its outlet. However, the temperature distribution became more uniform towards the adsorber outlet still with more significant temperature difference observed during the beginning of adsorption process.

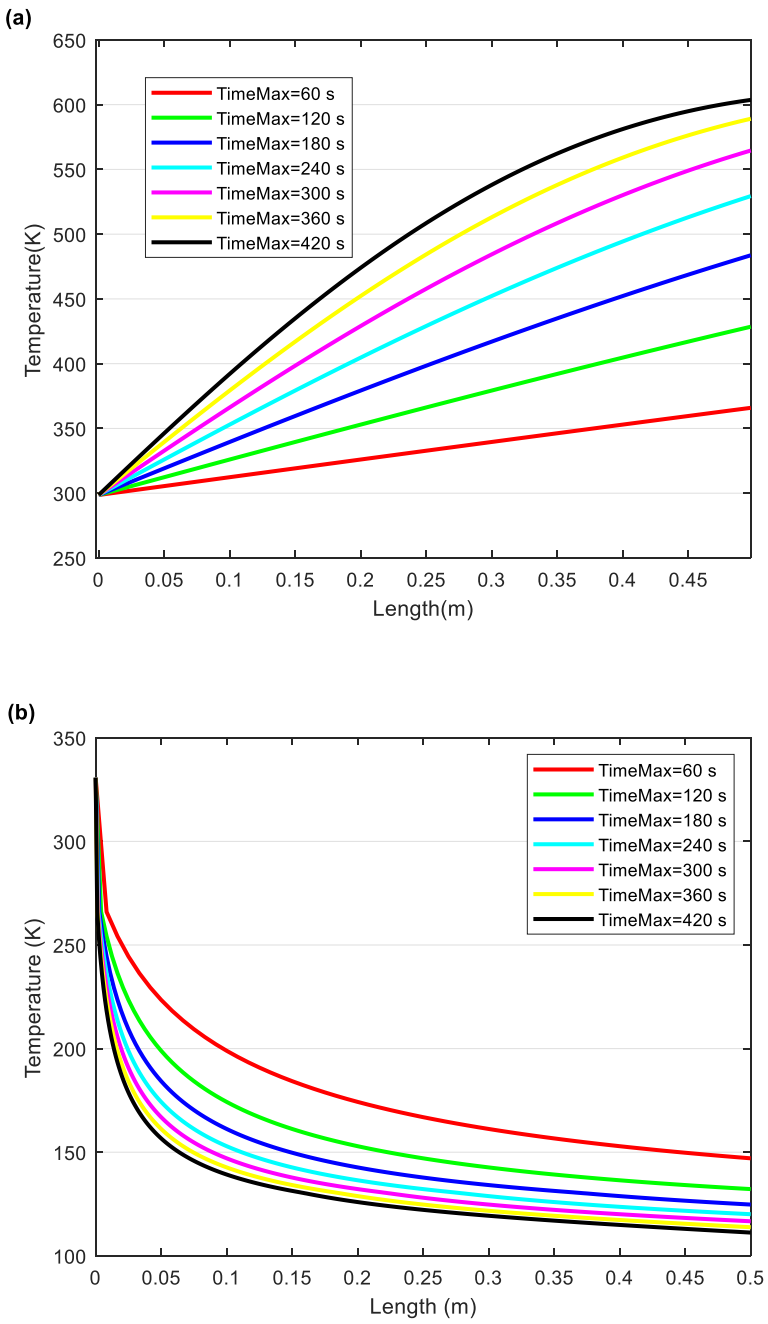


Fig 6-11 Temperature profile after the first 60 s along (a) desorber during desorption process (b) adsorber during adsorption process

6.2.2 Pressure profile along the desorber and adsorber

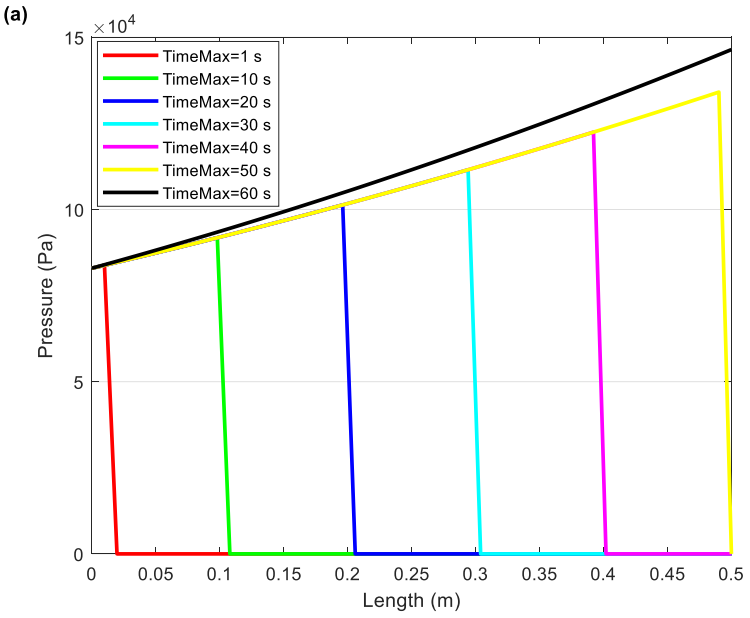
6.2.2.1 In the first 60 s

Fig 6-12 shows the pressure distribution along both desorber and the adsorber in the first 60 s of each of desorption and adsorption processes. There is a close

resemblance with the profile previously observed for temperature along both desorber and adsorber within this same period.

From Fig 6-12a, it is shown that the heating of the moving desiccant particles from the very first second (1 s) as they enter into the desorber through its inlet for desorption process, appears not to cause a corresponding rise in their pressure not until after 50 s. Apparently, there is an appreciably rise at 60 s in the desiccant pressure as they move from the desorber inlet to its outlet.

Similar trend is observed along the adsorber as shown in Fig 6-12b where there is irregular pressure pattern until the adsorption time of 60 s where there is an observable pressure drop. Therefore, there seems to be a turbulent (irregular) pressure distribution along the desorber and the adsorber earlier than 60 s.



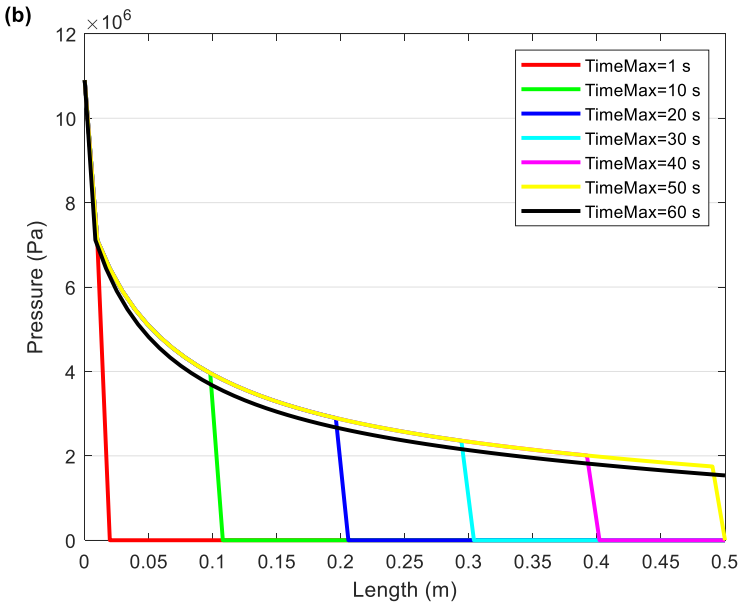


Fig 6-12 Pressure profile in the first 60 s along (a) desorber during desorption process (b) adsorber during adsorption process

6.2.2.2 Within the second 60 s

Fig 6-13 shows the pressure distributions obtained along the desorber and the adsorber by increasing the cycle time from 60 s to 120 s for each of desorption and adsorption processes respectively. Apparently, as previously observed in the case of temperature profile for this same cycle time range and also unlike the profile earlier observed for cycle time less than 60 s, there is more regular pressure profile along both desorber and adsorber. As observed from Fig 6-13 a, for every 10 s rise in the cycle time, there is a progressive rise in the pressure from the start to the end of desorption process as the desiccant particles migrate from the inlet to the outlet of desorber with more significant pressure difference observed towards desorber outlet.

Conversely, as shown in Fig 6-13 b, for every 10 s rise in the adsorption cycle time, the pressure dropped from the start to the end of adsorption process as

the desiccant particles migrate from the inlet to the outlet of adsorber but with less significant pressure difference towards the end of adsorption.

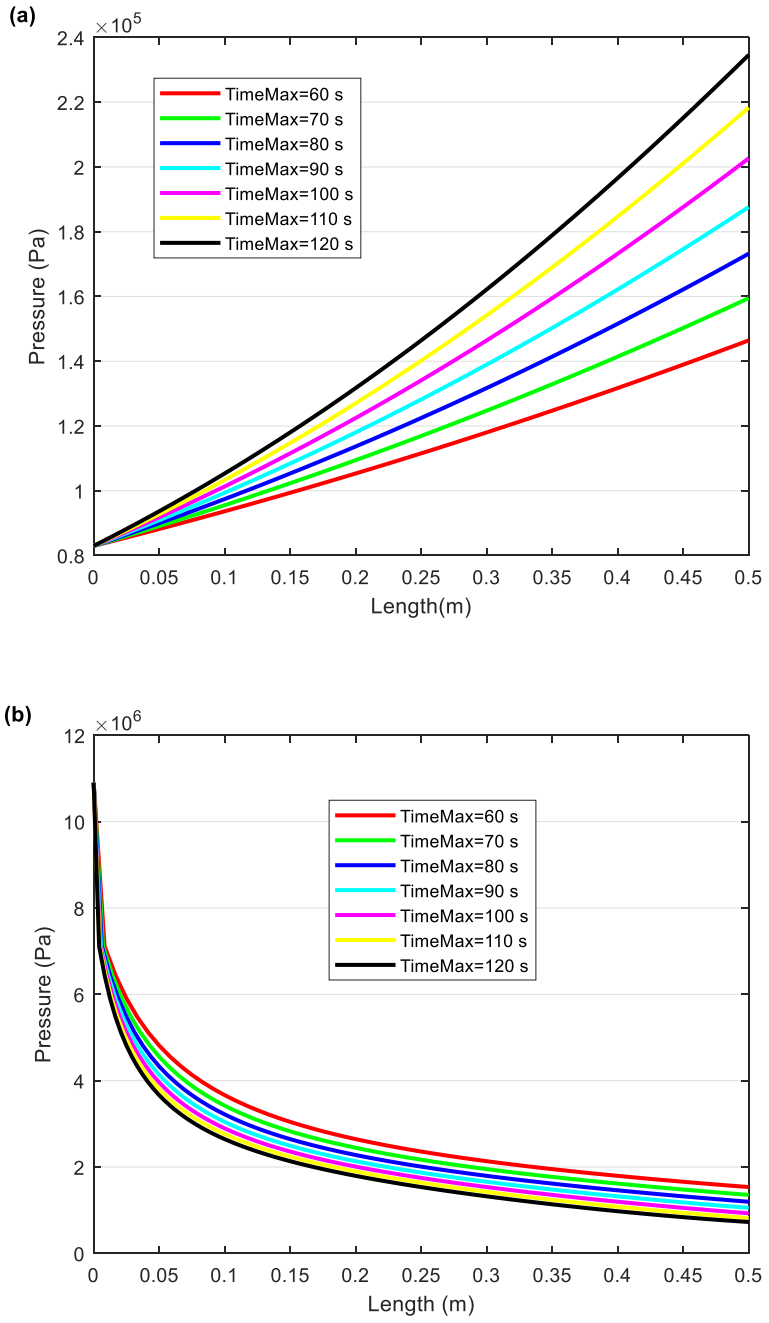


Fig 6-13 Pressure profile within the second 60 s along (a) desorber during desorption process (b) adsorber during adsorption process

6.2.2.3 After the first 60 s

Like in the case of temperature profiles and also from the pressure distribution trends observed previously concerning cycle time less than 60s and above 60 s up to 120s, the cycle time is further increased from 60 s to 420 s for each of desorption and adsorption in order to have a detailed view of the pressure distributions along both desorber and adsorber respectively.

As shown in Fig 6-14 a, during the progressive heating of the desiccant particles as they transit the desorber, for every 60 s increase in time, there is more significant pressure increase observed near the desorber outlet throughout the desorption than at its inlet.

On the other hand, during the progressive cooling of the desiccant particles as they transit the adsorber, for every 60 s increase in time as shown in Fig 6-14 b, there is more significant pressure drop at about one-third of the adsorber length. This pressure reduction continued till the adsorber outlet for shorter cycle time. It was noticed that the pressure immediately increased at about half adsorber length for cycle time after 180 s. However, more significant pressure difference was observed during the beginning of adsorption process.

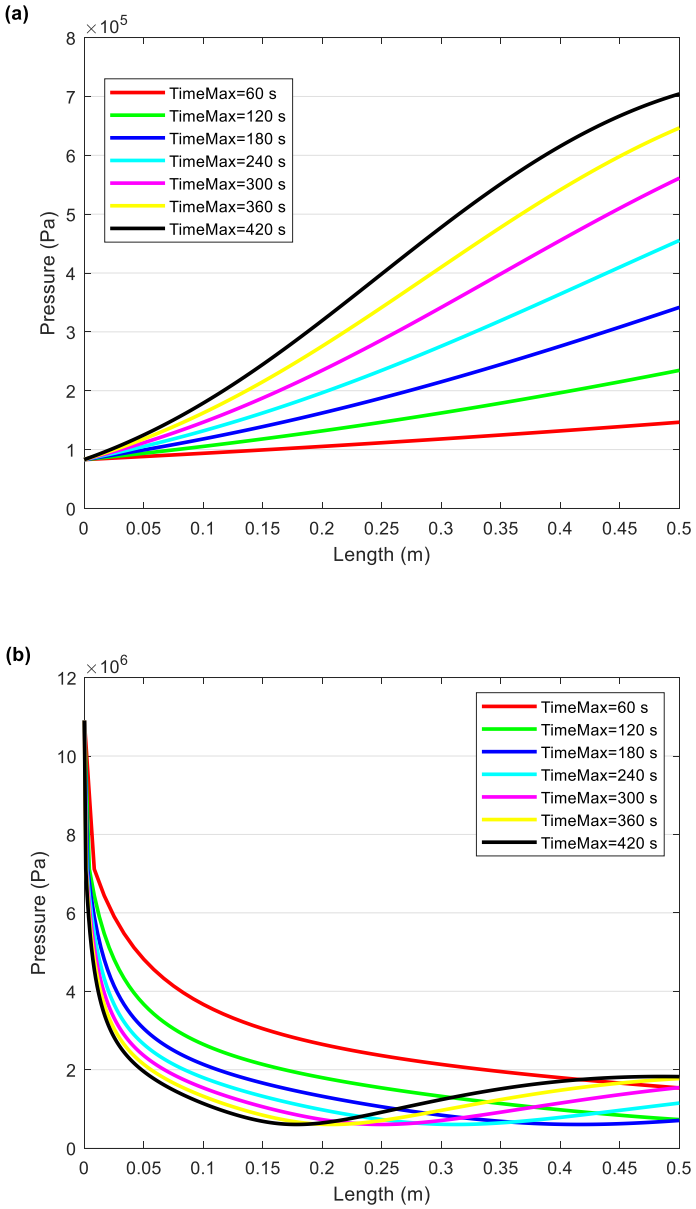


Fig 6-14 Pressure profile after the first 60 s along (a) desorber during desorption process (b) adsorber during adsorption process

6.2.3 Adsorption quantity profile along the desorber and adsorber

6.2.3.1 In the first 60 s

The Adsorption quantity profile along the desorber and adsorber in the first 60 s of each of desorption and adsorption processes is shown in Fig 6-15. From Fig 6-15a, it is obvious that there is no regular pattern for the adsorption quantity until after 50 s after which there is slight reduction in the adsorption

quantity as the desiccant particles move from the desorber inlet to its outlet. A similar trend can be observed along the adsorber as shown in Fig 6-15b where there is also no regular pattern for the adsorption quantity until 60 s into the adsorption process where there is an observable slight adsorption quantity increase. This further confirms the turbulent (irregular) temperature and pressure profiles earlier observed along the desorber and the adsorber in the first 60 s of desorption and adsorption respectively.

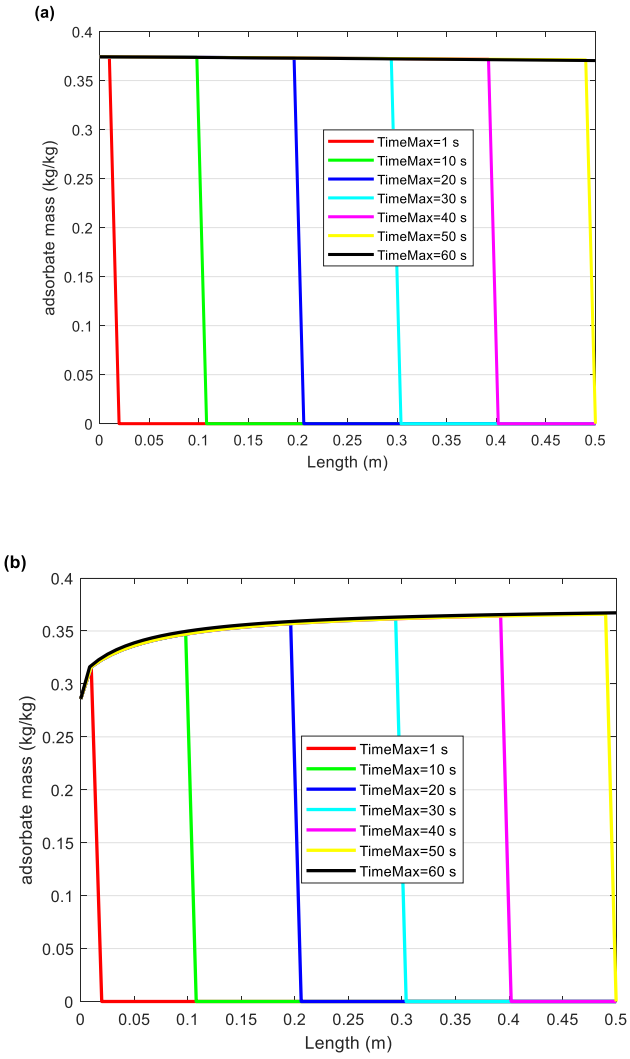


Fig 6-15 Adsorption quantity profile in the first 60 s along (a) desorber during desorption process (b) adsorber during adsorption process

6.2.3.2 Within the second 60 s

Fig 6-16 presents the adsorption quantity profile obtained along the desorber and the adsorber by increasing the cycle time from 60 s to 120 s for each of desorption and adsorption processes respectively. Unlike the profile previously observed before 60 s, there is more regular adsorption quantity profile this time around along both desorber and adsorber.

As observed from Fig 6-16a, for every 10 s rise in the desorption cycle time, there is a progressive reduction in the adsorption quantity from the start to the end of desorption process as the desiccant particles migrate from the inlet to the outlet of desorber with more significant difference towards the desorber outlet.

Conversely, as observed from Fig 6-16b, for every 10 s rise in the adsorption cycle time, though there is a progressive rise in the adsorption quantity from the start to the end of adsorption process as the desiccant particles migrate from the inlet to the outlet of adsorber but with less observable difference towards the end of adsorption.

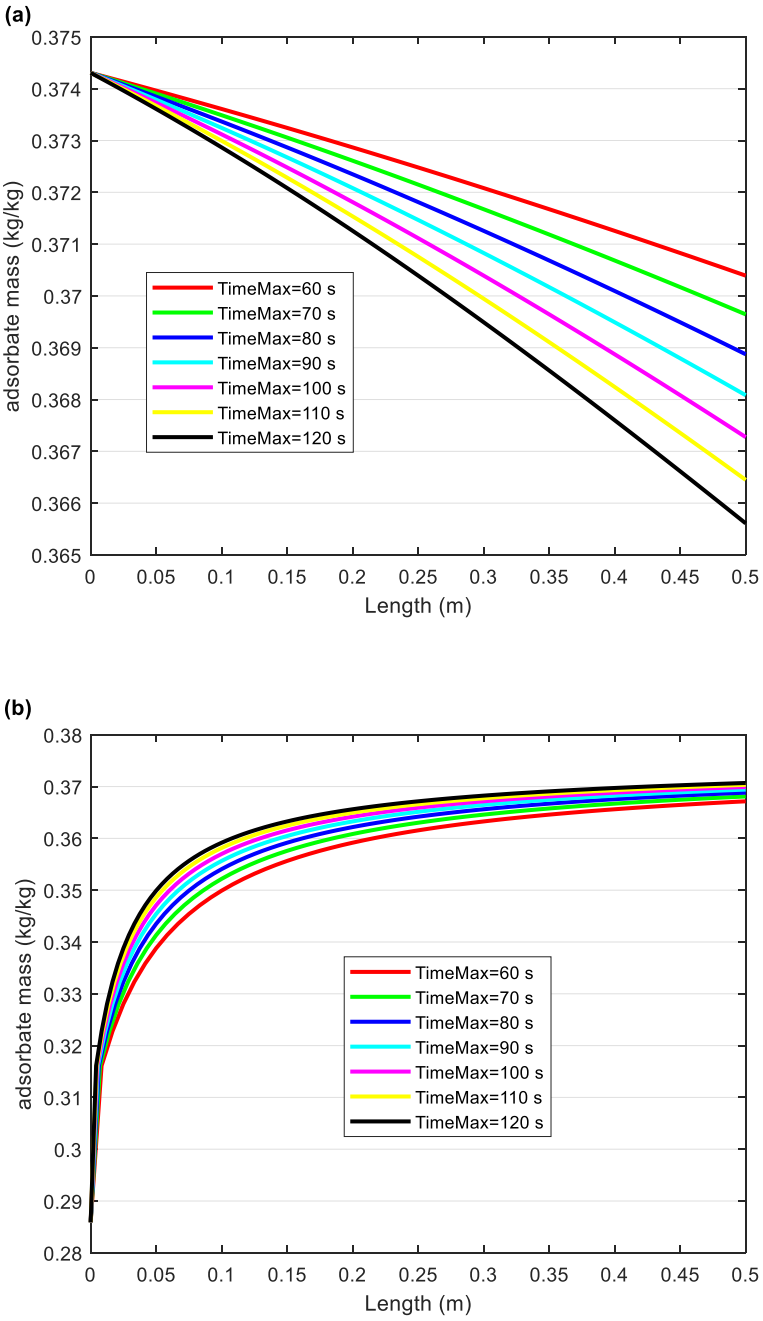
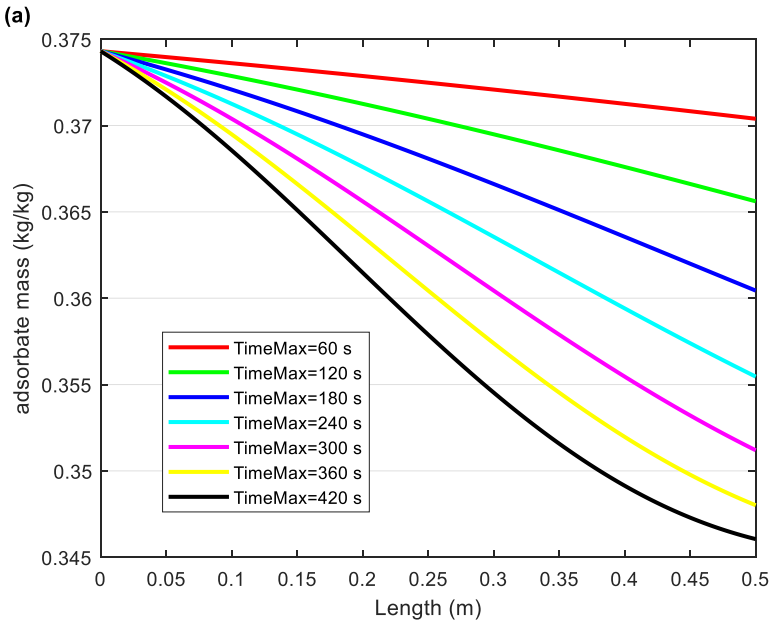


Fig 6-16 Adsorption quantity profile within the second 60 s along (a) desorber during desorption process (b) adsorber during adsorption process

6.2.3.3 After the first 60 s

Moreover, in order to have a comprehensive view of the adsorption concentration profile along both desorber and adsorber as previously investigated on both temperature and pressure, the cycle time is increased from

60 s to 420 s for each of desorption and adsorption. As shown in Fig 6-17a, during the progressive heating of the desiccant particles during desorption process as they transit the desorber, for every 60 s increase in time, there is more significant reduction in the adsorption quantity near the desorber outlet during the beginning of desorption process than at its inlet. However, during the progressive cooling of the desiccant particles as they transit the adsorber during adsorption process, as shown in Fig 6-17b, for every 60 s increase in time, there is more significant increase in the adsorption quantity at the adsorber inlet during the beginning of adsorption process than at the end.



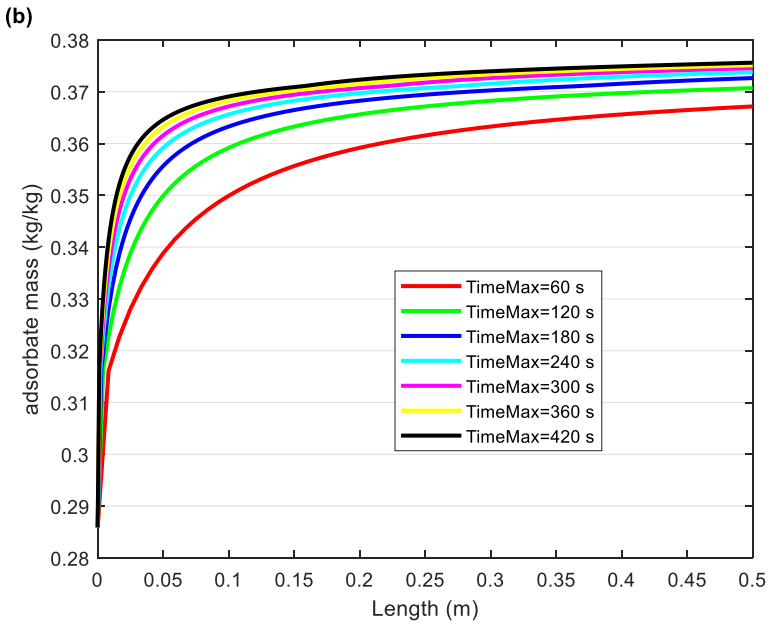


Fig 6-17 Adsorption quantity profile after the first 60 s along (a) desorber during desorption process (b) adsorber during adsorption process

6.3 Parametric analysis

A parametric analysis was conducted using the developed computer model to evaluate the effects of various operational parameters on the CFAR system thermal performance. The design parameters selected for consideration are those that play a significant role in the system performance. The purpose of this study is to demonstrate how the performance of this solid desiccant adsorption refrigeration system would change during its practical use.

6.3.1 Effect of cycle time

Fig 6-18 shows the effect of cycle time on the CFAR system thermal performance. The total cycle time was varied from 60 s each to 420 s, with 50/50 proportion for both desorption and adsorption processes with other parameters taken from Table 5-4. As shown in Fig 6-18, the system COP decreases in the first 240 seconds of the desorption time and gradually

increases thereafter. This can be explained by the fact that, the heat added to the moving desiccant particles as they migrate through the desorber within the shorter times are only used for the sensible heating of the desiccant and the adsorbate and not for the effective desorption of the adsorbate from the desiccant. The COP gradually increases with longer cycle time as this allows more adsorbate to be desorbed from the desiccant, thus better regeneration process.

However, as shown in Fig 6-18**,** the SCP of the CFAR system gradually decreases with increasing cycle time. It can be particularly seen that the SCP drastically reduces by 26% between 60 s and 120s and subsequently by at least 7% for every addition of 60 s to the cycle length. This reduction trend in the SCP is because longer adsorption times allowed the desiccant particles to reach saturation faster which reduces their adsorbate uptake capability. Hence, less adsorbate is adsorbed over time. In addition, longer cycles time implied a reduction in the number of cycles over a particular period of operating times which further explains the reduction in the SCP. Although the COP increases with longer cycle time but one cannot indefinitely increase the cycle time because the dried desiccant particles would be kept in the desorber for too long a time and the inputted energy will be wasted. Therefore, if a higher COP is desired, increasing the cycle time from 60 s to 360 s could be most favourable.

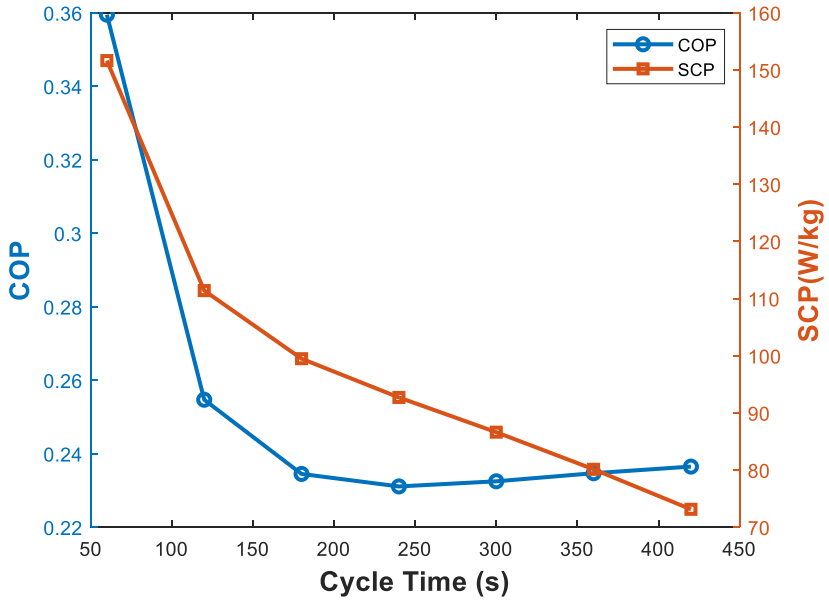


Fig 6-18 System performance for various cycle times

6.3.2 Effect of Desiccant flow velocity

In order to investigate the effect of the desiccant flow velocity on the system performance, the desiccant flow velocity for both desorption and adsorption processes were varied from 0.05 m/s to 0.35 m/s while other parameters were taken from Table 5-4. Fig 6-19 summaries the relationships between the system COP, SCP and desiccant flow velocity. Comparing the effects of the desiccant flow velocity on both system performance indices, one distinctive difference observed in this study is that varying the desiccant flow velocity has a positive effect on the SCP and a negative effect on the COP.

Fig 6-19 shows that at higher desiccant flow velocities, since the heat input doesn't change, the moving desiccant particles were not given considerable time to be effectively heated as they transit the desorber and so cannot desorb the adsorbate fully, hence the decreased COP.

Obviously, by increasing the desiccant flow velocity from 0.05 m/s to 0.35 m/s, the SCP increased by amost 119%. This is because, during the adsorption process, increasing the desiccant flow velocity implies a shorter cycle time which indicates that the desiccant temperature dropped faster. Therefore, getting an optimum velocity for the moving desiccant should be desired because, if the velocity is faster than the optimum velocity, the moving desiccant would not fully desorb the adsorbate because of the short desorption cycle. On the other hand, if it is too slow or slower than the optimum, the process time would be too long which make the dried desiccant particles to be unnecessary kept within the desorber which wastes the inputted energy and thus makes the CFAR system performance worse.

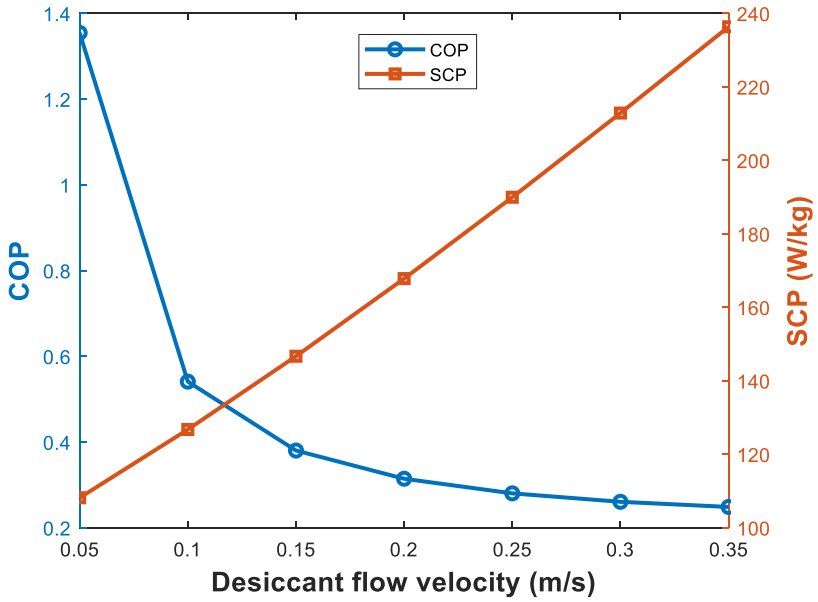


Fig 6-19 System performance for various desiccant flow velocities

6.3.3 Effect of desorber bed temperature

The desorber bed temperature of the CFAR system was varied from 30 ℃ to 90 ℃ with other parameters taken from Table 5-4. As observed from Fig 6-20, both the system COP and SCP are observed to be positively affected by

increasing the desorber bed temperature with about 100% rise in both COP and SCP.

This is because at higher desorber temperature, the moving desiccant particles are given more time to be heated in the desorber before reaching the saturation pressure corresponding to the condenser temperature at which desorption process starts. This favours more adsorbate desorption from the desorber into the condenser and consequently more adsorbate vapours are adsorbed into the adsorber. Hence, better system performance (both COP and SCP). However, as shown in Fig 6-20, a further increase in the desorber temperature would yield a drop in the system performance. This is because the additional heat added was only used for the sensible heating of the adsorbent and the adsorbate and not for further adsorbate desorption.

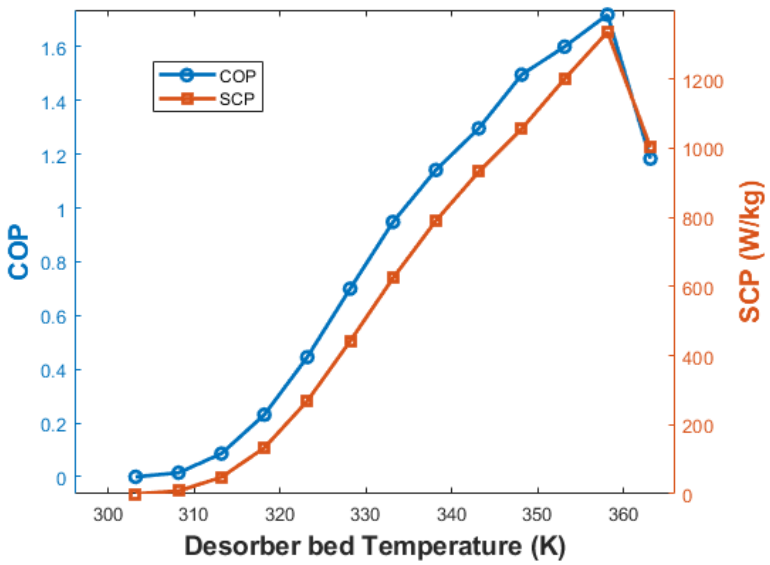


Fig 6-20 System performance for various desorber bed temperatures

6.3.4 Effects of adsorber bed temperature

This time around, the adsorber bed temperature was varied from 5 ℃ to 20 ℃ in order to investigate its effect on the system performance with other

parameters taken from Table 5-4. Both the COP and the SCP are observed in Fig 6-21 to be negatively affected by increasing the temperature of the adsorber bed with the COP decreasing from 0.86 to 0.08 and the SCP reducing from 213.16 W/kg to 34.34 W/kg. Higher adsorber bed temperature implies that the pressure at which the adsorbate vapour exits the evaporator is high. The simple implication of this is that, the moving desiccant particles in the adsober would have to start adsorbing the adsorbate at this said higher temperature which eventually reduces their adsorbate uptake capacity during the adsorption process. Therefore, this higher adsorber bed temperature during the adsorption process reduces the adsorbate uptake capacity of the adsorbent which consequently reduces the system performance. This is because higher adsorbent bed temperature implies an increase in the overall system working temperature range which directly increases the pressure ratio which in turn does not only hinder the flow of adsorbate vapour from the evaporator to the adsorber during the adsorption process, but also the regeneration of the adsorbent.

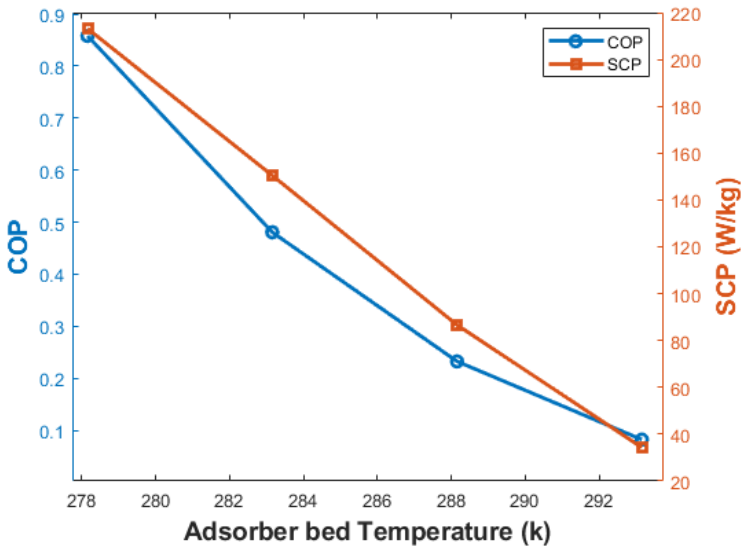


Fig 6-21 System performance for various adsorber bed temperatures

6.4 Summary

This chapter presents the analysis and discussion of the results of the numerical simulation carried out on both the circulatory/separation unit (cyclone) and the adsorption refrigeration unit. Parametric analyses were carried out on both the cyclone and the adsorption refrigeration unit by investigating into the effects of various design and operational parameters on the overall CFAR system performance.

From the cyclone results, it is shown that the designed cyclone is an energy efficient, high efficiency one as it has an overall separation/collection efficiency of 99%. This implies that with the little fan power input of 51.75 Watts, 99% of the total mass of the solid adsorbent particles fed into it is being separated and enters with a flow rate of 0.32 kg/s at a terminal settling velocity of 0.49 m/s into the refrigeration unit for regeneration and subsequently complete the adsorption refrigeration cycle.

It was also observed that there seems to be a turbulent (irregular) temperature, pressure and adsorption concentration profile along the desorber and the adsorber for cycle time shorter than 60 s for both desorption and adsorption processes. However, on the part of temperature or pressure profile, increasing the cycle time from 60 s to 120 s for each of desorption and adsorption processes resulted in a progressive increase in temperature or pressure from the start to the end of desorption process with more significant temperature or pressure difference observed towards the desorber outlet. Meanwhile there is a progressive temperature or pressure drop from the start to the end of adsorption process but with less significant temperature or pressure difference towards the end of adsorption. Regarding the adsorption concentration profile for this cycle

time range, for every 10 s rise in the desorption cycle time, there is a progressive reduction in the adsorption quantity from the start to the end of desorption process with more significant difference towards the desorber outlet. Conversely, there is a progressive rise in the adsorption quantity from the start to the end of adsorption process for every 10 s rise in the adsorption cycle time but with less observable difference towards the end of adsorption.

Increasing the cycle time further from 60 s to 420 s for each of desorption and adsorption in order to have a comprehensive view of the temperature, pressure and adsorption quantity distributions along both desorber and adsorber respectively showed that:

(a) for every 60 s increase in desorption time, there was more significant temperature increase near the desorber outlet during the beginning of desorption process than at its inlet but the temperature distribution became more uniform at the end of desorption cycle. Whereas for every 60 s increase in adsorption time, there was more significant temperature drop at about one-third of the adsorber length throughout the adsorption period than at its outlet. However, the temperature distribution became more uniform towards the adsorber outlet still with more significant temperature difference observed during the beginning of adsorption process.

(b) for every 60 s increase in desorption time, more significant pressure increase was observed near the desorber outlet throughout the desorption than at its inlet whereas for every 60 s increase in adsorption time, there was, at about one-third of the adsorber length, more significant pressure drop which continued till the adsorber outlet for shorter cycle times but immediately

increased at about half adsorber length for cycle time greater than 180 s. However, more significant pressure difference was observed during the beginning of adsorption process.

(c) Regarding the adsorption quantity profile, for every 60 s increase in desorption time, there was more significant reduction in the adsorption quantity near the desorber outlet during the beginning of desorption process than at its inlet. Conversely, there was more significant increase in the adsorption quantity at the adsorber inlet during the beginning of adsorption process than at the end for every 60 s increase in adsorption time.

The results of the parametric studies conducted on the adsorption refrigeration unit to further analyse the system performance under various operating conditions are also presented. Four main parameters that play a significant role in the system performance were selected and varied: cycle time, desiccant flow velocities, desorber bed temperature and adsorber bed temperature.

It was observed that the COP of the CFAR system increased with longer cycle time while the SCP gradually decreased with increasing cycle time. It was particularly observed that the SCP drastically reduced by 26% between 60 s and 120s and subsequently by at least 7% for every addition of 60 s to the cycle time. Even though the COP increased with longer cycle time but one cannot indefinitely increase the cycle time because the dried desiccant particles would be kept in the desorber for too long a time and the inputted energy will be wasted. Therefore, if a higher COP is desired, increasing the cycle time from 60 s to 360 s could be most favourable.

The parametric study also revealed that increasing the desiccant flow velocity would have a positive effect on the SCP and a negative effect on the COP. Therefore, getting an optimum velocity for the moving desiccant velocity for the CFAR system should be desired because, if the velocity is faster than the optimum velocity, the moving desiccant would not fully desorb the adsorbate because of the short desorption cycle. On the other hand, if it is too slow or slower than the optimum, the process time would be too long which make the dried desiccant particles to be unecessary kept within the desorber which wastes the inputted energy and thus makes the CFAR system performance worse.

Also, both the system COP and SCP were observed to be positively affected by increasing the desorber bed temperature. This is because at higher desorber bed temperature, the moving desiccant particles are given more time to be heated in the desorber before reaching the saturation pressure corresponding to the condenser temperature at which desorption process starts. This favours more adsorbate desorption from the desorber into the condenser and consequently more adsorbate are adsorbed into the adsorber. Hence, better system performance. However, increasing the desorber bed temperature further would yield a drop in the system performance.

Both the COP and the SCP were observed to be negatively affected by increasing the adsorber bed temperature This is because at higher adsorber bed temperature, the pressure at which the adsorbate exits the evaporator is high. The simple implication of this is that, the moving desiccant particles in the adsober would have to start adsorbing the adsorbate at this said higher temperature which eventually reduces their adsorbate uptake capacity during

the adsorption process. Therefore, this higher adsorbent temperature during the adsorption process reduces the adsorbate uptake capacity of the adsorbent which consequently reduces the system performance. Hence, lower adsorber bed temperature seemed more preferable.

Chapter 7: Conclusion and Future Work

7.1 Conclusion

In this research study, a novel circulating fluidized adsorption refrigeration (CFAR) system for continuous operation mode was proposed, designed and modelled. This new configuration involves the continuous circulation of fluidized adsorbate-laden-solid desiccant by means of a gas-solid cyclone separator. This novel design offered an effective solution to those technical limitations (like intermittent refrigeration production, refrigerant leakage with sealing issues, thermal stress induction, adsorbent deterioration, mechanical complexities etc.) often encountered in fixed adsorption beds and existing adsorption systems. Therefore, the design novelty and the major contributions to knowledge of this research project are summarised below.

7.1.1 Design novelty

The key novelty of this research work can be summarised as follow:

i. It is a continuous process which can produce refrigeration continuously thereby overcoming the bottleneck of intermittent cold production associated with fixed beds.

ii. Once the system is started up, concentration, pressure and temperature profiles are formed and become time invariant, which simplifies the issue of unnecessary load on the evaporator as it is with fixed beds.

iii. In contrast to conventional fixed-bed adsorbers and other continuous systems in the literature, this system does not only stand out because of

its continuous cold production, but also because adsorption and desorption processes occur separately (that is, they are separated spatially) and can thus be optimized maximally.

iv. The issue of switching between beds and the use of a reversible pump in the previous works are overcome here. Hence the valves complexity and thermal stress induced in the bed by switching between heating and cooling is completely solved.

v. Heat source and heat sink heat exchangers are therefore localised.

vi. The investigation on the effects of the particle (product, which is the adsorbent in this present study) exit diameter,d_{pe}, on the cyclone performance rather than the effect of gas exit diameter which has been broadly researched in the literature.

7.1.2 Contribution to knowledge

The key contributions of this research work can be summarised as follow:

i. Detailed design, study, investigation and evaluation (in terms of credits and limitations) of the various possible alternative configurations of solid desiccant cooling/heating systems with the purpose of identifying the best configuration most suitable to fill those identified research gaps.

ii. The incorporation of solid-gas cyclone separator which is known for its low capital cost, low maintenance needs, less risk of wear due to absence of moving parts, long-term reliability, relative power economy

and its ability to reuse separated particles, is one of the key feature or contribution of this design.

iii. Detailed computer modelling of the novel design to investigate its performance parameters was carried out which involved model formulation for the separation circuit (cyclone) and mathematical formulations for the modelling of the heat and mass transfer of the adsorption cooling/heating circuit. The performance of the separation circuit (cyclone) was investigated by writing a computer code using MATLAB software to determine the speed of adsorbent flow. Subsequently, from the discretised governing equations of energy and mass conservation combined with the associated boundary conditions and the adsorbent flow speed already determined, a computer code using MATLAB software was developed to determine and optimize the overall system performance parameters.

iv. The results from the investigation on the effects of the particle (product, which is the adsorbent in this present study) exit diameter, d_{pe}, on the cyclone performance rather than the effect of gas exit diameter which has been broadly researched in the literature would be useful for chemical industries, pharmaceutical industry, food processing industry, nanotechnology etc., in ensuring efficient products separation and recovery from the air stream without damaging their (products) characteristics.

7.2 Future work

- Although this research has shown a remarkable potential of using the circulatory fluidized adsorption refrigeration (CFAR) system to generate cooling, a further research can be considered to explore further opportunities geared towards improving the refrigerator performance as well as its applicability.
- The real CFAR system with fluidized solid desiccant could be constructed based on the design in this research, and then tested in the laboratory for its applicability. The test results could be compared with the numerical results in this work. Further analysis could provide addition insights. There is need for the construction of the small design (like a prototype) of the CFAR system.
- There is need for the laboratory evaluation and testing of the small scale prototype of the CFAR system.
- It is also necessary to determine the economic and environmental viability of the system.

References

1. Odesola, I.F. and M.A. Oluleye, *Thermodynamic Analysis and Simulation of Combined Adsorption Heating and Cooling System.* Journal of Engineering Research, 2012. **17**(2): p. 43-55.
2. Choudhury, B., et al., *An overview of developments in adsorption refrigeration systems towards a sustainable way of cooling.* Applied Energy, 2013. **104**: p. 554-567.
3. Wang, D.C., et al., *A review on adsorption refrigeration technology and adsorption deterioration in physical adsorption systems.* Renewable and Sustainable Energy Reviews, 2010. **14**(1): p. 344-353.
4. Vedavalli, R., *Energy for development [electronic resource] : twenty-first century challenges of reform and liberalization in developing countries / Rangaswamy Vedavalli*, ed. I. ebrary. 2007, London ; New York: London ; New York : Anthem Press.
5. Bejan, A. and A.D. Kraus, *Heat transfer handbook*. 2003, Hoboken, NJ: Hoboken, NJ: Wiley.
6. NEXTIAS. *World Population Prospects Report 2022.* *https://www.nextias.com/current-affairs/12-07-2022/world-population-prospects-report-2022 Accessed: 29th July, 2023*.
7. Aliyu, A.S., J.O. Dada, and I.K. Adam, *Current status and future prospects of renewable energy in Nigeria.* Renewable and Sustainable Energy Reviews, 2015. **48**: p. 336-346.
8. Hadj Ammar, M.A., B. Benhaoua, and F. Bouras, *Thermodynamic analysis and performance of an adsorption refrigeration system driven by solar collector.* Applied Thermal Engineering, 2017. **112**: p. 1289-1296.
9. Wang, D., et al., *Investigation of adsorption performance deterioration in silica gel–water adsorption refrigeration.* Energy Conversion and Management, 2012. **58**: p. 157-162.
10. Sleiti, A.K., W.A. Al-Ammari, and M. Al-Khawaja, *Review of innovative approaches of thermo-mechanical refrigeration systems using low grade heat.* International Journal of Energy Research, 2020. **44**(13): p. 9808-9838.
11. Tassou, S.A., et al., *A review of emerging technologies for food refrigeration applications.* Applied Thermal Engineering, 2010. **30**(4): p. 263-276.
12. Enibe, S.O., *Solar refrigeration for rural applications.* Renewable Energy, 1997. **12**(2): p. 157-167.
13. Anyanwu, E.E. and C.I. Ezekwe, *Design, construction and test run of a solid adsorption solar refrigerator using activated carbon/methanol, as adsorbent/adsorbate pair.* Energy Conversion and Management, 2003. **44**(18): p. 2879-2892.
14. Sarbu, I. and C. Sebarchievici, *General review of solar-powered closed sorption refrigeration systems.* Energy Conversion and Management, 2015. **105**: p. 403-422.
15. N'Tsoukpoe, K.E., D. Yamegueu, and J. Bassole, *Solar sorption refrigeration in Africa.* Renewable and Sustainable Energy Reviews, 2014. **35**: p. 318-335.
16. Sehgal, S., et al., *A comprehensive review of recent developments in falling-film, spray, bubble and microchannel absorbers for absorption systems.* Renewable and Sustainable Energy Reviews, 2021. **142**: p. 110807.
17. Ali, F.A.F. and A.M.E. Yoonis, *Absorption Refrigeration Cycle Technology*, in *Cooling Technologies*, B.-H. David, Editor. 2023, IntechOpen: Rijeka. p. Ch. 1.
18. Li, M., *Run-around energy recovery system with a porous solid desiccant*, in *Department of Mechanical Engineering*

19. Goyal, P., et al., *Adsorption refrigeration technology – An overview of theory and its solar energy applications.* Renewable and Sustainable Energy Reviews, 2016. **53**: p. 1389-1410.
20. Oluleye, M.A., *Thermodynamic Analysis and Simulation of a Combined Adsorption Heating and Cooling System*, in *Department of Mechanical Engineering, Faculty of Technology*. 2011, University of Ibadan, Nigeria: Ibadan, Nigeria.
21. Fernandes, M.S., et al., *Review and future trends of solar adsorption refrigeration systems.* Renewable and Sustainable Energy Reviews, 2014. **39**: p. 102-123.
22. Meunier, F., *Adsorptive cooling: a clean technology.* Clean Products and Processes, 2001. **3**(1): p. 8-20.
23. Wang, R., L. Wang, and J. Wu, *Adsorption Refrigeration Technology : Theory and Application*. 2014, Somerset, SINGAPORE: Wiley.
24. Pons, M. and J. Guilleminot, *Design of an experimental solar-powered, solid-adsorption ice maker.* Journal of solar energy engineering, 1986. **108**(4): p. 332-337.
25. Sakoda, A. and M. Suzuki, *Simultaneous transport of heat and adsorbate in closed type adsorption cooling system utilizing solar heat.* Journal of Solar Energy Engineering, Transactions of the ASME, 1986. **108**(3): p. 239-245.
26. Tan, Y., et al., *Study of solar powered adsorption ice maker.* Taiyangneng Xuebao/Acta Energiae Solaris Sinica, 1992. **13**(3): p. 255-258.
27. Boubakri, A., et al., *Experimental study of adsorptive solar-powered ice makers in Agadir (Morocco)—1. Performance in actual site.* Renewable Energy, 1992. **2**(1): p. 7-13.
28. Boubakri, A., et al., *Experimental study of adsorptive solar-powered ice makers in Agadir (Morocco)—2. Influences of meteorological parameters.* Renewable Energy, 1992. **2**(1): p. 15-21.
29. Critoph, R.E., Z. Tamainot-Telto, and E. Munyebvu, *Solar sorption refrigerator.* Renewable Energy, 1997. **12**(4): p. 409-417.
30. Sumathy, K. and L. Zhongfu, *Experiments with solar-powered adsorption ice-maker.* Renewable Energy, 1999. **16**(1): p. 704-707.
31. Boubakri, A., J.J. Guilleminot, and F. Meunier, *Adsorptive solar powered ice maker: experiments and model.* Solar Energy, 2000. **69**(3): p. 249-263.
32. Boubakri, A., *A new conception of an adsorptive solar-powered ice maker.* Renewable Energy, 2003. **28**(5): p. 831-842.
33. Boubakri, A., *Performance of an adsorptive solar ice maker operating with a single double function heat exchanger (evaporator/condenser).* Renewable Energy, 2006. **31**(11): p. 1799-1812.
34. Leite, A.P.F. and M. Daguenet, *Performance of a new solid adsorption ice maker with solar energy regeneration.* Energy Conversion and Management, 2000. **41**(15): p. 1625-1647.
35. Li, M., et al., *Experimental study on dynamic performance analysis of a flat-plate solar solid-adsorption refrigeration for ice maker.* Renewable Energy, 2002. **27**(2): p. 211-221.

36. Buchter, F., P. Dind, and M. Pons, *An experimental solar-powered adsorptive refrigerator tested in Burkina-Faso.* International Journal of Refrigeration, 2003. **26**(1): p. 79-86.
37. Li, C.H., R.Z. Wang, and Y.J. Dai, *Simulation and economic analysis of a solar-powered adsorption refrigerator using an evacuated tube for thermal insulation.* Renewable Energy, 2003. **28**(2): p. 249-269.
38. Anyanwu, E.E., *Review of solid adsorption solar refrigerator I: an overview of the refrigeration cycle.* Energy Conversion and Management, 2003. **44**(2): p. 301-312.
39. Lemmini, F. and A. Errougani, *Building and experimentation of a solar powered adsorption refrigerator.* Renewable Energy, 2005. **30**(13): p. 1989-2003.
40. Lemmini, F. and A. Errougani, *Experimentation of a solar adsorption refrigerator in Morocco.* Renewable Energy, 2007. **32**(15): p. 2629-2641.
41. Anyanwu, E.E. and N.V. Ogueke, *Transient analysis and performance prediction of a solid adsorption solar refrigerator.* Applied Thermal Engineering, 2007. **27**(14): p. 2514-2523.
42. Ogueke, N.V. and E.E. Anyanwu, *Design improvements for a collector/generator/adsorber of a solid adsorption solar refrigerator.* Renewable Energy, 2008. **33**(11): p. 2428-2440.
43. Saha, B.B., et al., *Evaluation of minimum desorption temperatures of thermal compressors in adsorption refrigeration cycles.* International Journal of Refrigeration, 2006. **29**(7): p. 1175-1181.
44. Leite, A.P.F., et al., *Experimental thermodynamic cycles and performance analysis of a solar-powered adsorptive icemaker in hot humid climate.* Renewable Energy, 2007. **32**(4): p. 697-712.
45. González, M.I. and L.R. Rodríguez, *Solar powered adsorption refrigerator with CPC collection system: Collector design and experimental test.* Energy Conversion and Management, 2007. **48**(9): p. 2587-2594.
46. González, M.I., L.R. Rodríguez, and J.H. Lucio, *Evaluation of thermal parameters and simulation of a solar-powered, solid-sorption chiller with a CPC collector.* Renewable Energy, 2009. **34**(3): p. 570-577.
47. Maggio, G., et al., *Simulation of a solid sorption ice-maker based on the novel composite sorbent "lithium chloride in silica gel pores".* Applied Thermal Engineering, 2009. **29**(8): p. 1714-1720.
48. Hassan, H.Z., A.A. Mohamad, and R. Bennacer, *Simulation of an adsorption solar cooling system.* Energy, 2011. **36**(1): p. 530-537.
49. Omisanya, N., et al., *Performance of a zeolite–water adsorption refrigerator.* Advances in Applied Science Research, 2012. **3**(6): p. 3737-3745.
50. Laidi, M. and S. Hanini, *Optimal solar COP prediction of a solar-assisted adsorption refrigeration system working with activated carbon/methanol as working pairs using direct and inverse artificial neural network.* International Journal of Refrigeration, 2013. **36**(1): p. 247-257.
51. Abu-Hamdeh, N.H., K.A. Alnefaie, and K.H. Almitani, *Design and performance characteristics of solar adsorption refrigeration system using parabolic trough collector: Experimental and statistical optimization technique.* Energy Conversion and Management, 2013. **74**: p. 162-170.
52. Omisanya, N.O., et al., *Comparison of Experimental Measurements and Simulation of Solar (Zeolite4A-Water) Adsorption Refrigerator Using Trnsys and Matlab Softwares.* Review of Applied Physics, 2013. **2**(4): p. 114-127.

53. Anjorin, S.A. and E.I. Bello, *Performance evaluation of a solar powered solid adsorption refrigerator under a tropical humid climate.* European Journal of Engineering and Technology, 2015. **3**(No. 4): p. 43-56.
54. Fatih, B., et al. *Design and analysis of a laboratory cooling adsorption machine working with pair silicagel/water*. in *2015 3rd International Renewable and Sustainable Energy Conference (IRSEC)*. 2015.
55. Bouzeffour, F., B. Khelidj, and M. Tahar abbes, *Experimental investigation of a solar adsorption refrigeration system working with silicagel/water pair: A case study for Bou-Ismail solar data.* Solar Energy, 2016. **131**: p. 165-175.
56. Wang, R.Z., *Performance improvement of adsorption cooling by heat and mass recovery operation.* International Journal of Refrigeration, 2001. **24**(7): p. 602-611.
57. Wang, R.Z., *Adsorption refrigeration research in Shanghai Jiao Tong University.* Renewable and Sustainable Energy Reviews, 2001. **5**(1): p. 1-37.
58. Miles, D.J., et al., *Gas fired sorption heat pump development.* Heat Recovery Systems and CHP, 1993. **13**(4): p. 347-351.
59. Jones, J.A., *Regenerative adsorbent heat pump*. 1991, US Patent 50,463,319.
60. Jones, J.A., *Sorption refrigeration research at JPL/NASA.* Heat Recovery Systems and CHP, 1993. **13**(4): p. 363-371.
61. Sumathy, K., K.H. Yeung, and L. Yong, *Technology development in the solar adsorption refrigeration systems.* Progress in Energy and Combustion Science, 2003. **29**(4): p. 301-327.
62. Bataineh, K. and Y. Taamneh, *Review and recent improvements of solar sorption cooling systems.* Energy and Buildings, 2016. **128**: p. 22-37.
63. Akahira, A., et al., *Mass recovery adsorption refrigeration cycle—improving cooling capacity.* International Journal of Refrigeration, 2004. **27**(3): p. 225-234.
64. Liu, Y.L., R.Z. Wang, and Z.Z. Xia, *Experimental study on a continuous adsorption water chiller with novel design.* International Journal of Refrigeration, 2005. **28**(2): p. 218-230.
65. Wang, D.C., et al., *Study of a novel silica gel–water adsorption chiller. Part I. Design and performance prediction.* International Journal of Refrigeration, 2005. **28**(7): p. 1073-1083.
66. Wang, D.C., et al., *Study of a novel silica gel–water adsorption chiller. Part II. Experimental study.* International Journal of Refrigeration, 2005. **28**(7): p. 1084-1091.
67. Fadar, A.E., A. Mimet, and M. Pérez-García, *Modelling and performance study of a continuous adsorption refrigeration system driven by parabolic trough solar collector.* Solar Energy, 2009. **83**(6): p. 850-861.
68. Baiju, V. and C. Muraleedharan, *Performance study of a two stage solar adsorption refrigeration system.* IJEST, 2011. **3**(7): p. 5754-5764.
69. Shelton, S.V., W.J. Wepfer, and D.J. Miles, *External fluid heating of a porous bed.* Chemical Engineering Communications, 2007. **71**(1): p. 39-52.
70. Shelton, S.H., W.J. Wepfer, and S.H. Shelton, *Ramp Wave Analysis of the Solid/Vapor Heat Pump.* Journal of Energy Resources Technology, Transactions of the ASME, 1990. **112**(1): p. 69-78.
71. Miles, D.J. and S.V. Shelton, *Design and testing of a solid-sorption heat-pump system.* Applied Thermal Engineering, 1996. **16**(5): p. 389-394.
72. Jones, J.A. *Carbon/ammonia regenerative adsorption heat pump*. in *International Absorption Heat Pump Conference, ASME-AES*. 1994.

73. Amar, N.B., L.M. Sun, and F. Meunier, *Numerical analysis of adsorptive temperature wave regenerative heat pump.* Applied Thermal Engineering, 1996. **16**(5 SPEC. ISS.): p. 405-418.
74. Spinner, B., *Ammonia-based thermochemical transformers.* Heat Recovery Systems and CHP, 1993. **13**(4): p. 301-307.
75. Sun, L.M., Y. Feng, and M. Pons, *Numerical investigation of adsorptive heat pump systems with thermal wave heat regeneration under uniform-pressure conditions.* International Journal of Heat and Mass Transfer, 1997. **40**(2): p. 281-293.
76. Chahbani, M.H., J. Labidi, and J. Paris, *Modeling of adsorption heat pumps with heat regeneration.* Applied Thermal Engineering, 2004. **24**(2): p. 431-447.
77. Critoph, R.E., *Forced convection adsorption cycle with packed bed heat regeneration: Cycle à adsorption à convection forcée avec régénération thermique du lit fixe.* International Journal of Refrigeration, 1999. **22**(1): p. 38-46.
78. Critoph, R.E., *Forced convection adsorption cycles.* Applied Thermal Engineering, 1998. **18**(9): p. 799-807.
79. Lai, H.-M., *An enhanced adsorption cycle operated by periodic reversal forced convection.* Applied Thermal Engineering, 2000. **20**(7): p. 595-617.
80. Douss, N. and F. Meunier, *Experimental study of cascading adsorption cycles.* Chemical Engineering Science, 1989. **44**(2): p. 225-235.
81. Saha, B.B., A. Akisawa, and T. Kashiwagi, *Solar/waste heat driven two-stage adsorption chiller: the prototype.* Renewable Energy, 2001. **23**(1): p. 93-101.
82. Saha, B.B., et al., *Performance evaluation of a low-temperature waste heat driven multi-bed adsorption chiller.* International Journal of Multiphase Flow, 2003. **29**(8): p. 1249-1263.
83. Shu, J., et al., *Research on an adsorption–absorption cascading multi-effect refrigeration cycle.* J Engng Thermophys, 2001. **5**: p. 546-548.
84. Saha, B.B., E.C. Boelman, and T. Kashiwagi, *Computational analysis of an advanced adsorption-refrigeration cycle.* Energy, 1995. **20**(10): p. 983-994.
85. Saha, B.B. and T. Kashiwagi, *Experimental investigation of an advanced adsorption refrigeration cycle.* ASHRAE Transactions, 1997. **103**(pt 2): p. 50-58.
86. Saha, B.B., et al., *Waste heat driven dual-mode, multi-stage, multi-bed regenerative adsorption system.* International Journal of Refrigeration, 2003. **26**(7): p. 749-757.
87. Critoph, R.E., *Simulation of a continuous multiple-bed regenerative adsorption cycle.* International Journal of Refrigeration, 2001. **24**(5): p. 428-437.
88. Wang, Q., et al., *Experimental investigation on a fluidized-bed adsorber/desorber for the adsorption refrigeration system.* International Journal of Refrigeration, 2012. **35**(3): p. 694-700.
89. Hassan, H.Z., A.A. Mohamad, and H.A. Al-Ansary, *Development of a continuously operating solar-driven adsorption cooling system: Thermodynamic analysis and parametric study.* Applied Thermal Engineering, 2012. **48**: p. 332-341.
90. Hassan, H.Z. and A.A. Mohamad, *Thermodynamic analysis and theoretical study of a continuous operation solar-powered adsorption refrigeration system.* Energy, 2013. **61**: p. 167-178.

91. Hassan, H.Z., et al., *Dynamic analysis of the CTAR (constant temperature adsorption refrigeration) cycle.* Energy, 2014. **77**: p. 852-858.
92. Tchernev, D.I., *Solar air conditioning and refrigeration systems utilizing zeolites.* In: Proceedings of the meeting of commissions E1–E2, International Institute of Refrigeration, 1982: p. 209–215
93. Wang, R.Z., et al., *An energy efficient hybrid system of solar powered water heater and adsorption ice maker.* Solar Energy, 2000. **68**(2): p. 189-195.
94. Wang, R.Z., et al., *Research on a combined adsorption heating and cooling system.* Applied Thermal Engineering, 2002. **22**(6): p. 603-617.
95. Zhang, X.J. and R.Z. Wang, *Design and performance simulation of a new solar continuous solid adsorption refrigeration and heating hybrid system.* Renewable Energy, 2002. **27**(3): p. 401-415.
96. Suleiman, R., et al., *Transient simulation of a flat plate solar collector powered adsorption refrigeration system.* International Journal of Renewable Energy Research, 2012. **2**(4): p. 657-664.
97. Banker, N.D., et al., *Performance studies on mechanical+adsorption hybrid compression refrigeration cycles with HFC 134a.* International Journal of Refrigeration, 2008. **31**(8): p. 1398-1406.
98. Banker, N.D., et al., *Activated carbon+HFC 134a based two stage thermal compression adsorption refrigeration using low grade thermal energy sources.* Applied Thermal Engineering, 2009. **29**(11): p. 2257-2264.
99. Banker, N.D., et al., *Development and transient performance results of a single stage activated carbon – HFC 134a closed cycle adsorption cooling system.* Applied Thermal Engineering, 2010. **30**(10): p. 1126-1132.
100. Mitra, S., et al., *Performance evaluation and determination of minimum desorption temperature of a two-stage air cooled silica gel/water adsorption system.* Applied Energy, 2017. **206**: p. 507-518.
101. Mitra, S., et al., *Modeling study of two-stage, multi-bed air cooled silica gel+water adsorption cooling cum desalination system.* Applied Thermal Engineering, 2017. **114**: p. 704-712.
102. Tchernev, D.I., *Solar air conditioning and refrigeration systems utilizing zeolites.* In: Proceedings of the meeting of commissions E1–E2, International Institute of Refrigeration, 1982: p. 209–215.
103. NPTEL, N.C.E.D.-I.J.i.o.I.a.I.F.b.M., *Module 5: Separation Equipment*. p. 1-34.
104. Gabelman, A., P.E., *Adsorption basics: Part 2. Chemical Engineering Progress, 113(8), 38-45. .* 2017.
105. Jing, H. and R.H.B. Exell, *Adsorptive properties of activated charcoal/methanol combinations.* Renewable Energy, 1993. **3**(6): p. 567-575.
106. Meunier, F. and N. Douss, *Performance of adsorption heat pumps; Active carbon-methanol and zeolite-water pairs.* ASHRAE Transactions (American Society of Heating, Refrigerating and Air-Conditioning Engineers);(United States), 1990. **96**(CONF-9006117--).
107. saVRee, s.D.I.M. *Cyclone Separator working principle (Dust Separator)*. 2022 7th July,2022]; Available from: https://savree.com/en/encyclopedia/cyclone-separator-working-principle-dust-separator#:~:text=There%20are%20two%20main%20designs,particles%20from%20a%20gas%20stream.&text=Hydrocyclones%20are%20used%20for%20separating%20fluids%20of%20different%20densities.
108. Rietema, K. and C.G. Verver, *Cyclones in industry: a collection of papers on the principles and utilization of industrial cyclones, originally presented at the*

two symposia on this subject, organized in 1953 and 1958 by the Royal Dutch Institute of Engineers and the Royal Netherlands Chemical Society. 1961.
109. Fushimi, C., et al., *Recent Progress in Efficient Gas–Solid Cyclone Separators with a High Solids Loading for Large-scale Fluidized Beds †.* Kona, 2021. **38**: p. 94-109.
110. Trefz, M. and E. Muschelknautz, *Extended cyclone theory for gas flows with high solids concentrations.* Chemical Engineering and Technology, 1993. **16**(3): p. 153-160.
111. Muschelknautz, E. and V. Greif, *Fundamental and practical aspects of cyclones.* Circulating Fluidized Bed Technology IV, 1994: p. 20.
112. Grace, J.R., A.A. Avidan, and T.M. Knowlton, *Circulating fluidized beds / edited by J.R. Grace, A.A. Avidan and T.M. Knowlton*. 1st ed. ed. 1997, London: London : Blackie Academic & Professional.
113. Muschelknautz, U., *Design and Calculation Methods for Uniflow Cyclones*. 2019, New York: Access Intelligence LLC: New York. p. 52-63.
114. Okedere, O.B., et al., *Usefulness of particulate cyclone in air pollution control.* Management of environmental quality, 2013. **24**(6): p. 771-781.
115. Chermisinoff, P., *Air Pollution Control and Design for Industry*. 1993, New York, NY.: Marcel Dekker Inc,.
116. Trimech, T.I.I. *Cyclone*. 2021 [cited 2022 July 7th, 2022]; Available from: https://www.trimechindia.com/cyclone.html.
117. Hoffmann, A.C. and L.E. Stein, *Gas Cyclones and Swirl Tubes: Principles, Design and Operation*. Second ed. 2008, (2nd edition) Springer Berlin, Heidelberg New York. 422.
118. Muschelknautz, E. and W. Krambrock, *Aerodynamische Beiwerte des Zyklonabscheiders aufgrund neuer und verbesserter Messungen.* Chemie Ingenieur Technik, 1970. **42**(5): p. 247-255.
119. Elsayed, K. and C. Lacor, *Optimization of the cyclone separator geometry for minimum pressure drop using mathematical models and CFD simulations.* Chemical Engineering Science, 2010. **65**(22): p. 6048-6058.
120. Stairmand, C.J., *Pressure drop in cyclone separators.* Engineering, 1949. **168**(B): p. 409-412.
121. Lapple, C.E., *Processes use many collector types. Chemical Eng. 58(5): 144-151.* 1951.
122. Pesaran, A., et al., *Review article: Numerical simulation of adsorption heat pumps.* Energy, 2016. **100**: p. 310-320.
123. Yong, L. and K. Sumathy, *Review of mathematical investigation on the closed adsorption heat pump and cooling systems.* Renewable and Sustainable Energy Reviews, 2002. **6**(4): p. 305-338.
124. Teng, W.S., K.C. Leong, and A. Chakraborty, *Revisiting adsorption cooling cycle from mathematical modelling to system development.* Renewable and Sustainable Energy Reviews, 2016. **63**: p. 315-332.
125. Wang, L.W., R.Z. Wang, and R.G. Oliveira, *A review on adsorption working pairs for refrigeration.* Renewable and Sustainable Energy Reviews, 2009. **13**(3): p. 518-534.
126. Qasem, N.A.A. and M.A.I. El-Shaarawi, *Improving ice productivity and performance for an activated carbon/methanol solar adsorption ice-maker.* Solar Energy, 2013. **98**: p. 523-542.
127. Mauran, S., P. Prades, and F. L'Haridon, *Heat and mass transfer in consolidated reacting beds for thermochemical systems.* Heat Recovery Systems and CHP, 1993. **13**(4): p. 315-319.

128. Bejan, A., *Heat transfer handbook / Adrian Bejan, Allan D. Kraus*, ed. A.D. Kraus. 2003, Hoboken, N.J.: Hoboken, N.J. : John Wiley & Sons.
129. Peary, H.R. and H.C. Chilton, *Chemical engineering handbook. 5thed. New York: McGraw-Hill. .* 1973.
130. Hoekstra, A.J., *Gas Flow Field and Collection Efficiency of Cyclone Separators*. 2000, Ph.D. Thesis, Technical University Delft.
131. Zhao, B., H. Shen, and Y. Kang, *Development of a symmetrical spiral inlet to improve cyclone separator performance.* Powder Technology, 2004. **145**(1): p. 47-50.
132. Jafarnezhad, A., et al., *Performance improvement of a cyclone separator using different shapes of vortex finder under high-temperature operating condition.* Journal of the Brazilian Society of Mechanical Sciences and Engineering, 2021. **43**(2).
133. El-Batsh, H.M., *Improving cyclone performance by proper selection of the exit pipe.* Applied Mathematical Modelling, 2013. **37**(7): p. 5286-5303.
134. Gil, A., L. Romeo, and C. Cortes, *Effect of the solid loading on a pressurized fluidized bed combustors cyclone with pneumatic extraction of solids.* Chemical Engineering & Technology, 2002. **25**: p. 407-415.
135. Morin, M., et al., *Effect of solid loading and inlet aspect ratio on cyclone efficiency and pressure drop: Experimental study and CFD simulations.* Powder Technology, 2021. **377**: p. 174-185.

Appendices

Appendix A: Computer code written in MATLAB script file for the separation circuit (cyclone)

```
%CYCLONEDEIGN.m
clear
close all
clc
%%%%%%%%%%%%%%%%%%%%%%%%%%%%%%%%%%%%%%%%%%%%%%%%%%%%%%%%%%%%%%%%%%%%%%%%%%%%

%CYCLONE PHYSICAL PARAMETERS
d=0.1;              % (m) Cyclone diameter
r=d/2;              % (m) Cyclone radius
a=0.62*d;           % (m)cyclone inlet height
b=0.24*d;           % (m)cyclone inlet width
d_v=0.62*d;         % (m) Vortex finder diameter
r_v=d_v/2;          % (m) Vortex finder radius
H_t=4.24*d;         % (m) Cyclone total height
H_cyl=1.62*d;       % (m)Cylinder height
H_con=2.62*d;       % (m)Cone height
S=a+d/8;            % (m) Vortex finder height inside the cyclone
d_pe=0.38*d;        % (m)Particle exit diameter
r_pe=d_pe/2;        % (m)Particle exit radius
L_o=1.62*d;         % (m)Vortex finder height outside the cyclone
Epsilon= 0.046*10^(-3); %(m)absolute roughness of the inside
surface of the cyclone wall(= 0.046mm for commercial steel)
%%%%%%%%%%%%%%%%%%%%%%%%%%%%%%%%%%%%%%%%%%%%%%%%%%%%%%%%%%%%%%%%%%%%%%%%%%%%

%GAS PROPERTIES
rho_gas=1.2;            % (kg/m^3) Density of the circulating gas
V_in = 30;              % (m/s) mean gas inlet velocity
mu_gas=1.8*10^(-5);     % (Pa.s)  gas dynamic viscosity
g=9.81;                 % (m/s^2) Acceleration due to gravity

%%%%%%%%%%%%%%%%%%%%%%%%%%%%%%%%%%%%%%%%%%%%%%%%%%%%%%%%%%%%%%%%%%%%%%%%%%%%

%PARTICLE PARAMETERS
rho_p=370;              % (kg/m^3) Density of the solid adsorbent
particles
C_o=6;                  % (kg/kg)incoming solid loading in
cyclone inlet
C_o2=C_o/0.83;          % (kg/m^3)incoming solid loadino in
cyclone inlet
m=2;                    % () exponential factor/slope
n=20;                   % () no of size fraction
M_sf=6;                 % (kg) mass of solid adsorbent fed into
the cyclone

%%%%%%%%%%%%%%%%%%%%%%%%%%%%%%%%%%%%%%%%%%%%%%%%%%%%%%%%%%%%%%%%%%%%%%%%%%%%


%ESTIMATION OF CUT SIZE DIAMETER
Q = a*b*V_in % (m^3/s) gas(particle laden)volumetric flow rate
```

```
Ut_50=Q/(2*pi*r_v*(H_t-S));  %(m/s) terminal radial velocity of
X_50 in the inner vortex
r_in=r-(b/2);              %(m)  radial position of the center
of cyclone/inlet mean inlet radius
Ext=b/r;
alpha=(1/Ext)*(1-(sqrt(1+4*((Ext/2)^2-(Ext/2))*sqrt(1-(((1-
(Ext^2))*(2*Ext-Ext^2))/(1+C_o))))));
r_cm=sqrt(r*r_v);                          % (m) mean cyclone
radius
V_m=(0.9*Q)/(pi*(r^2-r_cm^2));             % (m) mean (wall)
axial velocity
Re_ge=(rho_gas*V_m*d_v)/mu_gas;            % () exit pipe
Reynolds number
Re_c=Re_ge/(4*H_t/d_v*((d/d_v)-1));        % () cyclone Reynolds
number

f_sw_con=0.323*(Re_c^(-0.623));      % () gas friction factor
for smooth (conical)cyclone wall

f_sw_cyl=1.51*(Re_c^(-1.0));         % () gas friction factor
for smooth (cylindrical)cyclone wall

Rel_rough=(Epsilon/r);

if Rel_rough>0.0006
   f_rw_con=(log10((1.60/((Rel_rough)-0.000599))^2.38))^(-
2)*(1+((2.25*10^5)/(Re_c^(2)*((Rel_rough)-0.000599)^0.213)))^-
1; % gas friction factor for rough(conical) cyclone wall
   f_rw_cyl=(log10((1.29/((Rel_rough)-0.000599))^2.59))^(-
2)*(1+((2.14*10^5)/(Re_c^(1.64))))^-1; % gas friction factor
for rough cyclone wall

   else
    Rel_rough=0.0006;
    f_rw_con=(log10((1.60/((Rel_rough)-0.000599))^2.38))^(-
2)*(1+((2.25*10^5)/(Re_c^(2)*((Rel_rough)-0.000599)^0.213)))^-
1; % gas friction factor for rough(conical) cyclone wall
    f_rw_cyl=(log10((1.29/((Rel_rough)-0.000599))^2.59))^(-
2)*(1+((2.14*10^5)/(Re_c^(1.64))))^-1; % gas friction factor
for rough cyclone wall
end
f_sw= (f_sw_con + f_sw_cyl)/2;  % () mean gas friction factor
for smooth cyclone wall

f_rw= (f_rw_con + f_rw_cyl)/2; % () mean gas friction factor
for rough cyclone wall
f_gas=f_sw + f_rw;                % () gas friction factor
f_p=0.015*sqrt(C_o); % () solid (desiccant)particle friction
factor
f=f_gas+f_p;          % () Overall friction factor/coefficient
U_c=(V_in*r_in)/(alpha*r);
A_R=pi*((r^2)-(r_v^2)+2*r*(H_t-
H_con)+(r+r_pe)*sqrt((H_con^2)+((r-r_pe)^2))+2*r_v*S);
U_x =(U_c*(r/r_v))/(1+(f*A_R*U_c*(sqrt(r/r_v))/(2*Q))); %gas
tangential vel @ the inner core(vortex) radius (@ r_v)
X_50=sqrt((18*mu_gas*(0.9*Q))/(2*pi*(rho_p-
rho_gas)*(U_x^(2))*(H_t-S)));
Re_p=(rho_gas*Ut_50*X_50)/mu_gas;

if Re_p<=0.5   %particles settling in the Strokes'law regime
```

```
     X_50=sqrt((18*mu_gas*(0.9*Q))/(2*pi*(rho_p-
rho_gas)*(U_x^(2))*(H_t-S)));
else
  X_50=(5.18*mu_gas^0.375*rho_gas^0.25*Ut_50^0.875)/(((rho_p-
rho_gas)*U_x^2)/r_v)^0.625; %Strokes'law not holding
end
X_50=X_50*10^6;   %conversion of cut size diameter from meter
to micrometer

%%%%%%%%%%%%%%%%%%%%%%%%%%%%%%%%%%%%%%%%%%%%%%%%%%%%%%%%%%%%%%%%%%%%%%%

%ESTIMATION OF THE OVERALL SEPARATION EFFICIENCY

Xi=linspace(50,500,n);   %50:50:500;
X_50_vec=linspace(X_50,X_50,n);
Ni=1./(1+(X_50_vec./Xi).^m);
Wi=[0.03 0.02 0.06 0.04 0.06 0.04 0.11 0.09 0.09 0.06 0.09 0.06
0.06 0.04 0.03 0.02 0.03 0.02 0.03 0.02]; % mass fraction
X_median=median(Xi);
k=-0.11-0.10*log(C_o);
if C_o>=0.1
    C_oL=0.025*(X_50/X_median)*(10*C_o)^0.15;   %limiting
loading
else
   C_oL=0.025*(X_50/X_median)*(10*C_o)^k;
end

if C_o<C_oL     %condition of no saltation/mass loading
  Sep_Eff_total=Ni*Wi' ;
end
if C_o>C_oL     %saltation/mass loading condition occurs
  Sep_Eff_total= ((1-(C_oL/C_o))+(C_oL/C_o))*(Ni*Wi');
End

%%%%%%%%%%%%%%%%%%%%%%%%%%%%%%%%%%%%%%%%%%%%%%%%%%%%%%%%%%%%%%%%%%%%%%%

%ESTIMATION OF PRESSURE DROP
V_x=Q/(pi*r_v^2);
DeltaP_wall=(f*A_R*rho_gas*(U_c*U_x)^1.5)/(2*0.9*Q);
DeltaP_x=(2+3*(U_x/V_x)^1.33+(U_x/V_x)^2)*(rho_gas*V_x^2)/2;
DeltaP=DeltaP_wall+DeltaP_x;

%%%%%%%%%%%%%%%%%%%%%%%%%%%%%%%%%%%%%%%%%%%%%%%%%%%%%%%%%%%%%%%%%%%%%%%

%ESTIMATION OF THE MASS OF SOLID (ADSORBENT) COLLECTED
M_sc=Sep_Eff_total*M_sf;   %(kg) mass of solid collected

%%%%%%%%%%%%%%%%%%%%%%%%%%%%%%%%%%%%%%%%%%%%%%%%%%%%%%%%%%%%%%%%%%%%%%%

% NO OF EFFECTIVE TURNS
N_Eff_Turns=(1/a)*(H_cyl+H_con/2);

%%%%%%%%%%%%%%%%%%%%%%%%%%%%%%%%%%%%%%%%%%%%%%%%%%%%%%%%%%%%%%%%%%%%%%%

% POWER REQUIREMENT
P_f=Q*DeltaP;  %(Watts)fan power requirement
%%%%%%%%%%%%%%%%%%%%%%%%%%%%%%%%%%%%%%%%%%%%%%%%%%%%%%%%%%%%%%%%%%%%%%%

% SOLID ADSORBENT FLOW RATE
```

```
M_dot=C_o2*Q;  % (kg/s) mass flow rate of solid adsorbent

%%%%%%%%%%%%%%%%%%%%%%%%%%%%%%%%%%%%%%%%%%%%%%%%%%%%%%%%%%%%%%%%%%%%%%%%

% TERMINAL SETTLING VELOCITY OF THE SOLID ADSORBENT PARTICLES
Tau= (pi*d*N_Eff_Turns)/V_in;   % gas residence time
V_terminal= b/Tau;
```

Appendix B: Computer code written in MATLAB script file for the adsorption refrigeration circuit

```
%REFRIGERATION_CIRCUIT.m

% RESET MEMORY
clear
clc
clearvars


%DEFINITION OF CONSTANT PROPERTIES
Cpsc = 920;           % Specific heat of adsorbent (J/kg.K)
Cpads = 2534;         % Specific heat of adsorbate (J/kg.K)
rhosc = 370;          % Density of adsorbent (kg/m^3)
Lv=1102*10^3;         % Latent heat of vaporization of adsorbate
(J/kg)
qmax = 0.38;          % Maximum adsorption capacity (kg/kg)
ksc = 0.5;                % Thermal conductivity of adsorbent
(W/m.K)
Msc = 6*0.98;         % Mass of adsorbent (kg) (actually, 98% of
                        the total mass fed into the cyclone)
Mads = 0.032;         % Molar mass of adsorbate (kg/mol)
Hs = 1900*10^3;       % Heat of sorption (J/kg)


%ADSORPTIVE PARAMETERS
D=1.94*10^-8;             %  Adsorption parameter (K^-1)
n=2.59;                   %  Adsorption parameter
A=18.587;                 %  Adsorption parameter
B=3626.55;                %  Adsorption parameter
C=-34.29;                 %  Adsorption parameter
Ea = 40*10^3;             %  Activation energy (J/mol)
R=8.314;                  %  Universal gas constant (J/mol.K)
D_not=3.9*10^-2;                %   Arrrhenius equation Pre-
exponential
                              coefficient (m^2/s)
eps = 0.7;                %  Adsorbent porosity


%OPERATING PARAMETERS
Tamb = 26.9+273.15;               % Ambient temperature (K)
T_L=30+273.15;                    % Cooling temperature (K)
T_H=100+273.15;                   % Heating temperature  (K)
T_ave=(T_H+T_L)/2;                % Average system temperature
(K)
TC = 35+273.15;                   % Condenser temperature (K)
TE = 15+273.15;                   % Evaporator temperature(K)
PC = 133.33*exp(A-(B/(TC+C)));    % Condenser Pressure (Pa)
PE = 133.33*exp(A-(B/(TE+C)));    % Evaporator Pressure (Pa)
P_atm =133.33*exp(A-(B/(Tamb+C)));% Atmospheric pressure
                                    corresponding to Tamb
M_dot=0.3227;                     % Adsorbent flow rate (kg/s)
u_sc=0.49;                       % Velocity of adsorbent(m/s)



%SIMULATION PARAMETERS
H=0.5;                  % Height of adsorber/desorber (m)
```

```
dz= 0.01;                % Spatial step size(m)
z=0:dz:H;                % vector of z(numerical domain)
Nz=(H/dz)+1;             % Number of nodes on grids ()
dt = 0.000001;           % Time step ()
TimeMax = 60;            % Cycle time(s)
iterMax = TimeMax/dt;    % Number of iterations/time steps to
                         compute


%OTHER PARAMETERS
Ds=D_not*exp(-Ea/(R*T_ave)); % Effective diffusion coefficient
(m^2/s)
omega= (dt*Ds)/(eps*dz^2);
alphasc = dt*u_sc/(2*dz);
betasc = dt*ksc*(1-eps)/(dz*dz*rhosc);
alpha2sc = dt*u_sc/(2*eps*dz);
phi = (1-eps)*rhosc*R/(eps*Mads);


%INDICES
ibegin = 1;
sz=Nz+1;
iend = sz;


%INITIALISING (CREATING AN ARRAY (MATRIX) OF VARIABLES
q = zeros(1,sz);  %creating an array (Matrix) of zeros for q
T = zeros(1,sz);  %creating an array (Matrix) of zeros for T
Pads = zeros(1,sz);%creating an array (Matrix) of zeros for
Pads
qnew = zeros(1,sz);%creating an array (Matrix) of zeros for
qnew
Tnew= zeros(1,sz); %creating an array (Matrix) of zeros for
Tnew
Padsnew = zeros(1,sz);%creating an array (Matrix) of zeros for
Padsnew
Psat = zeros(1,sz);%creating an array (Matrix) of zeros for
Psat
gamma = zeros(1,sz);%creating an array (Matrix) of zeros for
gamma
qvar=zeros(1,sz);%creating an array (Matrix) of zeros for qvar
Tvar=zeros(1,sz);%creating an array (Matrix) of zeros for Tvar
Pvar=zeros(1,sz);%creating an array (Matrix) of zeros for Pvar
q(1, :)= qmax *ones(1,sz);
T(1,:) = (30+273.15)*ones(1,sz);
Pads(1,:) = PE*ones(1,sz);


% convergence loop controller
cond = 0;


%DESORPTION CYCLE

% SET INLET PARAMETERS FOR DESORPTION
q0 = qmax; % Maximum adsorption quantity
T_des = 30+273.15;

for time = 0:1:TimeMax

%SET INITIAL CONDITION (time = 0)
```

```
for i=ibegin:iend



Tnew(1,:)=
[303.1500,304.5225,305.8951,307.2676,308.6402,310.0127,311.3853
312.7578,314.1304,315.5029,316.8755,318.2480,319.6206,320.9931,
322.3657,323.7382,325.1108,326.4833,327.8559,329.2284,330.6010,
331.9735,333.3461,334.7186,336.0912,337.4637,338.8363,340.2088,
341.5814,342.9539,344.3265,345.6990,347.0716,348.4441,349.8167,
351.1892,352.5618,353.9343,355.3069,356.6794,358.0520,359.4245,
360.7971,362.1696];


Padsnew = 1.0e+04 *

[0.9840,1.0195,1.0549,1.0904,1.1259,1.1613,1.1968,1.2323,1.2678
1.3032,1.3387,1.3742,1.4097,1.4451,1.4806,1.5161,1.5515,1.5870,
1.6225,1.6580,1.6934,1.7289,1.7644,1.7998,1.8353,1.8708,1.9063,
1.9417,1.9772,2.0127,2.0481,2.0836,2.1191,2.1546,2.1900,2.2255,
2.2610,2.2964,2.3319,2.3674,2.4029,2.4383,2.4738,2.5093,2.5448,
2.5802,2.6157,2.6512,2.6866,2.7221,2.7576,2.7931];


qnew(1,:) =
    [0.3800,0.3733,0.3666,0.3599,0.3532,0.3465,0.3398,0.3331,
     0.3264,0.3196,0.3129,0.3062,0.2995,0.2928,0.2861,0.2794,
     0.2727,0.2660,0.2593,0.2526,0.2459,0.2392,0.2325,0.2258,
     0.2191,0.2124,0.2056,0.1989,0.1922,0.1855,0.1788,0.1721,
     0.1654,0.1587,0.1520,0.1453,0.1386,0.1319,0.1252,0.1185,
     0.1118,0.1051,0.0984,0.0916,0.0849,0.0782,0.0715,0.0648,
     0.0581,0.0514,0.0447,0.0380];
end

  for iter = 1:2:iterMax
        %disp(iter)


% AT INLET OF DESORBER (i=ibegin=1)
  for i=ibegin
    Tnew(1,ibegin) = T_des;
    Psat(1,ibegin) = 133.33*exp(A-(B/(Tnew(1,ibegin)+C)));
    qnew(1,ibegin)=q0*exp(-
D*(Tnew(1,ibegin)*log((Psat(1,ibegin))/PC))^n);

    Padsnew(1,ibegin) = (Pads(1,ibegin)*(1(2*omega)))
     +(Pads(1,ibegin+1)*(omega-alpha2sc))-
(phi*T(1,ibegin)*qnew(1,ibegin))..
       +(phi*T(1,ibegin)*q(1,ibegin));
  end


 % AFTER INLET/INNER NODES ALONG THE DESORBER LENGTH)(i=2:iend-
1)
  for i=ibegin+1:iend-1

   Psat(1,i) = 133.33*exp(A-(B/T(1,i)+C));
   qnew(1,i) =q0*exp(-D*(T(1,i)*log((Psat(1,ibegin))/PE))^n
```

```
      gamma(1,i) = Cpsc+(q(1,i)*Cpads);
   Tnew(1,i)=(T(1,i+1)*((betasc/gamma(1,i))-
alphasc))+(T(1,i)*(1-
   (2*betasc/gamma(1,i))))+(T(1,i-
    1)*((betasc/gamma(1,i))+alphasc))+(Hs*(qnew(1,i)-
q(1,i))/gamma(1,i));

   Pads(1,i) = (Pads(1,i-1)*(omega+alpha2sc))+(Pads(1,i)*(1-
   (2*omega)))+(Pads(1,i+1)*(omega-alpha2sc))-
   (phi*T(1,i)*qnew(1,i))+(phi*T(1,i)*q(1,i));

  end

% AT OUTLET OF DESORBER(i = iend)
  for i=iend
      Psat(1,iend) = 133.33*exp(A-(B/T(1,iend)+C));
      qnew(1,iend)=q0*exp(-
D*(T(1,iend)*log((Psat(1,ibegin))/PE))^n);

          gamma(1,iend) = Cpsc+(q(1,i)*Cpads);
      Tnew(1,iend)=(T(1,iend)*(1-
(2*betasc/gamma(1,iend))))+(T(1,iend-
       1)*((betasc/gamma(1,iend))+alphasc))+(Hs*(qnew(1,iend)-
       q(1,iend))/gamma(1,iend));


      Padsnew(1,iend)=(Pads(1,iend-
1)*(omega+alpha2sc))+(Pads(1,iend)*(1-
      (2*omega)))-
(phi*T(1,iend)*qnew(1,iend))+(phi*T(1,iend)*q(1,iend));
  end

 %UPDATING VARIABLES
         for i=ibegin:iend

            T(1,i)=Tnew(1,i);
            Pads(1,i)=Padsnew(1,i);
            q(1,i)=qnew(1,i);

           Tvar(1,time+1)=abs(Tnew(1,i));
           Pvar(1,time+1)=abs(Padsnew(1,i));
           qvar(1,time+1)=abs(qnew(1,i));
        end
   end

%CHECK FOR CONVERGENCE
      for i=ibegin:iend
              if (q(1,iend-1)-q(1,iend))<0.01
                 disp('converged');
                 cond = 1;
                break;
             end
             if cond ==true
                 break;
             end
      end


 end

        % Boundary conditions
```

```
        T_des_outlet = Tnew(1,iend);
        Pads_des_outlet = Padsnew(1,iend);
        q_des_outlet = qnew(1,iend);

%%%%%%%%%%%%%%%%%%%%%%%%%%%%%%%%%%%%%%%%%%%%%%%%%%%%%%%%%%%%%%%%%%%%%%%%%%%%
%%%%%%%%%%%%%%%%%%%%%%%%%%%%%%%%%%%%%%%%%%%%%%%%%%%%%%%%%%%%%%%%%%%%%%%%%%%%
%%%%%%%%%%%%%%%%%%%%%%%%%%%%%%

%ADSORPTION CYCLE

% SET INLET PARAMETERS FOR ADSORPTION

q0 = qmax;
T_ads = 80+273.15;

for time = TimeMax+1:1:2*TimeMax


  for iter = 1:2:iterMax

        %disp(iter)


% AT INLET OF ADSORBER (i=ibegin=1)
  for i=ibegin

% imposing the boundary conditions that the conditions at the
adsorber inlet is equivalent to those at the desorber outlet

Tnew(1,ibegin) = T_des_outlet; %  Temperature at adsorber
                          inlet = Temperature at desorber outlet
Padsnew(1,ibegin)  =  Pads_des_outlet;%   Pressure  at  adsorber
inlet
                                    =   pressure   at   desorber
outlet
qnew(1,ibegin)   =   q_des_outlet;   %   Adsorption   quantity   at
adsorber
                  inlet   =   adsorption   quantity   at   desorber
outlet
  end


% AFTER INLET/INNER NODES ALONG THE ADSORBER LENGTH)(i=2:iend-
1)
  for i=ibegin+1:iend-1

Psat(1,i) = 133.33*exp(A-(B/T(1,i)+C));
qnew(1,i) =q0*exp(-D*(T(1,i)*log((Psat(1,ibegin))/PE))^n);
   gamma(1,i) = Cpsc+(q(1,i)*Cpads);
Tnew(1,i)            =            (T(1,i+1)*((betasc/gamma(1,i))-
alphasc))+(T(1,i)*(1-

(2*betasc/gamma(1,i))))+(T(1,i1)*((betasc/gamma(1,i))+alphasc))
              +(Hs*(qnew(1,i)-q(1,i))/gamma(1,i));
Padsnew(1,i)   =   (Pads(1,i-1)*(omega+alpha2sc))+(Pads(1,i)*(1-
(2*omega)))

+(Pads(1,i+1)*(omegaalpha2sc))(phi*T(1,i)*qnew(1,i))
               +(phi*T(1,i)*q(1,i));
```

```
  end


% AT OUTLET OF ADSORBER (i = iend)
  for i=iend

Psat(1,iend) = 133.33*exp(A-(B/T(1,iend)+C));
qnew(1,iend)=q0*exp(-D*(T(1,iend)*log((Psat(1,ibegin))/PC))^n);

  gamma(1,iend) = Cpsc+(q(1,i)*Cpads);
Tnew(1,iend)=(T(1,iend)*(1-
(2*betasc/gamma(1,iend))))+(T(1,iend-

1)*((betasc/gamma(1,iend))+alphasc))+(Hs*(qnew(1,iend)-
                q(1,iend))/gamma(1,iend));

Padsnew(1,iend)=(Pads(1,iend-
1)*(omega+alpha2sc))+(Pads(1,iend)*(1-
          (2*omega)))-
(phi*T(1,iend)*qnew(1,iend))+(phi*T(1,iend)*q(1,iend));
  end


 %UPDATING VARIABLES
         for i=ibegin:iend
            T(1,i)=Tnew(1,i);
            Pads(1,i)=Padsnew(1,i);
            q(1,i)=qnew(1,i);

           Tvar(1,time+1)=abs(Tnew(1,i));
           Pvar(1,time+1)=abs(Padsnew(1,i));
           qvar(1,time+1)=abs(qnew(1,i));
         end
   end

%CHECK FOR CONVERGENCE
      for i=ibegin:iend
             if (q(1,iend)-q(1,iend-1))<0.01
                disp('converged');
                 cond = 1;
               break;
            end
             if cond ==true
                 break;
             end
     end

 end
```